To the Graduate Council:

I am submitting herewith a dissertation written by Leonardo Resende Allain entitled "Optical Sensors in Harsh Environments: Determination of Concentrated Strong Acids and Bases for Process Control." I have examined the final copy of this dissertation for form and content and recommend that it be accepted in partial fulfillment of the requirements for the degree of Doctor of Philosophy, with a major in Chemistry.

Ziling Xue, Major Professor

We have read this dissertation
and recommend its acceptance:

Accepted for the Council:

Associate Vice Chancellor and
Dean of The Graduate School

Optical Sensors in Harsh Environments: Determination of Concentrated Strong Acids and Bases for Process Control

A Dissertation

Presented for the

Doctor of Philosophy

Degree

The University of Tennessee, Knoxville

Leonardo Resende Allain

December 1999

DEDICATION

This dissertation is dedicated to my family,

from whom I draw support,

encouragement, and good-humor.

ACKNOWLEDGEMENTS

Throughout the years I have spent at the University of Tennessee, I discovered a small universe of people whose help, friendship, and guidance deserve proper gratitude and appreciation. I could not start this list without first acknowledging my research advisor, Dr. Ziling (Ben) Xue, for his consistent guidance, support, and persistence in achieving and maintaining high standards. I would also like to thank the members of my committee, Professors Ronald Magid, George Schweitzer, and Otto Schwarz, for their guidance and commitment. Special thanks go to Drs. David C. Joy and David Beach for assistance in obtaining scanning electron micrographs and film thickness measurements, respectively. My appreciation is also extended to Drs. John F. Willey and Arlene A. Garrison, who have always encouraged helpful discussions.

I am grateful to the electronic and glass shop staff, especially, Johnny Jones, Bill Gurley, Arthur Pratt, and Elder Mellon, for assisting me so efficiently and cheerfully. I also owe thanks to several other people in this department, including, but not limited to, Dr. Charmaine Mamantov, Jan McGuire, Maria Motoyama, Rachelle Allen, Teresa Turner, and Carol Moulton.

I would especially like to thank my coworkers and colleagues here, including Dr. Liting Li, Dr. Lenore McAlexander, Dr. Jonathan Diminnie, Vivian Liu, Dr. Zhongzhi Wu, Dr. Yvette Yang, Kevin Bennett, Jonathan Morrell, Mark Burleigh, Bryan Fagan, Terry Yost, Tianniu Chen, Hee-Jung Im, Jaime Blanton, Andrew Canada, Dr. Hu Cai, Erin Myers, and John and Cheri Clavier. I have met good, spirited friends in all of you and am flattered to have had you as part of my everyday life.

I am particularly appreciative of my undergraduate research advisor, Professor Carlos Alberto Filgueiras, for being such a cheerful friend over the years and for inspiring me with his cultivation and sense of humor.

Finally, I am, as always, grateful for the constant and steadfast encouragement of my parents, brothers, and sister, and my friends in Brazil. I also would like to thank my friends Mark Arena and Edivania Feijo, Don Rosen, Joe Meyer, Domenic Sabella, and my cousin, Simone Resende Nunes. You have all significantly improved the quality of my life during the past years.

The research described in this dissertation was financially supported by the Measurement and Control Engineering Center (MCEC) at the UTK College of Engineering and its member companies [3M, ABB, Amoco, Ciba Specialty Chemicals, Coates Consulting, Dow Corning, DuPont, Eastman Chemical, Elf Aquitaine, Equistar Chemicals, Exxon, Goodyear, Hercules, Imperial Chemical Industries (ICI), Kaiser Optical, Lubrizol, Oak Ridge National Laboratory, Solutia, and Union Carbide]. American Holographic is also recognized for the donation of a Rainbow Meter spectrometer. I would also like to acknowledge the following research grants and institutions for their financial support: DuPont Young Professor Award, Camille Dreyfus Teacher-Scholar Award, and the University of Tennessee at Knoxville.

ABSTRACT

This dissertation describes the development of optical sensors for the determination of concentrated strong acid and alkali for process control in harsh environments. An overview of the Ph. D. research is given in Chapter 1, along with a summary of optical sensors, and Hammett acidity functions. Chapter 2 describes a portable fiber-optic sensor system for on-line high acidity ($[H^+]$ = 1 - 11 M) measurements. The sensor consists of a thin-film silica support prepared through a sol-gel process and doped with a low p*K*a indicator. The sensors are mechanically and chemically stable in acid for a period of at least 9 months. The performance of the sensors in this test period had a relative standard deviation of less than 2.0% with no re-calibration. The sensor response time was short (1 - 5 s), and a small hysteresis was observed during reproducibility measurements with 2 - 10 M HCl solutions. The use of the sensor in solutions containing a large amount of salts and organic compounds is also discussed. In Chapter 3, sensors for the spectrometric determination of hydroxide ($[OH^-]$ = 1 - 10 M) are discussed. Such a sensor consists of a support prepared with a blend of organic polymers and SiO_2/ZrO_2, and an immobilized high p*K*a dye. The hydrophilic nature of inorganic oxides and their chemical stability in concentrated alkali make them attractive as support materials for sensors. The organic polymers provide a stronger mechanical support and better dye immobilization. Composites of SiO_2/ZrO_2 with organic polymers were found to produce sensors with high mechanical stability and fast response. The performance of the sensors showed a relative standard deviation of less than 2%. The response time was short (5 s), and a small hysteresis was observed in

reproducibility measurements with 1 - 4 M NaOH solutions. The diffusion kinetics and hysteresis performance of the sensors were also evaluated. Chapter 4 describes the effect of salts, present in the acid analyte matrix, on the acid sensors. To correct the salt effect on sensor response, a dual-sensor approach has been developed. A novel linear relationship between $\left(\partial A/\partial C_{salt}\right)_{C_{acid}}$ and $\left(dA/dC_{acid}\right)_{C_{salt}=0}$ (A = absorbance of the indicator doped in the sensor film; C_{acid} = acid concentration; C_{salt} = salt concentration) was discovered. The dual-sensor approach to correct the salt effect was based on a set of non-linear equations derived from this relationship. Finally, in Chapter 5, the importance of response hysteresis in our sensor systems is presented. The hysteresis of sensor response was found to be the major component of the analytical error in our optical sensor systems. A correlation between sensor response time and hysteresis was observed. Sensors with fast response times had a small hysteresis. A variety of techniques have been developed to reduce the hysteresis in our sensor response.

TABLE OF CONTENTS

Chapter Page

1 Introduction 1

1.1 Sensor Applications in Industry 4

1.2 Optical Sensors 5

1.2.1 Beer-Lambert Law 5

1.2.2 Attenuation of Light in Optical Fibers 6

1.3 Characteristics of Optical Sensors 7

1.4 Measuring Acidity: an Overview 10

1.4.1 Dilute Acid and Base Solutions - *Using Potentiometric pH as Standard* 10

1.4.2 Concentrated Acid and Base Solutions - *The Establishment of Acidity and Basicity Functions* 11

1.5 Overview of this Dissertation 14

1.6 The Equipment Used in the Current Study 15

2 Optical Sensors for High Acidity Determination 19

2.1 Introduction 19

2.1.1 Previous Research on Sensors for High Acidity Measurement 20

2.1.2 Our Approach to Acid Sensors 21

2.2 Experimental Section 23

2.2.1 Preparation of the Sol-Gel Sensor Films - Acid as a Catalyst (Sensors 1 – 5) 23

2.2.2 Preparation of Sol-Gel Sensor Films - Base as a Catalyst (Sensor 6) 24

2.2.3 Conditioning of the Films 24

2.3 Results and Discussion 25

2.3.1 The Sol-Gel Process and Doping of Indicators 25

2.3.2 The Indicator 28

2.3.3 Effects of Reagents, Catalysts, and Gelling Temperatures on the Sol-Gel Sensor Films 32

2.3.4 Response of the Sensor Films in Concentrated HCl 35

2.3.5 Sensor Response under Flow Conditions 38

2.3.6 Response Time and Sensor Morphology 42

2.3.7 Long-Term Reproducibility 48

2.3.8 Measurement of HCl Pickling Solutions 48

2.3.9 Attempted Construction of a Reflectance Probe 56

2.3.10 Measurement of Strong Acids in Organic Media 56

3 Optical Sensors for the Determination of Concentrated Hydroxide 62

3.1 Introduction 62

3.2 Experimental Section 64

3.2.1 Preparation of the SiO_2/ZrO_2-PSMMA Sensor (Sensor 7) 65

3.2.2 Preparation of the SiO_2/ZrO_2-Nafion Sensor (Sensor 8) 66

3.2.3 Preparation of the SiO_2/ZrO_2-Nafion-PSMMA Sensor (Sensor 9) 67

3.2.4 Preparation of SiO_2/ZrO_2 with a Chelating Agent (Sensor 10) 67

3.2.5 Preparation of ZrO_2 with $(CF_3)_2CO{\cdot}3H_2O$ (Sensor 11) 68

3.2.6 Preparation of SiO_2/ZrO_2 with Micelle Templating (Sensor 12) 68

3.2.7 Preparation of SiO_2/ZrO_2 with Emulsion Templating (Sensor 13) 68

3.2.8 Preparation of SiO_2/ZrO_2 with a TiO_2 Reflective Coating (Sensors 14 - 15) 69

3.2.9 Conditioning of the Films 70

3.3 Results and Discussion 70

3.3.1 The Metal-Oxide Support 71

3.3.2 The Composite Support 77

3.3.3 The Transducer Dyes 83

3.3.4 Response of the Sensor Films in Concentrated NaOH 86

3.3.5 Response Time 90

3.3.6 Long-Term Stability of the Sensors 95

3.3.7 Reflectance vs. Transmittance Sensors 95

3.3.8 Effect of Ionic Strength 100

4 Optical Sensors and the Salt Effect: A Dual-Transducer Approach to Acidity Determination in Salt-Containing Concentrated Strong Acids 105

4.1 Introduction 105

4.2 Experimental Section 108

4.2.1 Preparation of Sensor 16 109

4.2.2 Measurement Procedure 109

4.3 Results and Discussion 110

4.3.1 The Transducing Mechanism 110

4.3.2 The Salt-Effect 116

4.3.3 Dual Optical Transducer Approach 119

4.3.4 Indicator Absorbance and Acidity Function 129

4.3.5 Evaluation of Conductivity as a Secondary Concentration Transducer 134

5 Hysteresis in Optical Sensing and Its Impact on Analytical Error 138

5.1 Introduction 138

5.2 Experimental Section 140

5.3 Results and Discussion 141

5.3.1 Hysteresis in the Acid Sensor 141

5.3.2 Quantifying the Hysteresis Error in Acid Sensor Response 147

5.3.3 Hysteresis in the Base Sensors 149

5.3.4 Hysteresis and Response Time 149

References 158

Appendices 165

Appendix A 166

Appendix B 168

Vitae 171

LIST OF TABLES

Table Page

1.1 Current Customers of Laboratory Services 5

3.1 Thermodynamic Dissociation Constants for Thiazole Yellow GGM in Different Supports 87

5.1 Results from Analysis of Variance Applied to the Nine-Month Reproducibility Data (Sensor 2 Response in 2 M HCl under a Positive and a Negative Concentration Gradient) 145

5.2 Results from Analysis of Variance Applied to the Nine-Month Reproducibility Data (Sensor 2 Response in 6 M HCl under a Positive and a Negative Concentration Gradient) 146

5.3 Results from Analysis of Variance Applied to the Nine-Month Reproducibility Data (Sensor 2 Response in 2 M HCl in the First 4.5 Months and in the Second 4.5 Months) 148

LIST OF FIGURES

Figure Page

1.1. Schematic representation of the mode of gathering optical information: (a) a first generation, (b) a second generation, and (c) a third generation extrinsic optical chemical sensor. In (a), the optical information is obtained directly from the absorbing or fluorescing analyte. In (b), a transducer element such as an indicator layer is attached to the fiber end. In (c), a bioreactive or bioreceptice element, e.g., an enzyme layer, is added, which converts an otherwise unmeasurable parameter into a measurable one. Evidently the response times increase with the increasing complexity of the sensor. (Adapted from ref. 2a) 3

1.2. Top: Schematic of an optical fiber. Bottom: Path of light in a waveguide. α is the acceptance angle; n1 and n2 are refractive indices for core and cladding; θ is the critical angle for total reflection to occur. (Adapted from ref. 2a) 8

1.3. Schematic of the optical flow system 16

1.4. Schematic of the optical cells. In (a), the sensor element is a sol-gel coated glass slide, which can be easily removed from and placed in the optical cell. In (b), the sensor element consists of a sol-gel film directly coated onto the surface of one of the optical windows. The sensor element in (b) is thus fixed in the optical cell 18

2.1. The reactions in the sol-gel process 26

2.2. A generic sol-gel sensor preparation procedure 27

2.3. Equilibria of the three protonated forms of Bromocresol Purple 29

2.4. Typical spectra of Bromocresol Purple-doped Sensor 2 in HCl solutions 30

2.5. Distribution curves for the first ionization of BCP doped in a sol-gel thin film. The curves were fitted by a five degree polynomial 31

2.6. Scanning electron micrographs (SEM) of the sensors films: (a) base-catalyzed Sensor 6; (b) acid-catalyzed Sensor 2 33

2.7. Typical spectra of Bromocresol Green-doped Sensor 4 in HCl solutions 36

2.8. Typical spectra of Fast Green FCF-doped Sensor 3 in HCl solutions 37

2.9. Response reversibility of Sensor 2. The averages of the response in the range of 546 – 550 nm are shown 39

2.10. The response of BCP Sensor 2 in HCl solutions 40

2.11. Response of Sensor 2 under a continuous flow of 8 M HCl 41

2.12. Response kinetics for Sensor 2 in HCl solutions 44

2.13. Response kinetics for Sensor 2 under different washing conditions The sensor was initially kept in 6 M HCl 46

2.13. Response kinetics for BCP Sensors 1, 2, and 6 47

2.15. Response stability of Sensor 2 in a nine-month durability test. Sensor 2 was kept in 6 M HCl during the entire test period. The error bars are 2 σ (std. dev.) 49

2.16. Nine-month durability test of Sensor 2. The sensor film was kept in 6 M HCl during the entire test period, and evaluated periodically 50

2.17. The response of Sensor 2 in $HCl/FeCl_2$ solutions (75 g/L of Fe^{+2}) 53

2.18. The response of Sensor 2 in $HCl/FeCl_3$ solutions (50 g/L of Fe^{+3}) 54

2.19. The response of Sensor 2 in $HCl/FeCl_2$ solutions ([HCl] = 2.42 M) 55

2.20. Absorbance vs. salt concentration of Sensor 2 in $HCl/FeCl_2$ solutions ([HCl] = 2.42 M) 57

2.21. Response of Sensor 2 in solutions of H_2SO_4/benzene/acetone/water 59

2.22. Response of Sensor 2 in solutions of H_2SO_4/HOAc 60

2.23. Variation of H_0 with H_2SO_4 concentration in acetic acid with small amounts of water. Curves A to E contain, respectively, 0, 1, 5, 10, and 15% H_2O. Indicator was 4-chloro-2-nitroaniline, pK_{BH^+} = -1.03 in water. (Adapted from ref. 39) 61

3.1. Preparation of SiO_2/ZrO_2 with pre-hydrolysis of $Si(OMe)_4$ 73

3.2. Preparation of SiO_2/ZrO_2 with the use of a chelating agent to reduce the hydrolysis rate of $Zr(OBu^n)_4$ 75

3.3. Preparation of SiO_2/ZrO_2 with the use of $(CF_3)_2CO{\cdot}3H_2O$ as a slow H_2O-releasing agent 76

3.4. Preparation of a composite SiO_2/ZrO_2-organic polymer sensor 79

3.5. SEM of the surface of the sensor films: (a) a SiO_2/ZrO_2 sensor; (b) a SiO_2/ZrO_2 sensor doped with TiO_2 powder (Sensor 14); (c) a SiO_2/ZrO_2-PSMMA-Nafion composite sensor (Sensor 9) 81

3.6. Equilibrium involving the protonated and deprotonated forms of Thiazole Yellow GGM 85

3.7. Typical transmittance spectra of Sensor 7 in NaOH solutions (concentrations in % w/v) 88

3.8. Calibration curve of Sensor 7 in NaOH solutions 89

3.9. Response reproducibility of Sensor 8 in NaOH solutions (concentrations in % w/v) 91

3.10. Response kinetics of Sensors 7 – 9 under a positive concentration gradient, from H_2O to 12% w/v NaOH 92

3.11. Response kinetics of Sensors 7 – 9 under a negative concentration gradient, from 12% w/v NaOH to H_2O 93

3.12. Exponential dependence of the response time and PSMMA composition of Sensor 7. Response times were calculated using sensor absorbance changes from 12% w/v NaOH to H_2O 94

3.13. Long-term stability test of Sensor 7 96

3.14. Long-term stability test of Sensor 8 97

3.15. Long-term stability test of Sensor 9 98

3.16. Long-term stability test of Sensor 8. Response was corrected by dividing the transmittance at λ_{max} by $\lambda_{isosbestic}$ 99

3.17. Typical reflectance spectra of Thiazole Yellow GGM-doped Sensor 14 in NaOH solutions (concentrations in % w/v) 101

3.18. Typical reflectance spectra of Alizarin Yellow-doped Sensor 15 in NaOH solutions (concentrations in % w/v) 102

3.19. Effect of ionic strength: sensor response vs. Na_2S concentration. NaOH concentration was fixed at 2 M 103

4.1. Calibration plot of A vs. [HCl] for Bromocresol Purple Sensor 2 114

4.2. Theoretical plot of A vs. 10^{-H_0} for Sensor 2. H_0 is a Hammett acidity function for HCl 115

4.3. Response of Fastgreen FCF Sensor 3 in $CaCl_2$/HCl solutions ([HCl] = 2.42 M) 117

4.4. Response of Bromocresol Green Sensor 4 in $CaCl_2$/HCl solutions ([HCl] = 2.42 M) 118

4.5. Response of Bromocresol Purple Sensor 2 in $CaCl_2$/HCl solutions 120

4.6. Response of Acid Blue 147 Sensor 5 in $CaCl_2$/HCl solutions 121

4.7. Response of Neutral Red Sensor 16 in $CaCl_2$/HCl solutions 122

4.8. Plot of $\left(dA/dC_{acid}\right)_{C_{salt}=0}$ vs. $\left(\partial A/\partial C_{salt}\right)_{C_{acid}}$. A is the absorbance of Sensor 2 in $CaCl_2$/HCl solutions 123

4.9. Plot of $\left(dA/dC_{acid}\right)_{C_{salt}=0}$ vs. $\left(\partial A/\partial C_{salt}\right)_{C_{acid}}$. A is the absorbance of Sensor 5 in $CaCl_2$/HCl solutions 124

4.10. Plot of $\left(dA/dC_{acid}\right)_{C_{salt}=0}$ vs. $\left(\partial A/\partial C_{salt}\right)_{C_{acid}}$. A is the absorbance of Sensor 16 in $CaCl_2$/HCl solutions 125

4.11. Plot of computed (C_{salt}, [HCl]) pairs for given absorbance readings from Sensors 2 and 16 128

4.12. Comparison of errors in [HCl] measurements using Sensors 2 and 16, in the presence of $CaCl_2$, before and after the corrections 130

4.13. Validation plot of predicted vs. actual $CaCl_2$ concentrations in HCl/$CaCl_2$ solutions. Predicted values were computed by a signal deconvolution

algorithm using data from Sensors 2 and 16 131

4.14. Effect of NaCl on ionization of indicators from ref. 67: •, diphenylamine in 0.05 M HCl; o, diphenylamine in 0.1 M HCl; Δ, p-nitroaniline in 0.1 M HCl; ×, 2,4-dichloroaniline in 0.01 M HCl 132

4.15. Conductance of $FeCl_3$/HCl solutions as a function of $FeCl_3$ concentration ([HCl] = 2.42 M) 135

4.16. Conductance of $CaCl_2$/HCl solutions as a function of $CaCl_2$ and HCl concentrations 136

5.1. The hysteresis profile for Bromocresol Purple Sensor 2 142

5.2. Nine-month reproducibility test of Sensor 2 in 2 M HCl. The sensor was exposed to positive and negative acid concentration gradients 144

5.3. Hysteresis profile for Sensor 7 150

5.4. Hysteresis profile for Sensor 8 151

5.5. Hysteresis profile for Sensor 9 152

5.6. Plot of the response time vs. hysteresis magnitude for the hydroxide sensors (Sensors 7 – 9) 154

5.7. The logarithm of the buffer power per liter of water (B_w'/c) as a function of pH in the acidic region. Above pH = 3 and in the region between 0.6 and 3, the logarithm of buffer power is a linear function of pH with the equations given in the graph. Below pH = 0.6 there is a non-linear dependence, and, in extremely acidic solutions, the logarithm seems to approach a limiting value of 0.61. (Adapted from ref. 59) 155

5.8. The logarithm of the buffer power per liter of water (B_w'/c) as a function of pH in the alkaline region. Below pH = 13.6 the logarithm is a linear function of pH with the equation given in the graph. Above this pH there is a non-linear dependence, and, in strongly alkaline solutions, the logarithm seems to approach a limiting value of 0.84. (Adapted from ref. 59) 156

CHAPTER 1

Introduction

Human beings, along with other mammals, consciously interact with the universe that surrounds them by means of seven sensing mechanisms. Our ability to detect temperature and level variations is often ignored, but it is almost as important as the other more promptly recognized five senses. One cannot help being awed by the slow evolutionary process that brought the development of such senses, and their integration with a brain capable of information processing and storage.

If the better awareness of our surroundings, food supplies and predators was the main drive for this evolutive process, a parallel might be drawn with our own human enterprise of creating sensors that help us understand the world we modify.

A sensor can be viewed as the "primary element of a measurement chain, which converts the input variable into a signal suitable for measurement."[1] A sensing scheme is usually based on a transduction principle or mechanism. An input variable is transformed into an output variable through a transduction mechanism. Transduction principles are nothing less than known physical or chemical effects, which correlate observations in different domains. For example, the photoelectric effect is used to correlate the number of photons with electric current. The piezoelectric effect does the same for stress and electricity, and the Biot-Savart's law correlates magnetic field and voltage variations. In other words, sensing is based on transforming signals between different domains, from a domain we cannot directly access to one we can measure.

Our interest here lies in chemical sensors, where the primary transduction mechanism extracts chemical information (qualitative and/or quantitative chemical composition of a system) from its surrounding environment. Usually a series of other secondary transducers help transform the signal from the primary transducer to easily processable electrical signals. Through analog to digital converters, the electrical signals are then converted into digital data. As an example, Figure 1.1 indicates how optical information could be collected.[2a] In (a), the optical information is directly obtained from the absorbing/fluorescing analyte. In (b), a transducer element (absorbing or fluorescing indicator) is needed to extract optical information from the analyte. In (c), a bioreactive system, such as an enzyme layer, helps convert an otherwise unmeasurable analyte into measurable by-products. As expected, the response time increases with the number of transducing layers of the sensor.

Optical sensors and electrochemical sensors constitute the major categories of sensors used to extract chemical information from an analyte system. The importance of optical sensors has been growing in the past years, along with a variety of other types of sensors. Market studies show this trend (*vide infra*), as well as the increase in pertinent scientific publications. Janata's excellent literature review on chemical sensors[3] delineates well the latest research directions. The large growth in sensor research and development in the past 10 years has been facilitated by fundamental advances in interfacial chemistry, microscale-engineering technologies, as well as by a market demand for cleaner, more efficient, and better controlled industrial processes.

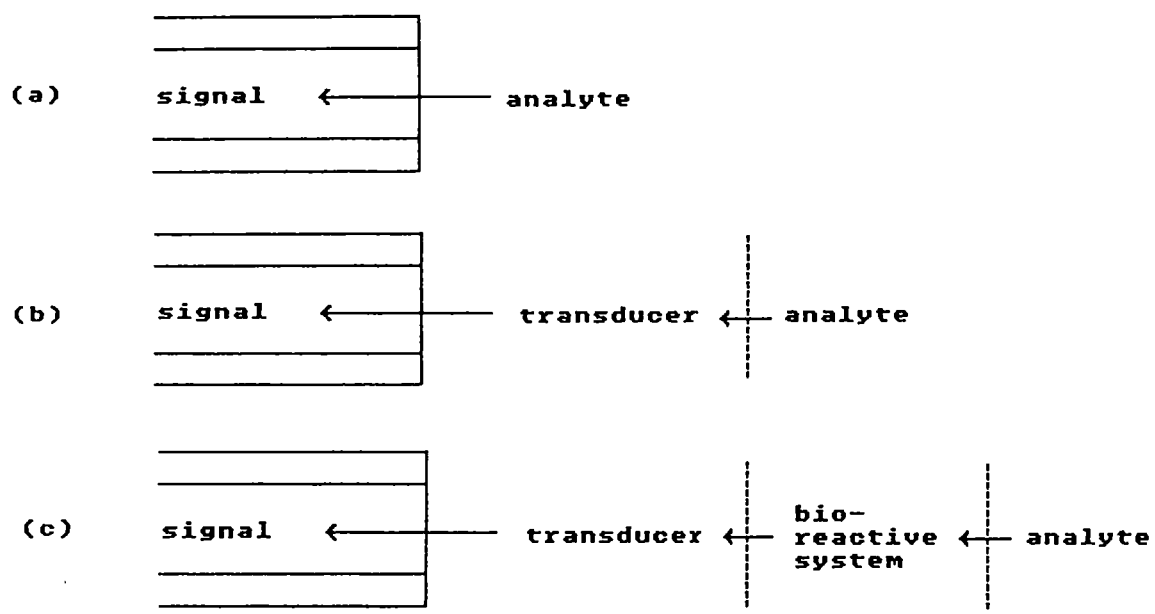

Figure 1.1. Schematic representation of the mode of gathering optical information: (a) a first generation, (b) a second generation, and (c) a third generation extrinsic optical chemical sensor. In (a), the optical information is obtained directly from the absorbing or fluorescing analyte. In (b), a transducer element such as an indicator layer is attached to the fiber end. In (c), a bioreactive or bioreceptice element, e.g., an enzyme layer, is added, which converts an otherwise unmeasurable parameter into a measurable one. Evidently the response times increase with the increasing complexity of the sensor. (Adapted from ref. 2a).

1.1 Sensor Applications in Industry

Sensor development has been greatly influenced by the needs of the market. For a number of years, the market has been fueled by electronic automation of processes and quality control. The large diversity in sensor applications can be observed in its stratified markets: in 1988, sensors for flow (U$ 1.8 billion), pressure (U$ 1.7 billion), speed (U$ 1.4 billion), chemical parameters (U$ 1.2 billion), level (U$ 1.15 billion), temperature (U$ 1.0 billion), and position (U$ 0.9 billion) had the highest world sales.[4]

Currently, the fiber optic chemical sensor market is less than 1% of the overall market for chemical sensors. Optical sensor technology is a relatively young area with bright growth potential. In the USA, according to Frost and Sullivan,[5] revenues for fiber optic chemical sensors in 1992 were $25.6 million, with approximately 3,600 units sold. In 1995 (the latest available data for the survey[5]), revenues were $34 million, with 4,900 units sold. The annual growth rate was 10% for that period.

The field sensor market currently accounts for $5 billion in annual sales.[6] The December 1995 issue of the Environmental Business Journal notes a strong trend to move environmental analysis from the lab to the field. Laboratory instrument sales decreased from 62% of environmental instrument sales in 1993 to 56% in 1995. Field instruments now account for 8% of environmental instrument sales. Once field instruments approach the quality of laboratory instruments, field analysis is predicted to dominate the market. Table 1.1 shows current customers of laboratory services:

Table 1.1 Current Customers of Laboratory Services

Customer	% of Purchase
Environmental firms*	51
Private Industry‡	32
Federal Government	9
Local Government	8

* Environmental firms include consulting and engineering firms, and hazardous waste management firms.

‡ Private industry encompasses business areas such as petroleum retailing, petroleum refining, chemicals manufacturing, utilities, mining, and agriculture.

This trend represents a large commercial opportunity for chemical sensors in both government and commercial sectors, especially since new sensor systems will benefit both the end users and firms that manufacture system-integrated equipment.

1.2 Optical Sensors

1.2.1 Beer-Lambert Law

One of the most important transduction principles in optical sensing is based on the Beer-Lambert law[7]. According to the Beer-Lambert law (Eq. 1.1), absorption of light (the first domain) is linearly proportional to the concentration of absorbing chemical species (the second domain).

$$A = \varepsilon \cdot b \cdot c \qquad \text{(Eq. 1.1)}$$

A = absorbance; ε = extinction coefficient; b = optical pathlength; c = concentration of the absorbing species.

At high concentrations (usually > 0.01 M), the average distances between ions or molecules of the absorbing species are small, and each particle affects the charge distribution of its neighbors. This interaction can alter the UV-visible spectrum of the absorbing species, shifting the absorbing wavelengths to higher or lower frequencies (hypsochromic and bathochromic shifts, respectively). Such an absorption shift usually leads to departures from linearity in Beer's law.

For some optical sensing applications, the analyte of interest may be present in multimolar concentrations. If the analyte were the direct absorbing species one would expect severe deviations from Beer's law. If low levels of dyes with low binding affinity (p*K*a) for the analyte are used, one can estimate the concentration of the analyte. The dye acts as a transducer, transforming one domain (dye concentration) into another (analyte concentration). The optical signal ultimately comes from the absorbing or fluorescence properties of the dyes, and the analyte concentration is inferred. That is the reason why specificity for the analyte-dye interaction has to be high enough to avoid interference from other species, which could produce a false estimation of concentration.

1.2.2 Attenuation of Light in Optical Fibers

Optical sensors have greatly benefited from the use of optical fibers, which allow the transmission of light over long distances. This feature provides sensors with the

flexibility for field or on-line analysis. The cost-effective mass production of fibers is a direct result of the demand created by the communication industry, which utilizes optical fibers to transfer high volumes of data. For common fibers, such as multimode step-index fibers, light is conducted through a center core surrounded by a cladding with lower refractive index (Figure 1.2). A successive number of total reflections of the incoming light beam occur at the core/cladding interface, guiding the light through the fiber with a very low level of intensity loss. The intensity loss, also known as power attenuation, is the result of the absorption intrinsic to the materials (silica and organic polymers such as polymethylmethacrylate and polystyrene) in the optical fibers and, to a lesser extent, from Rayleigh and Raman scattering. Plastic-based optical fibers have by far the highest loss in the visible spectrum in comparison to silica. The attenuation at 650 nm is < 10 dB/km for silica fibers, as compared to 100 – 200 dB/km for plastic fibers [1dB = 10 $\log(P_{output}/P_{input})$, where P is the power or energy].[2b]

1.3 Characteristics of Optical Sensors

Most optical sensors consist of a support (also referred to as matrix, membrane, or platform) that hosts an indicator, or transducer dye, sensitive to a specific analyte. The indicator is immobilized in the support by either chemical (covalent or electrostatic immobilization) or physical means (doping, entrapment).

The most important features that need to be addressed in designing an optical sensor are:

(a) *Long-term stability*: The transducer dye should not, in principle, degrade or leach from the membrane in the long term, making the system reliable and without the need of

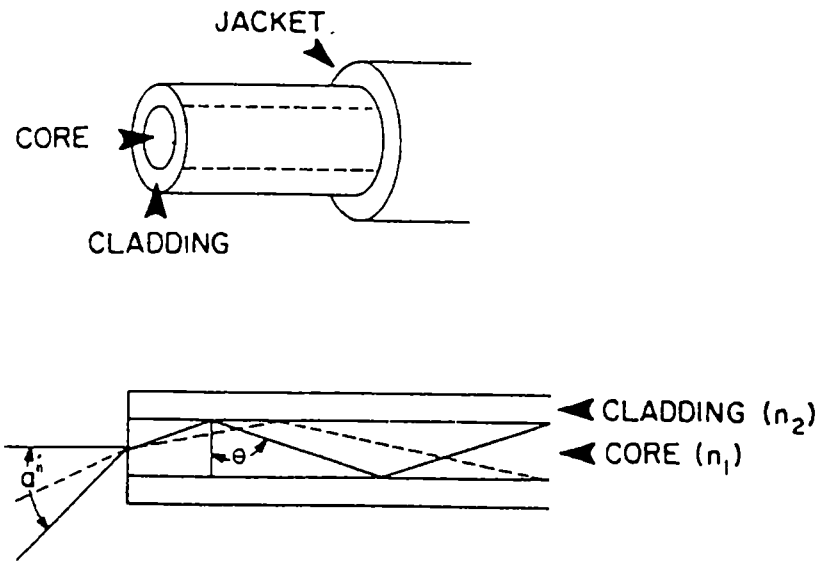

Figure 1.2. Top: Schematic of an optical fiber. Bottom: Path of light in a waveguide. α is the acceptance angle; n_1 and n_2 are refractive indices for core and cladding; θ is the critical angle for total reflection to occur. (Adapted from ref. 2a).

re-calibration. To achieve this, the host matrix should be mechanically and chemically stable in the testing environment. Chemometrical tools can be used to further improve the robustness of the long-term calibration.

(b) *Fast response time*: For on-line measurements it is indispensable to have real time data. The response time depends on the mass transfer rate of the analyte across the sensor interface. Therefore, the morphological characteristics of the sensor, such as thickness and porosity distribution, play an important role in controlling the response time. Furthermore, the interactions between the solvent and the sensor interface have a profound effect on the sensor response time. One of the most important consequences of long sensor response time is that it leads to severe hysteresis.

(c) *Hysteresis of response*: Although commonly ignored, hysteresis can be the major component of analytical error, as demonstrated in our work (Chapter 5). Hysteresis is a ubiquitous phenomenon, having its origin in the rate of analyte diffusion across a membrane. In some cases, hysteresis is so pronounced that the sensor reversibility is jeopardized.

(d) *Interferences*: Wavelength interference and chemical contamination are major sources of measurement bias. To avoid wavelength interference, simultaneous sensors with different absorbing dyes are required to allow measurements at different wavelengths. For deeply colored solutions a reflectance measurement may be desired. Chemical interference occurs if an indicator reacts with a contaminant, such as metal ion, to

produce other species. Thus, a careful selection of indicators is needed to avoid interference. Temperature and ionic strength are important factors, as they affect the p*K*a of the transducer dye. Interference bias caused by ionic strength changes in the analyte solution is an important issue in optical sensors, and is often not appropriately dealt with.

1.4 Measuring Acidity: an Overview

1.4.1 Dilute Acid and Base Solutions - *Using Potentiometric pH as Standard*

Brønsted first proposed in the early 1920's the definition of acids and bases in terms of proton transfer equilibria. According to his definition, the ionization in water of an acid HA and a base B can be written as:

$$HA + H_2O = A^- + H_3O^+ \qquad \text{(Eq. 1.2)}$$

$$B + H_3O^+ = BH^+ + H_2O \qquad \text{(Eq. 1.3)}$$

The extent of ionization of acids and bases in water directly depends on the activity of H_3O^+ ions in solution, denoted by $\{H^+\}$, via the equilibrium constants for Eqs. 1.2 and 1.3. The acidity of a dilute aqueous solution reflects the activity of hydrogen ions in such solution. However, due to thermodynamic restrictions, the activity of individual species cannot be measured experimentally.[8] The acidity scale was thus created based on a conventional standard, i.e., the potentiometric measurement of a hydrogen cell.

$$Pt|H_{2(g)}|\text{acid solution} \,||\, KCl_{(aq)}|AgCl|Ag$$

For convenience, H^+-sensitive glass electrodes are normally used instead of the standard hydrogen gas cell. The pH of an unknown solution can be measured by comparison to a well-defined standard (indicated by the superscript 0) by the following formula (Eq. 1.4).

$$pH = pH^0 + \frac{2.304\,F}{RT}(E - E^0) \qquad \text{(Eq. 1.4)}$$

where pH^0 is the pH of a standard solution, and E and E^0 are the electromotive forces of the hydrogen cell for an unknown and a standard solution, respectively.

As a consequence, pH cannot be independently measured, and the equality $pH = -\log\{H^+\}$ cannot be definitely established. The reference buffer solutions for the measurement of pH are defined by the National Bureau of Standards.[9]

1.4.2 Concentrated Acid and Base Solutions - *The Establishment of Acidity and Basicity Functions*

pH as a useful measure of acidity breaks down for concentrated solutions with ionic strength greater than 0.1 M. Other quantitative scales are needed to express the acidity (or basicity) in the more concentrated solutions. The work of Hammett and Deyrup of Columbia University during the early 1930's provided a quantitative scale.[10,11] In concentrated acid, for example, Hammett and Deyrup suggested a convenient measure of acidity by the spectrophotometric determination of the extent of protonation of weak basic indicators in acid solution (Eq. 1.5).

$$B + H^+ = BH^+ \qquad \text{(Eq. 1.5)}$$

In dilute acid solutions, the protonation of B will be related to pH by the equilibrium:

$$K_{BH^+} = \frac{\{H^+\}\cdot\{B\}}{\{BH^+\}} = \frac{\{H^+\}\cdot[B]}{[BH^+]}\cdot\frac{f_B}{f_{BH^+}} \qquad \text{(Eq. 1.6)}$$

$$pH = pK_{BH^+} - \log\left(\frac{[BH^+]}{[B]}\right) + \log\left(\frac{f_B}{f_{BH^+}}\right) \qquad \text{(Eq. 1.7)}$$

where [S] is the molar concentration of a chemical species S, and {S} is its activity; f_S is the activity coefficient for species S, defined by the expression $\{S\} = f_S[S]$.

At low ionic strength, f_B approaches unity, and f_{BH^+} can be calculated using the Hückel-Debye approximation. However, in concentrated solutions with ionic strength over 0.1 M, f_B deviates from unity by over 25%, and this approach will produce large errors. The Hammett acidity function, H_0, as defined in Eq. 1.8, was introduced as a quantitative measurement of acidity in concentrated solutions.

$$H_0 = pK_{BH^+} - \log\left(\frac{[BH^+]}{[B]}\right) = -\log\left(\frac{\{H^+\}\cdot f_B}{f_{BH^+}}\right) \qquad \text{(Eq. 1.8)}$$

H_0 is independent of the bases (indicators) used to measure it, provided that (f_B/f_{BH}^+) is identical for all bases in the same acid solution. Bases (indicators) with similar structures usually have close ratios f_B/f_{BH}^+, but deviations often occur if bases with different structures are used.

At low ionic strengths, H_0 approaches pH, and is identical to pH at infinite dilution. For pure water, H_0 = pH = 7.00 at 25 °C and 1 atm, and for solutions of increasing acidity H_0 decreases.

In the acidity function defined in Eq. 1.8, the ionization ratio ([BH^+]/[B]) is usually measured spectrophotometrically. The pK_{BH}^+ is derived from the plot of ([BH^+]/[B]) as a function of acid concentration. At infinite dilution, all activity coefficients approach unity, and Eq. 1.8 becomes Eq. 1.9. Thus, extrapolating the function defined by Eq. 1.8 to [H^+] = 0 will give pK_{BH}^+, the thermodynamic dissociation constant that refers to the pure solvent as a standard state.

$$pK_{BH^+} = \log\left(\frac{[BH^+]}{[B]}\right) - \log[H^+] \qquad \text{(Eq. 1.9)}$$

When the acidity function concept was first introduced, it was hoped that there would be a unique H_0 function, applicable to a specific acid, which would be independent of the bases used to measure it. This acidity function would be the universal standard for this specific acid. The condition for such universal standard acidity function is that the ratio f_B/f_{BH}^+ (Eq. 1.8) are the same for all neutral bases. It is recognized now that this

condition is seldom satisfied, and structurally diverse bases give (f_B/f_{BH}^+) ratios that differ from that of the primary amine series used by Hammett.[8]

In the case of basicity functions, usually denoted by $H_$, the indicators used are neutral acids before deprotonation in concentrated hydroxide and negatively charged afterwards.[8]

1.5 Overview of this Dissertation

The objective of the work described in this dissertation is to develop optical sensors for the determination of concentrated strong acids and concentrated strong bases, both important bulk feedstocks in the chemical industry. We opted to build our sensor elements using chemically stable absorbing dyes that are immobilized in a porous metal-oxide membrane. The preparation of the optical sensors for concentrated strong acids is described in Chapter 2. A SiO_2 membrane doped with low p*K*a dyes has been developed and used to continuously monitor HCl without re-calibration for at least nine months. The response time is very fast (< 2 s) and the sensor can be used in some organic media.

Sensors for the measurement of concentrated hydroxides are described in Chapter 3. Our sensor element consists of high p*K*a indicators immobilized in a composite membrane (organic polymer/metal-oxide phase). Our sensor elements are chemically and mechanically stable in the very harsh alkali environment, and allow a fast and reversible response.

Chapter 4 describes a dual-transducer procedure that can be used to correct measurement bias caused by the presence of large amounts of salts in acid solutions.

Finally, in Chapter 5, our studies of sensor hysteresis are reported, and the connection between response time and hysteresis is presented. Response hysteresis was found to be the major component of the analytical error for our optical sensors.

1.6 The Equipment Used in the Current Study

Visible spectra were recorded either by a Hewlett-Packard HP 8452A diode array spectrometer with a deuterium light source and 1.0 cm quartz cells or by a portable diode array spectrometer described below.

A scheme of the fiber-optic sensor system used in our work is shown in Figure 1.3. This system provides a low-cost and portable spectrometer suitable for field sensor applications. A single array portable spectrometer (Rainbow Meter system) by American Holographic Inc. (Fitchburg, MA 01420) was used. This dual-beam spectrometer contains a single silicon diode array of 128 channels. The collection of light from the reference and sample cells is simultaneous, each using 64 of the 128 channels. The spectrometer itself consists of an integrated opto-electronic device ($6.5 \times 6.5 \times 14$ cm^3) and a standard RS-232 host interface box ($13 \times 4 \times 18$ cm^3). The light source for this spectrometer is a xenon flashlamp (EG&G LS-1102-5 FlashPac; maximum output energy per flash: 360 mJ; maximum flash rate: 55 Hz; dimensions: $3 \times 8.5 \times 18$ cm^3). The bifurcated fiber-optic bundle, after passing through a fiber bundle coupler (to adjust light intensity), was split into two source fiber bundles. These source fiber bundles were then placed into cylindrical Pyrex glass tubes, which were exposed to the sample solutions in the spectrometer cells. The ends of the detector fiber bundles were also placed in similar Pyrex glass tubes. The glass tubes (diameter = 0.8 cm) were firmly held in the cells.

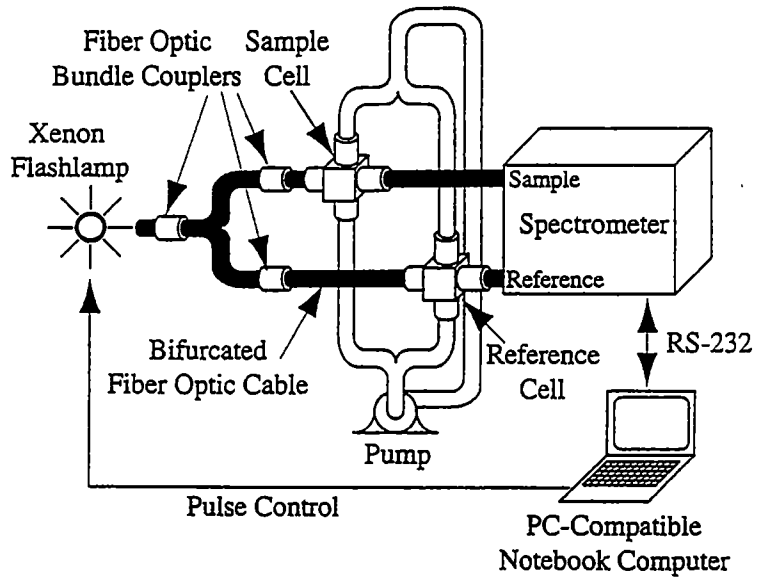

Figure 1.3. Schematic of the optical flow system.

Two types of Teflon cells were designed, and each type consisted of a sample cell and a reference cell. In the first type (Figure 1.4a), the sensor films were coated on removable Pyrex glass slides (width = 1.1 cm) which were placed between the ends of the glass tubes. The glass slides were placed in a Teflon cell, leaving a 0.7 mm space along the optical path for contact with the flowing liquid sample. In the second type (Figure 1.4b), the sensor films were directly coated on the Pyrex glass tubes that were fixed in the cells.

For all studies reported in Chapters 2 – 5, the set up in Figure 1.4a was used. This set up allows quick replacement of the glass sensor slides in the optical cells, without disturbing the optical configuration. In comparison, replacing the sensors coated on the end of the glass tubes in Figure 1.4b cells requires the disassembly of these optical cells, which disturbs the optical configuration.

For concentrated acid monitoring, a flow system was used. Through Teflon tubing, the spectroscopic cells were connected to an acid reservoir and a diaphragmatic pump to form an acid flow system. The acid solutions were pumped into the sample and reference acid cells, each having a volume of 5.5 mL, at a rate of 45 mL/min.

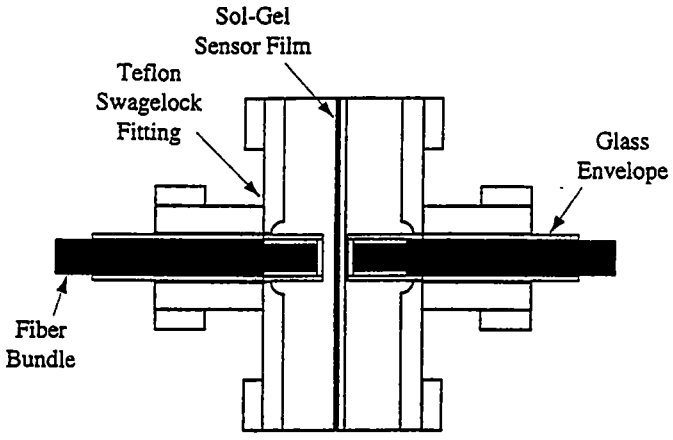

(a)

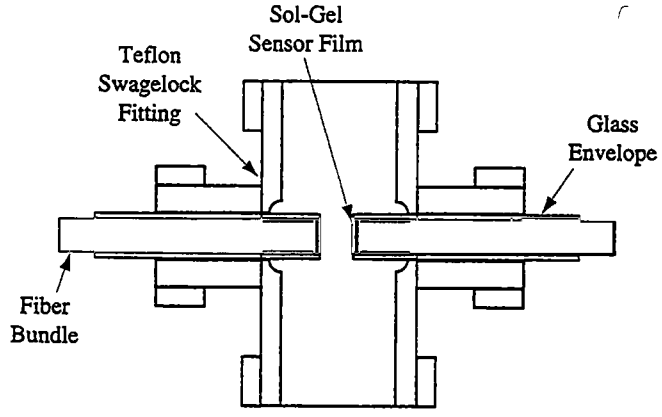

(b)

Figure 1.4. Schematic of the optical cells. In (a), the sensor element is a sol-gel coated glass slide, which can be easily removed from and placed in the optical cell. In (b), the sensor element consists of a sol-gel film directly coated onto the surface of one of the optical windows. The sensor element in (b) is thus fixed in the optical cell.

CHAPTER 2

Optical Sensors for High Acidity Determination

2.1 Introduction

Sensor systems designed to monitor high acidity continue to represent a challenge for chemists and engineers. Concentrated strong acids such as HCl, HNO_3, and H_2SO_4 are among the largest volume chemicals manufactured in the world, and are of major industrial importance.[12a-c,13a-c] They are widely used in many industrial processes such as the production of basic chemicals, steel, copper, fertilizers, pharmaceuticals, gasoline, synthetic fibers, plastics, electronic chips (e.g., GaAs[14]), batteries, and pesticides.[12a-c] In the U.S. alone, the annual consumption of HCl, HNO_3, and H_2SO_4 is ca. 6, 7, and 40 million tons, respectively. The commercial value of these acids exceeds $6 billion. However, rapid and reliable methods for their on-line determination and quality control are limited, mainly because of the harsh and corrosive nature of these acids and their high concentrations.[2c,12a-c,15,16] Classical off-line titration still forms the basis for acid content determination, and is one of the primary methods in many industrial processes.[12a-c] In such a traditional approach, a fixed volume of an acid solution is removed from the system and titrated with a base. Off-line titrations are generally time-consuming and labor-intensive, and thus costly. Lack of on-line sensing and monitoring often leads to waste of chemicals and poor quality control. Another challenge to the development of on-line acid sensors is the presence of other chemicals in industrial processes. Chemicals

such as $FeCl_n$ (n = 2, 3) in pickling HCl solutions will change the activities of acids,[17] complicating the measurement by introducing interference bias.

There is an urgent need to develop sensors for on-line monitoring of concentrated strong acids and the measurement of their acidity. The need for on-line analysis and new sensor materials was identified as one of the enabling technologies in *Technology Vision 2020: The U.S. Chemical Industry,* a task force report on the U.S. chemical industry's future growth and competitive advantage,[18a] and by the *Committee on New Sensor Technologies: Materials and Applications* appointed by the National Research Council.[18b]

2.1.1 Previous Research on Sensors for High Acidity Measurement

Electrochemical[15,19,20] and optical sensors developed for low acidity measurement in the pH range (pH > 1) do not perform adequately for high acidity (pH < 1) measurements, as severe deviations usually occur. In addition, the harsh and corrosive environments of these concentrated acids put severe limitations on the type of materials that could be used to construct sensors and their durability. Alternatives such as pre-dilution flow injection analysis (FIA) sampling techniques have been studied.[21] Optical sensors for high acidity based on fluorescent organic polymers and polymers doped with acid indicators have been reported, and efforts have been made to improve their stability, precision, and response time.[22] Another sensor was developed based on a Nafion cation-exchange membrane that allows acid from an external HNO_3 sample to reach a steady-state diffusion into an internal chamber containing a flowing reagent solution.[23] Several factors were found to influence the diffusion rate of acid, thus limiting the reliability of this system in industrial solutions. Recently, in an effort to reduce the annual acid cost of

millions of dollars in petroleum alkylation in a mid-sized oil refinery, a method was developed to monitor 89 – 91% H_2SO_4 based on its density measurement.[24] However, the this approach is currently limited to petroleum alkylation processing. As noted by the authors, this approach based on density measurements is possible in this process because the hydrocarbon concentration in the acid stream is kept reliably constant.

2.1.2 Our Approach to Acid Sensors

Our approach to optical sensors for high acidity measurement utilizes porous SiO_2 as the interface material. SiO_2 sol-gel has high optical transparency and chemical resistance to acid.[25] Furthermore, little or no heating is required in the sol-gel process and consequently the gel can be doped with thermally sensitive molecules.[26] Sol-gel approaches to sensors are of intense current interest. A chemical or enzyme is either physically encapsulated in or chemically bonded to silica, forming a transducer sensitive to pH, oxygen, or specific metabolites.[26]

Our approach to fast, highly sensitive, and durable sensors for the concentrated strong acids is based on porous SiO_2 films doped with an organic dye with low p*K*a. Upon exposure to a concentrated acid solution, H^+ ions diffuse into the porous SiO_2 film and react with the dye. Dye spectral changes are correlated to acid concentration, and monitored spectroscopically. A key issue to our approach is the porosity of the SiO_2 matrix. The pore size distribution is adjusted to be small enough to prevent severe indicator leaching and yet large enough to allow fast and reversible diffusion of the analyte to/from the SiO_2 matrix. There are several unique features and potential benefits associated with this approach to high acidity sensors:

(a) SiO_2 matrix is chemically and mechanically stable in extremely acidic environments. A mechanically stable film does not swell, peel off, or break apart in the analyte environment. In comparison, swelling is common for organic polymer hosts.

(b) Sol-gel SiO_2 possesses excellent optical transparency in the visible and near infrared region.

(c) The indicators are encapsulated in hydrophilic SiO_2 networks. In contrast, previous work on optical acid sensors was based on fluorescent or dye-doped hydrophobic organic polymers.[22] Hydrophilic SiO_2 materials interact with aqueous solutions intrinsically faster than hydrophobic organic polymers. Fast diffusion of H^+ ions is essential for a reversible operation with low hysteresis.

(d) Encapsulation of more than one indicator in sol-gel is possible as one approach for multi-transducer sensors. Multiple transducers are needed in many industrial systems where the presence of other chemicals changes the activity of acids and needs to be accounted for.

(e) The manufacturing of sol-gel sensors for high acidity monitoring is relatively inexpensive. This, coupled with the recently commercially available portable visible spectrometers (< $2,000[27]), makes the development of a low-cost fiber-optical sensor system possible.

The hydrophilic nature of inorganic silica sol-gels and their chemical stability in harsh highly acidic media make them attractive as matrices for sensors in aqueous strong acids. We describe here a durable acid sensor prepared using sol-gel methods for on-line high acidity measurements in a wide range ($[H^+]$ = 1 - 11 M). The stability, durability,

response time, and precision of the sensor system have been studied for the measurement of the concentrated strong acids.

2.2 Experimental Section

Spectroscopic measurements were conducted with the portable fiber optic system described in Chapter 1 (Figure 1.3) and by a standard HP 8452 diode array spectrometer using a 1.00 cm quartz cell. Acid solutions were standardized by titration with NaOH to the phenolphthalein end point. All chemicals (Aldrich, Sigma, and Mallinckodt) were used as received.

The sensors were prepared by casting the surface of either Pyrex glass slides or tube ends with sol-gel solutions *via* a spin coating process (1650 rpm). Prior to casting, the Pyrex glass surfaces were roughened and washed with KOH - 2-propanol solution. The surfaces were then rinsed with water, acetone, propanol, and methanol. The glass slides were mounted in a quartz cuvette with 1.0 cm optical path, and transmittance measurements were taken using a regular glass slide without any coating as a blank. Blank glass slides that were coated with sol-gel films without indicators were found to give results identical to those of a glass slide without any coating.

2.2.1 Preparation of the Sol-Gel Sensor Films - Acid as a Catalyst (Sensors 1 – 5)

Sensor 1: $Si(OMe)_4$ (200 μL), Bromocresol Purple (7 mg), HCl solution (0.01 M, 36 μL), methanol (180 μL), and CTAB (4.0 mg) were mixed and stirred together in a glass vial for 30 min to form a clear solution. The solution was then coated onto a glass surface *via* a spin coating process (1650 rpm). No more than 10 s of spinning was needed

for the sol-gel to produce a thin and viscous film. The sol-gel film was first dried in air for 3 days and then heated at 41 °C for 14 days in an oven.

Sensor 2: $Si(OMe)_4$ (200 μL), Bromocresol Purple (60 mg), HCl solution (0.01 M, 17 μL), H_2O (60 μL), methanol (130 μL), and CTAB (cetyltrimethylammonium bromide, a surfactant, 4.0 mg) were mixed and stirred together in a glass vial for 50 min to form a clear solution. The solution was then coated onto a glass surface *via* the spin coating process (1650 rpm) and gelled similarly as in the preparation of Sensor 1.

Sensors 3 – 5: They were prepared by procedures similar to that used in the preparation of Sensor 2 except that 6 mg of Fastgreen FCF, 55 mg of Bromocresol Green, and 12 mg of Acid Blue 147 (instead of BCP) were used to give Sensors 3 - 5, respectively.

2.2.2 Preparation of Sol-Gel Sensor Films - Base as a Catalyst (Sensor 6)

$Si(OMe)_4$ (200 μL), Bromocresol Purple (7 mg), NaOH solution (0.001 M, 36 μL), methanol (180 μL), and CTAB (4.0 mg) were mixed and stirred together in a glass vial for 30 min to give a clear solution. The solution was then coated onto a glass surface *via* the spin coating process (1650 rpm) and gelled as in the preparation of Sensors 1 - 2. The sol-gel film was first dried in air for 4 days and heated at 37 °C for 3 days in an oven.

2.2.3 Conditioning of the Films

The sensor films were pre-treated by first placing them in water for two days or until no appreciable leaching of the dyes was observed. The films were subsequently placed in concentrated HCl (ca. 18 h) until no further leaching of the dyes was detected spectrometrically.

2.3 Results and Discussion

2.3.1 The Sol-Gel Process and Doping of Indicators

The sol-gel process, first reported some 150 years ago, is attracting renewed interest for optical sensor applications.[28-30] The sol-gel process refers to a multitude of reactions which employ a wide variety of alkoxide precursors to prepare different products and has been applied most often to the production of glasses and ceramic oxides.[22] Typically, the sol-gel process involves a metal alkoxide such as $Si(OR)_4$, water, and a second solvent which acts as a porogen and miscibility agent. The particles that develop in the colloidal sol crosslink to form a gel which is subsequently dried to form a three-dimensional porous glass. Figure 2.1 illustrates the sol-gel reactions.

In sol-gel solutions, the rate, extent, and even the mechanisms of the reactions are profoundly affected and may be systematically influenced by many factors, such as the size of the alkoxide ligand on silicon, the solution pH, the types and concentrations of solvents, the temperature, and the presence of catalysts.[22] Each factor can affect the course of structure development and subsequent properties of the gel and the materials produced. Therefore, a multitude of variables may be adjusted to influence and tailor the structure and properties of sol-gel derived materials. Furthermore, little or no heating is required in the sol-gel process and consequently the gel can be doped with thermally sensitive molecules such as organic dyes, which would normally be precluded from incorporation into traditional inorganic hosts. Doping of sol-gel materials with organic and biological molecules has been widely studied and has shown interesting and unique properties. This technique has been used in a wide range of optical sensing applications.[21,23,24] Molecules or receptors are entrapped, and yet found accessible to

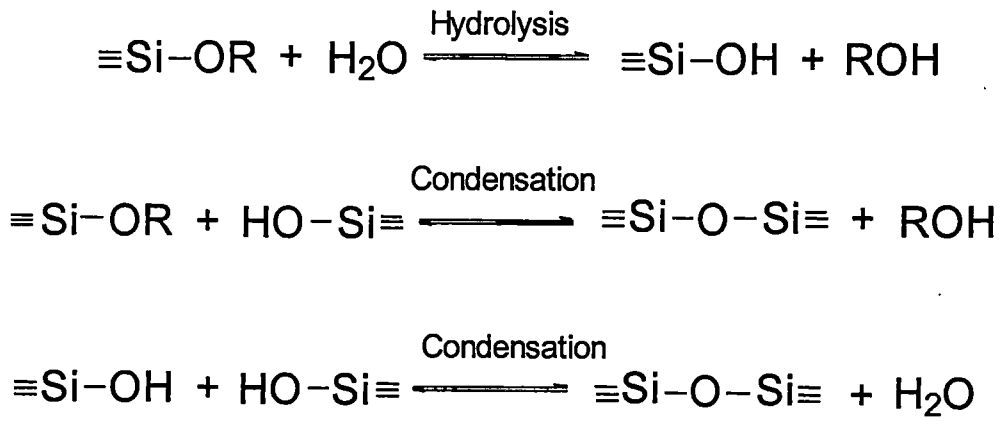

Figure 2.1. The reactions in the sol-gel process.

external reagents or analytes through the porous sol-gel network.[32,33]

Since the organic dyes used in the current project have been successfully doped in sol-gel matrices as pH sensors for low acidity solutions,[25,26] and these pH sensors are not designed for high-acidity systems, we thus have focused our attention on developing sol-gel processes that would produce stable and durable sensors for highly acidic solutions. In our approach, an organic dye is dissolved in an alcohol-containing sol-gel solution, allowing a homogeneous incorporation of the indicator in the final porous silica matrix. No micro-segregation was observed even when saturated alcoholic solutions of Bromocresol Purple (BCP) were used in the preparation. This process can be either acid- or base-catalyzed, and both catalysts were used to prepare the sensor films. Figure 2.2 shows the process of sensor preparation.

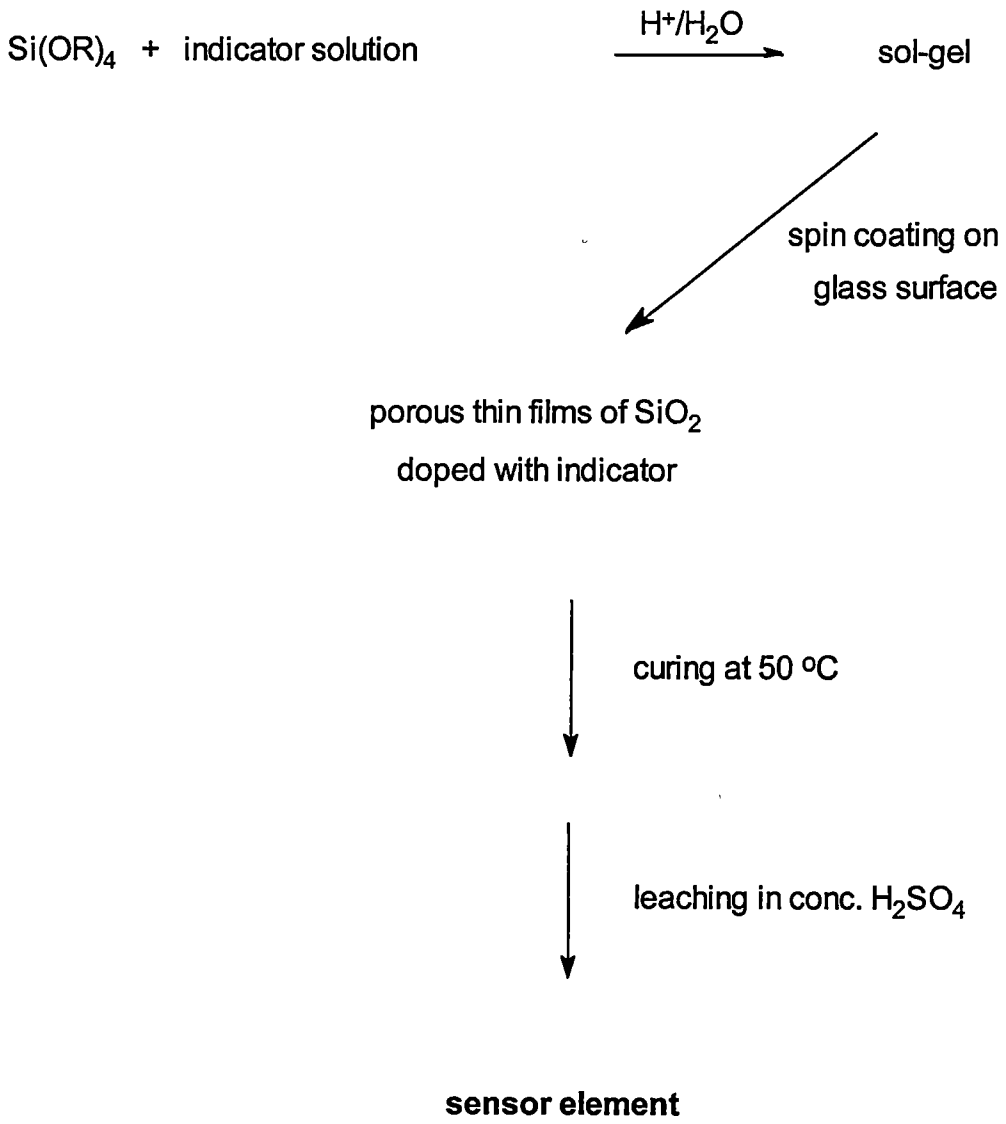

Figure 2.2. A generic sol-gel sensor preparation procedure.

2.3.2 The Indicator[34,35]

For acidities ranging from 1 to 11 M of [H^+], HCl solutions of several indicators were tested. Bromocresol Purple (BCP), Bromothymol Blue (BTB) and Chromazurol S (CAS) showed larger sensitivities in this concentration range. However, BTB was found to be not stable in highly acidic solutions. It faded in a few days after being exposed to concentrated HCl. CAS, on the other hand, was found to be chemically stable in concentrated HCl. However, CAS is a metallochromic indicator,[34a] and thus its use is limited to metal-free solutions. Other indicators used to prepare sensors include: Fast Green CFC (Sensor 3), Bromocresol Green (Sensor 4), Acid Blue 147 (Sensor 5), Ethyl Violet, Neutral Red, Xylene Cyanol FF, Methylene Violet, Night Blue, Victoria Blue, Brilliant Green, and Methylene Green Hue.

Bromocresol Purple, a member of the sulfonephthalein dyes, is chemically stable in concentrated HCl and H_2SO_4, and more resistant to oxidation than many other indicators.[34b] Like all other sulfonephthalein indicators, it has three different protonated forms, as shown in the equilibria in Figure 2.3.[36] The phenoxide form (III) predominates in basic conditions, whereas the anionic form (II) is favored in low acid concentrations. These two forms are responsible for the color change in the pH range ($pKa_2 = 6.3$).[36] BCP has thus been studied as an indicator in pH sensors for low acidity systems.[25a-b,26a] Form (II) is converted to the zwitterionic form (I) in highly acidic solutions, producing a color change from yellow to red. Two sets of pKa_1 values have been reported: -2.13 on the Hammett acidity scale[10,11] [$p(C_{acid}) = -0.75$, using the Sorensen pH scale] reported by Gupta and Reed,[36] and -2.00 on the Hammett acidity scale reported by Aragoni and coworkers[37] based on the data in ref. 11. We have found that this color change from

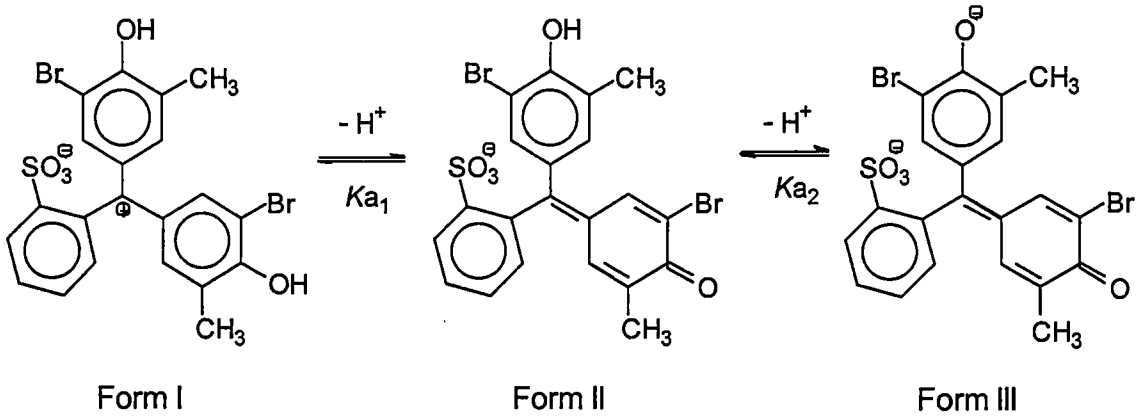

Figure 2.3. Equilibria of the three protonated forms of Bromocresol Purple.

II to I, which could be monitored spectrometrically, fits the acidity range studied.

The pKa$_1$ (sol-gel) of BCP in the sol-gel films was determined. From the [H^+]-dependent absorption spectra (Figure 2.4) of the indicator doped in the sol-gel in HCl solutions between 0.987 and 10.78 M, the absorption changes (ΔA) were found to be 0.138 and 0.284 for the anionic form (II) at 428 nm and zwitterionic form (I) at 530 nm, respectively. The absorbances at 428 nm were scaled to those at 530 nm to eliminate the extinction coefficient difference between the two forms, and the distribution curves for the first ionization of BCP are plotted in Figure 2.5. The two curves intersect at [H^+] = 5.83 M, which gives a pKa$_1$ (sol-gel) value of -0.77 ± 0.02 (-2.06 ± 0.08 on the Hammett acidity scale[11]) for BCP encapsulated in the sol-gel matrices. These values are within the

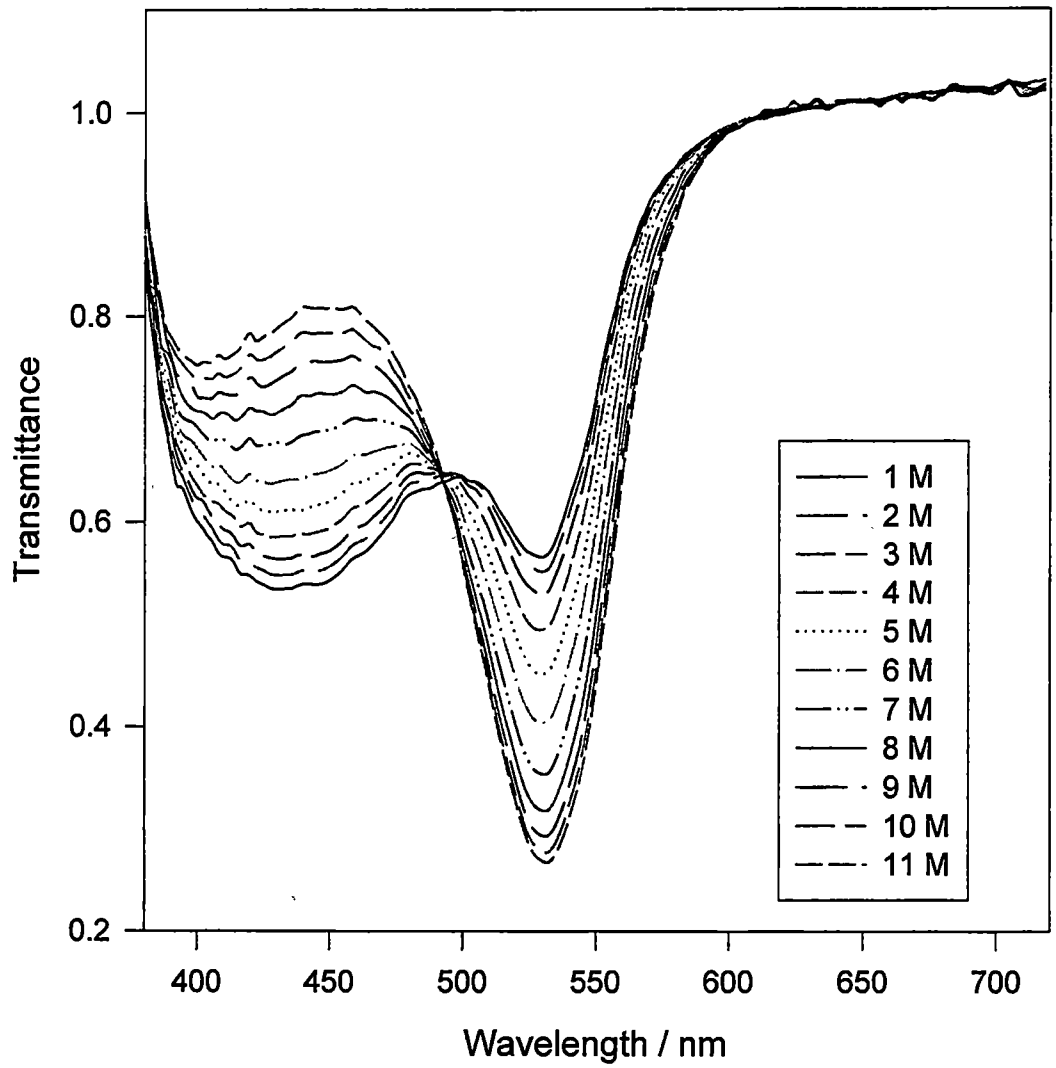

Figure 2.4. Typical spectra of Bromocresol Purple-doped Sensor 2 in HCl solutions.

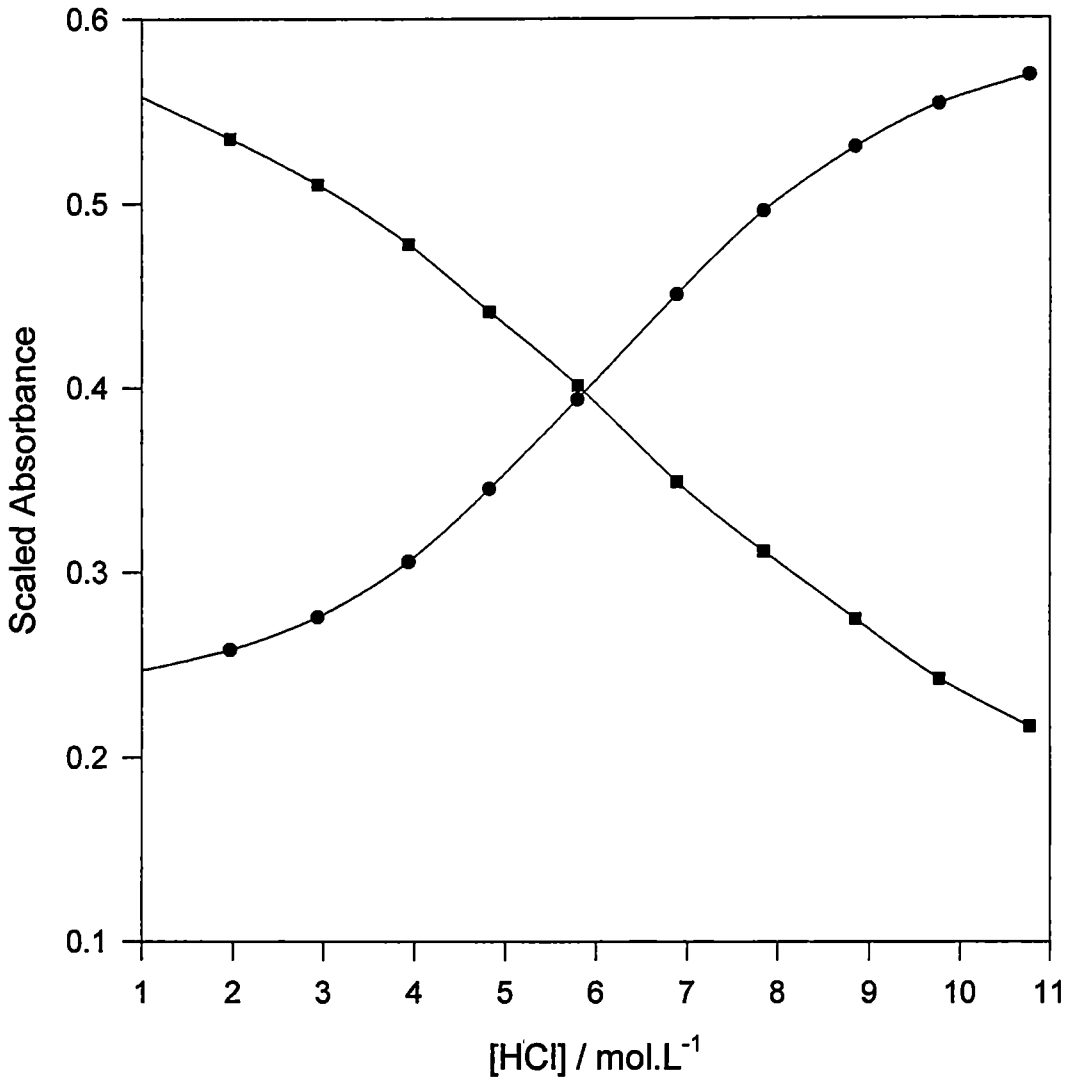

Figure 2.5. Distribution curves for the first ionization of BCP doped in a sol-gel thin film. The curves were fitted by a five degree polynomial.

two pKa_1 values reported earlier for dissolved BCP in HCl solutions.[36,37]

2.3.3 Effects of Reagents, Catalysts, and Gelling Temperatures on the Sol-Gel Sensor Films

Small variations in the catalyst or reagent ratios were found to have profound effects on the morphology of SiO_2 matrix, leading to either slow response time or dye leaching. It is very important to control the silicate synthesis to achieve the desirable fast kinetics and minimal indicator loss.

The catalysts in the sol-gel synthesis are perhaps the most important parameters on the sensor morphology and properties. The sol-gel films prepared by the acid- and base-catalyzed reactions were found to have distinctive surface morphology, response time and robustness. Their scanning electron micrographs (SEM) are shown in Figure 2.6. The SEM of a base-catalyzed sol-gel film (Figure 2.6a) shows a network of spherical particles packed together (diameter = 1.2 ± 0.4 μm), suggesting that the polymerization processes occur by the initial formation of colloidal silica globules followed by their aggregation. In contrast, the SEM of an acid-catalyzed sol-gel film (Figure 2.6b) reveals a much smoother surface. Our observations are in agreement with what has been reported in the literature.[26,28a] In the base-catalyzed sol-gel formation, hydrolysis is slower than condensation, and highly condensed and rather large particulate sols grow and aggregate to form the SiO_2 network. In contrast, the acid-catalyzed reactions promote hydrolysis, giving denser structures with small particulate sols that form polymeric backbones and branches.[26,28a] These structure differences greatly affect the H^+ diffusion rate in the sol-gel films and the cohesiveness of the films on substrates. Despite relatively faster

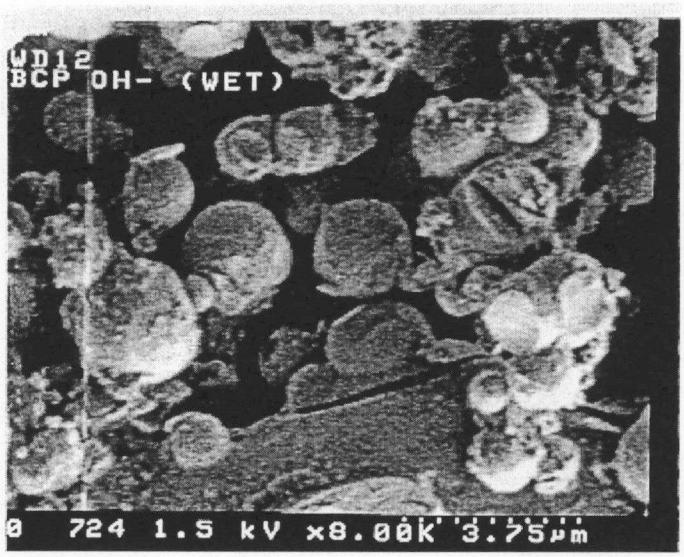

(a)

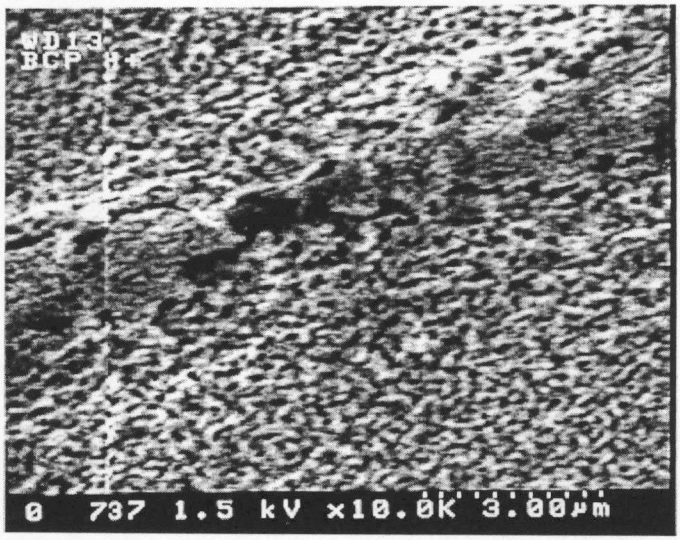

(b)

Figure 2.6. Scanning electron micrographs (SEM) of the sensors films: (a) base-catalyzed Sensor 6; (b) acid-catalyzed Sensor 2.

diffusion, base-catalyzed sol-gel films were more susceptible to degradation and indicator leaching than acid-catalyzed films.

$Si(OMe)_4$ was preferred for its faster hydrolysis rate in comparison with other silicon alkoxides;[28a] it reaches the gel-point considerably faster than other alkoxides. The ratios of $Si(OMe)_4$, MeOH, and H_2O were found to have an important effect on the viscosity and physical properties of the final sol-gel mixtures. A lower content of $Si(OMe)_4$ produced a sol-gel with low viscosity. Consequently the cast films were too thin, and the amount of the doped indicator confined to the short optical path was too small to produce a significant spectroscopic response. On the other hand, if the content of $Si(OMe)_4$ was large, the sol-gel mixture produced a more viscous solution. Thicker films were thus casted, giving a large but very slow spectroscopic response (*vide infra*). Therefore a careful selection of the ratios of $Si(OMe)_4$, MeOH, and H_2O is important to the quality of the sensor films.

The pre-treatment of the thin films by first placing them in water for two days and then in concentrated HCl (ca. 18 h) was found to be sufficient to stabilize the films and gave no spectrometrically observable leaching afterwards. We think that, in this pre-treatment process, indicator molecules entrapped in sol-gel voids of relatively large sizes may diffuse into the solution, leaving behind the indicator molecules entrapped in relatively small voids. The indicator molecules that remained in the sol-gel films after the pre-treatment did not readily leach out, thus providing stable sensor films.

The base-catalyzed sol-gel films were found to be more susceptible to degradation and leaching of indicators than acid-catalyzed films in the pre-treatment process. Total amount of indicator loss due to leaching in acid was 16% for the acid-catalyzed films

compared with 76% loss for the base-catalyzed films in the pre-treatment period. The long-term stability of these films in highly acidic media was also evaluated (*vide infra*).

The sol-gel films discussed to this point were prepared at a gelling temperature of 37 °C or 41 °C, as described in the experimental section. We also studied the gelling temperature effect on the properties of the sol-gel films. A gelling step at 200 °C for a sol-gel solution containing BCP was found to produce films of a poorer mechanical stability. The film thus prepared showed more fractures on its surface, as revealed by the SEM analysis, and a more pronounced leaching of the indicator than films prepared with a gelling step at 41 °C.

For the films of Sensor 2, which showed more promising results, their thickness was determined by profilometry measurements and found to be 2.7 ± 0.4 μm. The sol-gel films did not physically degrade even after repeated use.

2.3.4 Response of the Sensor Films in Concentrated HCl

Typical transmission spectra of Sensor 2 (Figure 2.4) in HCl solutions (2 to 10 M) show that there are two absorbance maxima at 430 and 550 nm. The longer wavelength absorption shows greater sensitivity. A well-defined isosbestic point is also observed. Sensors containing indicators with different p*K*a's show high sensitivities at different acid concentrations. Bromocresol Green (Sensor 4, spectra shown in Figure 2.7) has higher sensitivity for more concentrated HCl than BCP, whereas lower HCl concentrations can be better monitored with a Fastgreen FCF sensor (Sensor 3, spectra shown in Figure 2.8).

The response reversibility of this BCP sensor (Sensor 2) was also studied by exposing it to HCl solutions (2, 4, 6, 8, and 10 M) in both the incremental and

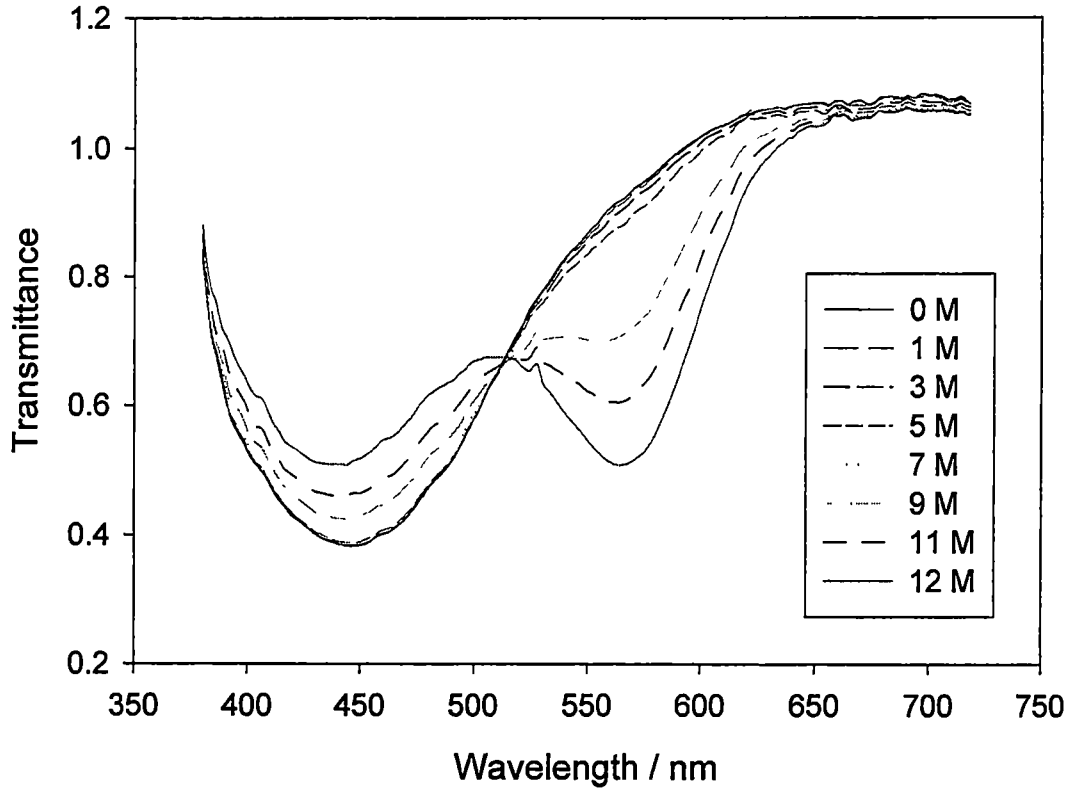

Figure 2.7. Typical spectra of Bromocresol Green-doped Sensor 4 in HCl solutions.

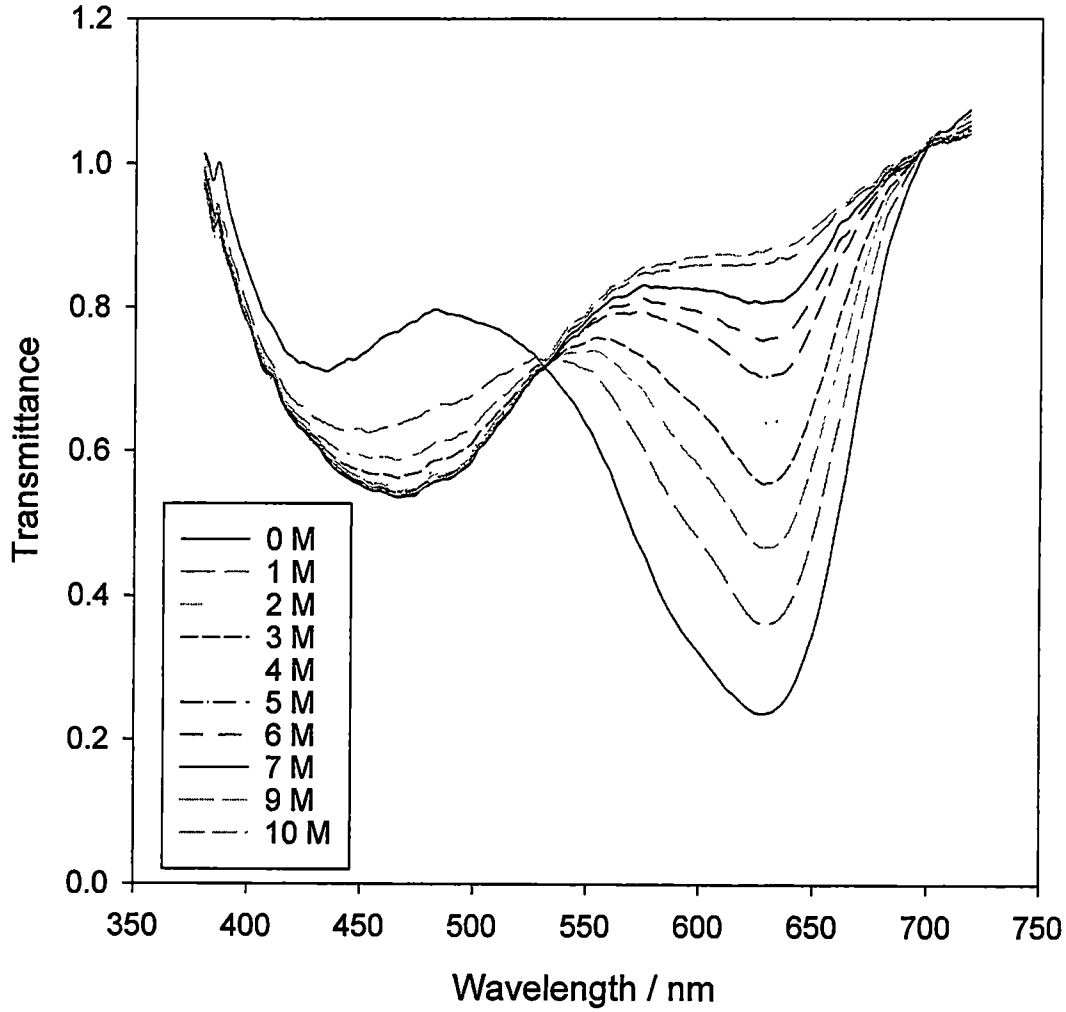

Figure 2.8. Typical spectra of Fast Green FCF-doped Sensor 3 in HCl solutions.

decremental direction (Figure 2.9). An excellent response time in both directions (1 - 5 s) was obtained, and the sensor film showed little hysteresis of response. A plot of the indicator absorbance at 530 nm vs. hydrochloric acid concentration is shown in Figure 2.10. The precision of the sensor has a relative standard deviation of less than 2.5% with respect to the total absorbance range for seven measurements at each point.

In order to compare the performance of acid- and base-catalyzed sol-gel sensors, a 12-week durability test was conducted. The results showed a progressive increase in transmittance for both sensors, which is consistent with loss of the indicator molecules due to slow leaching. However, leaching of the indicator for the base-catalyzed sol-gel films was found to be much more severe than for the acid-catalyzed films. The latter accumulated a loss of 4% of the total absorption range (at 530 nm) during a 12-week period, whereas the former showed a much greater loss, 22% (at 530 nm), of the indicator during the same period of time and under identical conditions. Therefore, we focused our efforts in developing acid-catalyzed sol-gel formulations.

2.3.5 Sensor Response under Flow Conditions

The portable optical system was coupled to a peristaltic pump, as discussed in Chapter 1. There are several potential problems in a continuous flow portable optical system. These include undesirable displacement of optical parts, entrapment of air bubbles along the optical path, deposition of particulate matter onto the sensor element, and faster chemical and mechanical degradation of the sensor films.

In our system, the entrapment of air bubbles was the only problem frequently encountered. Figure 2.11 shows the signal collection vs. time for Sensor 2,

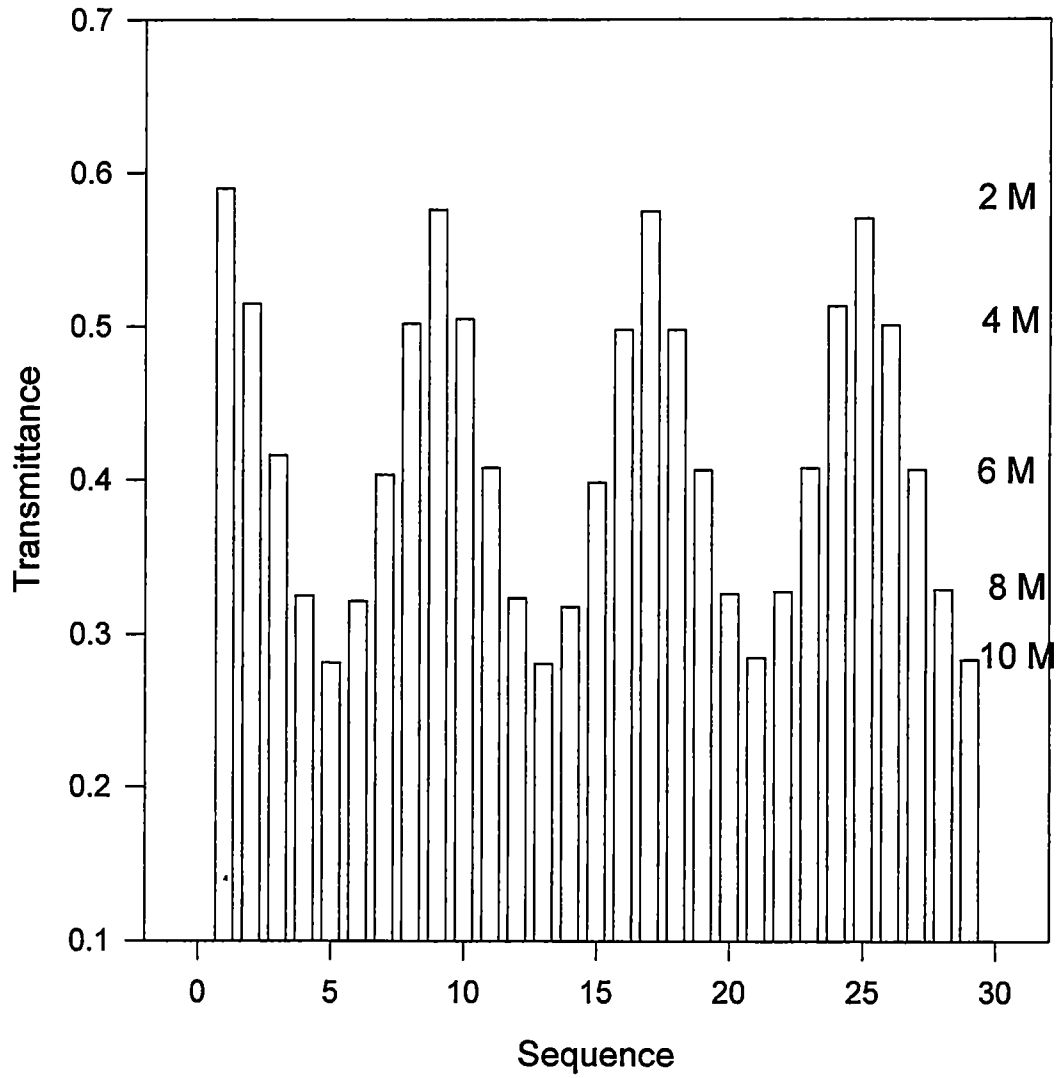

Figure 2.9. Response reversibility of Sensor 2. The averages of the response in the range of 546 – 550 nm are shown.

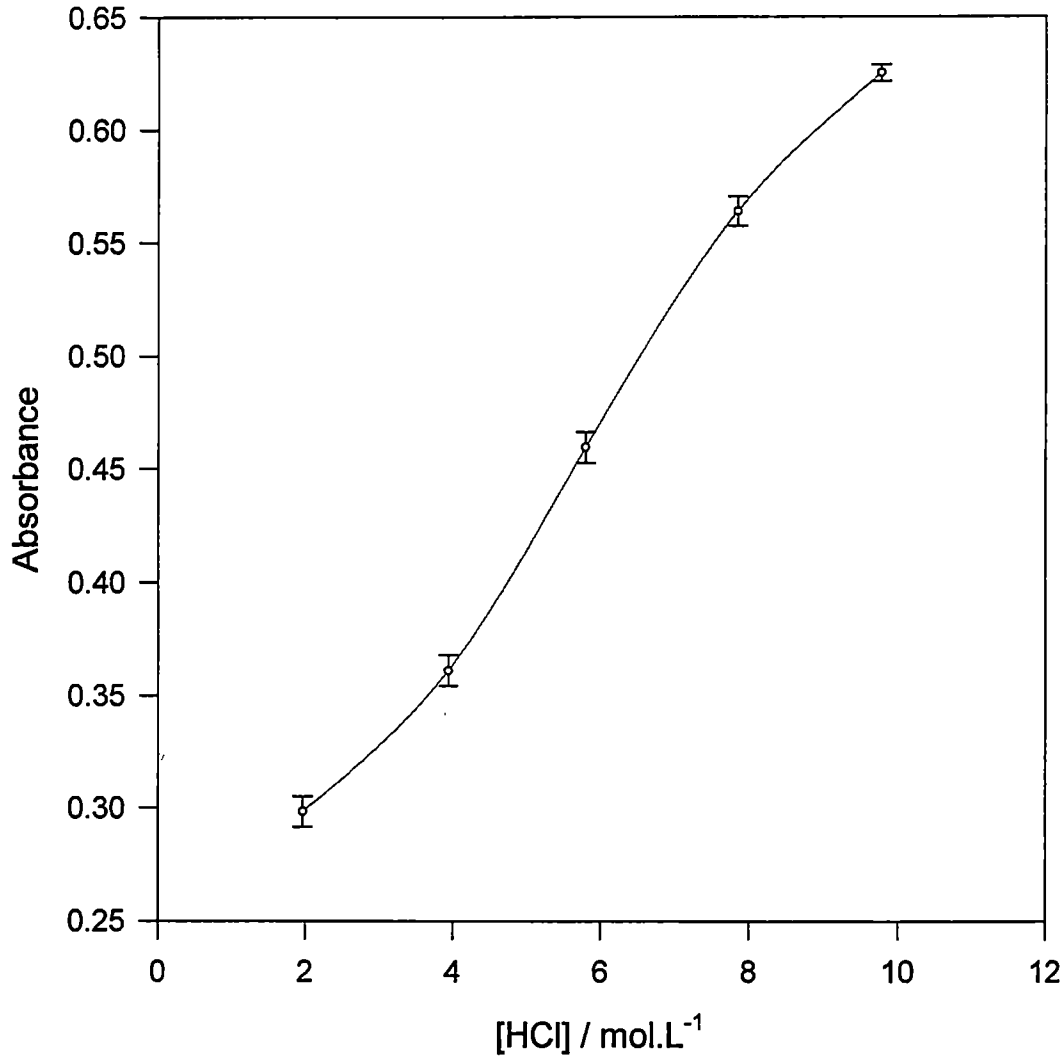

Figure 2.10. The response of BCP Sensor 2 in HCl solutions.

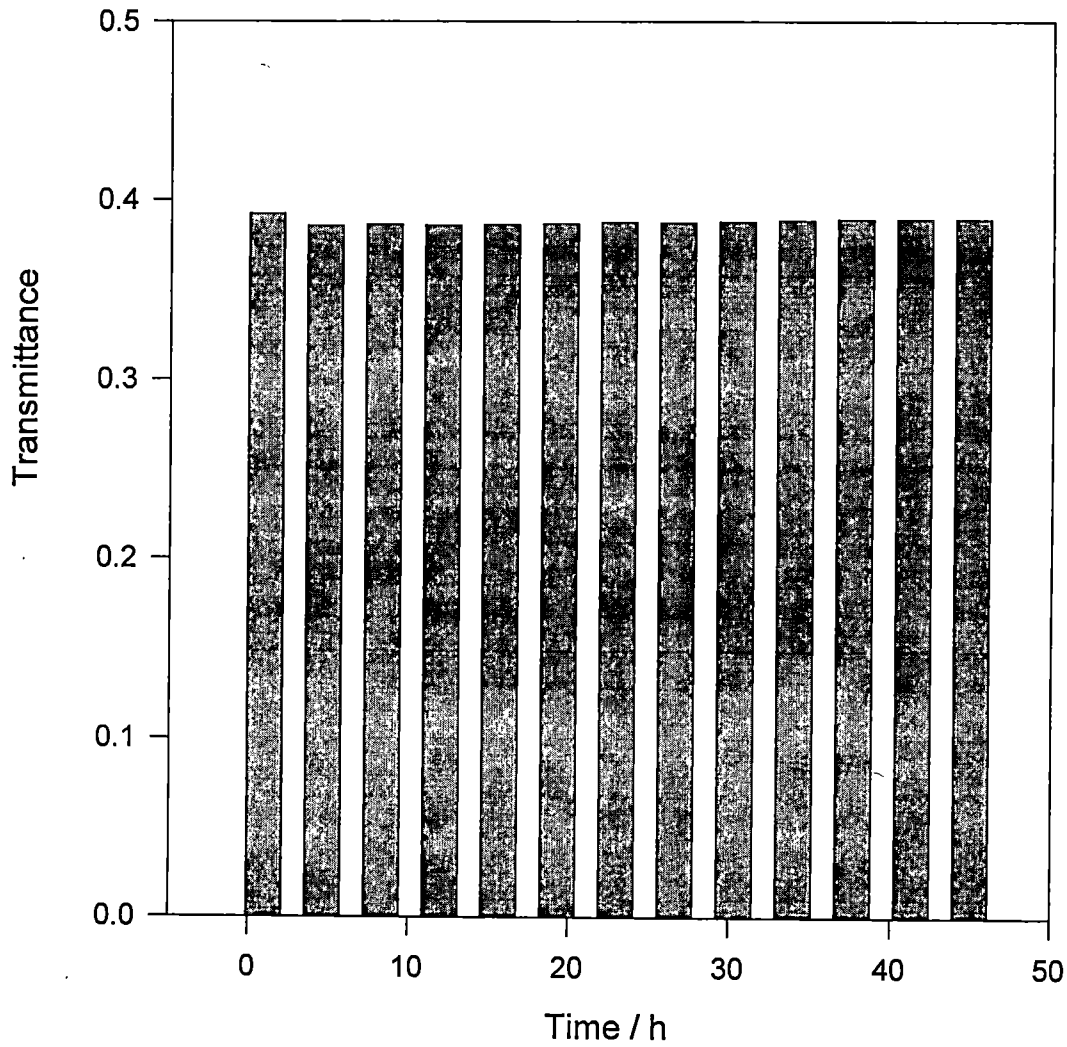

Figure 2.11. Response of Sensor 2 under a continuous flow of 8 M HCl.

subjected to 45 h of continuous flow of an 8 M HCl solution. The signal was steady, and the small variations observed being indistinguishable from the spectrometer error (± 0.0003 absorbance units).

2.3.6 Response Time and Sensor Morphology

The method to prepare Sensor 1 (Experimental Section) was used earlier in our studies, and was found to give stable acid-catalyzed sensor films. However the sensor films prepared by this method had a very slow response time (up to 300 min). On the other hand, our base-catalyzed sol-gel Sensor 6 had a much faster response time than the acid-catalyzed Sensor 1; shorter response times for base-catalyzed sol-gel sensors have also been reported in the pH region.[25a,26a] Yet the long-term stability of the base-catalyzed Sensor 6 was not ideal. The leaching of the indicator from Sensor 6 was found to be too severe to be of use in highly acidic media. These results directed us to focus on the formulation of the sol-gel reactions to preserve the stability of the acid-catalyzed films and improve their response time. This was achieved mainly by reducing the amount of the acid catalyst used in the preparation of Sensor 1 and adjusting the ratios of the reagents in the sol-gel reactions. After several tests, we found that the preparation method for Sensor 2 produced films with a very fast response time (1 - 5 s) and good stability. In comparison, the general response time of less than 1 min is required of chemical sensors.[15]

It is well known in sol-gel chemistry that the pH of the sol-gel solutions strongly influences the kinetics of the agglomeration of the sol (a colloidal suspension) and the structure of the xerogels,[26,28a] as shown in our SEM studies discussed earlier. Higher pH

conditions lead to condensed particulate sols and later highly porous particulate sols. On the other hand, lower pH processes lead to branched polymeric sols and dense xerogels with high surface area. The reduction in the amount of acid catalyst used (and thus higher pH in the sol-gel reactions) in the preparation of Sensor 2 may produce sol-gels with increased porosity and different morphology, which, in turn, increases the diffusion rate of hydronium ions. In addition to porosity increase, the reduced surface area in Sensor 2 may have changed the charge distribution on the sensor surface. Since the isoelectric point of silica sol-gel is close to pH = 2,[28b] the silanol-containing surface is vastly protonated in the highly acidic media in which our measurements were made. As a consequence, the surfaces of our sensor films were positively charged. The diffusion of species with positive charges, such as hydronium ions, through the positively charged sol-gel surface will be slower than through a neutral sol-gel surface (which exists above pH = 2).[28c] It is not clear if surface area and morphology differences between Sensor 1 and Sensor 2 lead to changes in the positively charged surface. If so, the surface charge changes may contribute to the sharp reduction in response time.

Our SiO_2-based sensors have a very fast response time (1 s) during H^+ intake, when exposed to acid. However a much slower washing of acid by deionized water from the sensor was observed. This slow removal of acid from the sensor increased response time dramatically, as shown in Figure 2.12. We initially suspected that the low buffering power of deionized water limited the amount of proton diffusion from the acid-soaked sensor element. After the flowing water caused a significant initial drop in the concentration of the acid surrounding the sensor element, further deprotonation of the entrapped indicator became a slow process.

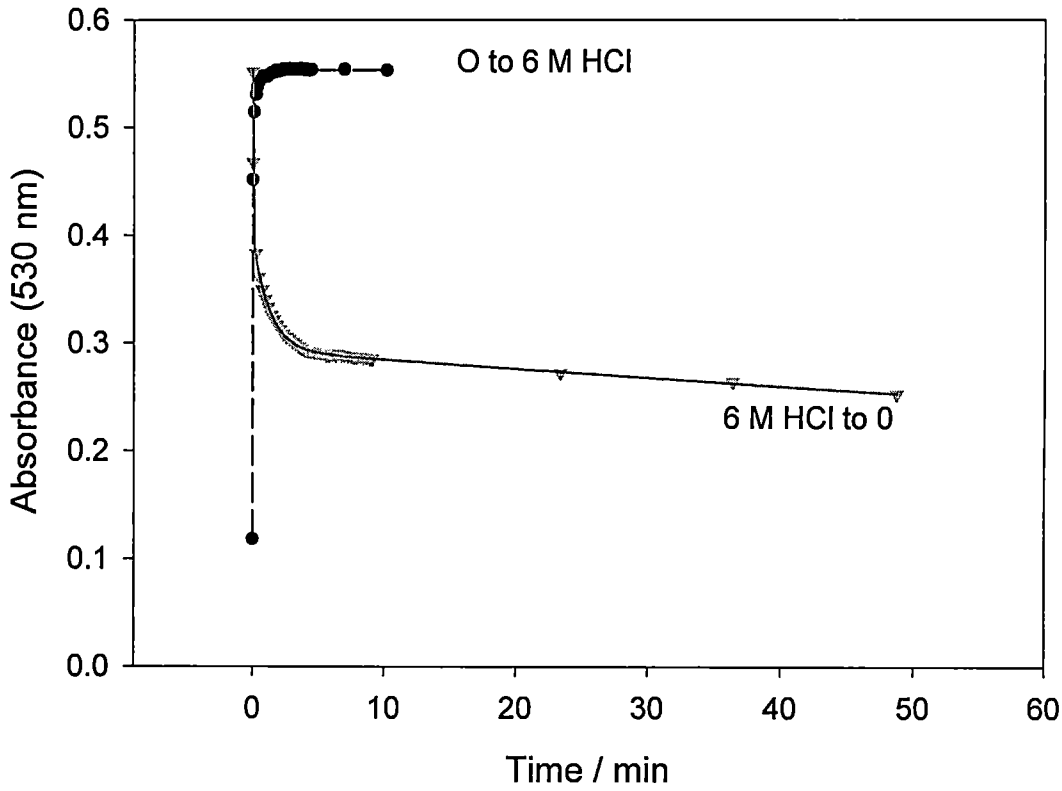

Figure 2.12. Response kinetics for Sensor 2 in HCl solutions.

To test the assumption that the low buffering power of water was responsible for the slow proton diffusion, a neutral buffer solution ($HPO_4^{-2}/H_2PO_4^-$) was used instead of deionized water to wash the acid-soaked sensor element. In such case, the decrease in response time was significant (Figure 2.13, curves a and b). Dilute and concentrated solutions of the buffer produced very similar results. However, to our surprise, dilute solutions of NaCl (≤ 0.01 M) were also found to reduce the response time as much as the phosphate buffer (Figure 2.13, curves b and c). This is a puzzling result, considering that at low concentrations, NaCl solutions have the same buffering power as pure water. Furthermore, many aqueous solutions with dissolved electrolytes (even tap water) seemed to have the same effect in promoting faster proton diffusion. Thus, it is apparently the presence of ions, rather than the buffer power, the major factor in acid removal from the sensor film. In Chapter 5, the importance of the buffer power of concentrated acidic solutions is addressed in our studies of hysteresis.

Since SiO_2 is protonated below pH = 2 in concentrated strong acids, the silica membrane is positively charged. H^+ transfer through such a positively charged surface involves a more complicated diffusion scheme, and is not fully understood at present. It is possible that electrolytes may help the H^+ diffusion by forming ionic double layers.

For slight changes in sol-gel formulation or processing, we observed remarkable differences in the sensor response time. Figure 2.14 shows the response kinetics profile for the three sensors studied here. These differences observed might be explained by changes in the film morphology, which brings a different charge density distribution on the positively charged, protonated membrane surface.

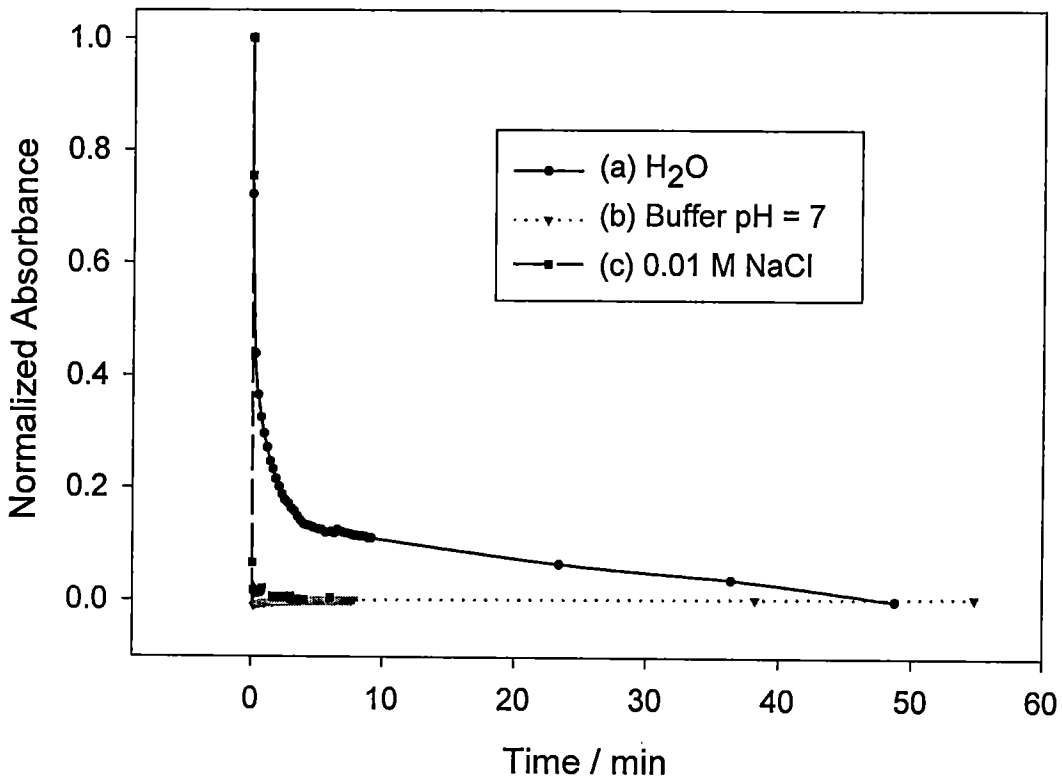

Figure 2.13. Response kinetics for Sensor 2 under different washing conditions. The sensor was initially kept in 6 M HCl.

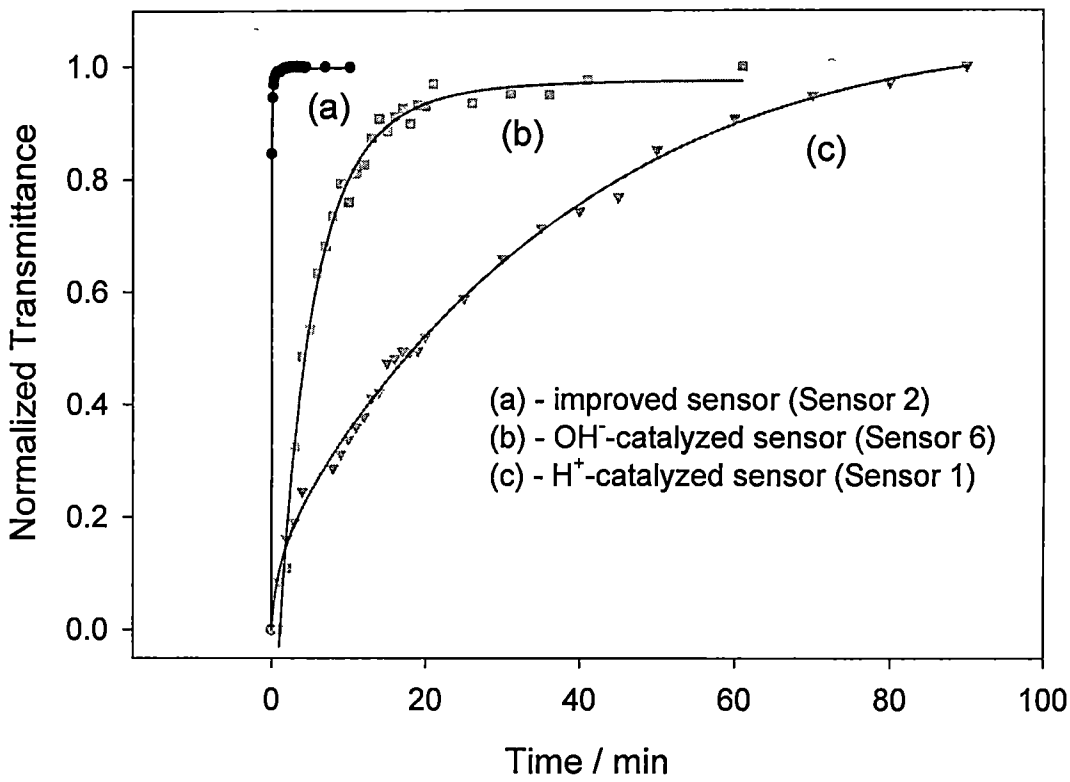

Figure 2.14. Response kinetics for BCP Sensors 1, 2, and 6.

2.3.7 Long-Term Reproducibility

One of the main impetuses of this work was to prepare an acid sensor system that could be used calibration-free for a relatively long period. In comparison, the signal drift in electrochemical sensors makes periodical recalibration necessary.

A nine-month durability test was performed with our BCP Sensor 2. The sensor element was kept in a 6 M HCl solution for nine months, except during measurements. About every two weeks, the sensor element was transferred to the spectrometer cell to test its response. It was exposed to HCl, with both incremental and decremental concentration cycles, in the following order: 6, 10, 6, 2, 0, 2, and 6 M. A maximum of 2% standard deviation relative to the response interval for 54 measurements at 6 M was observed. Only one initial calibration was conducted for these tests in the nine-month period, indicating that our sensor system was robust.

The mean transmittance, $<T>$, and standard deviation, σ, for the data for 10, 6, 2, and 0 M HCl in nine months are shown in Figure 2.15. To reduce the spectrometer error during the nine-month test period, the absorbance ratio (A_{max}/A_{isob}) was used, where A_{max} = absorbance at the wavelength of maximum sensitivity and A_{isob} = absorbance at the isosbestic wavelength. This approach was found sufficient to compensate for changes in the light power output and spectral baseline. The results of the long-term reproducibility tests after such correction are shown in Figure 2.16.

2.3.8 Measurement of HCl Pickling Solutions

Industrial acid streams are often loaded with salts of unknown composition. The number of chemical species and their concentration usually change in an industrial

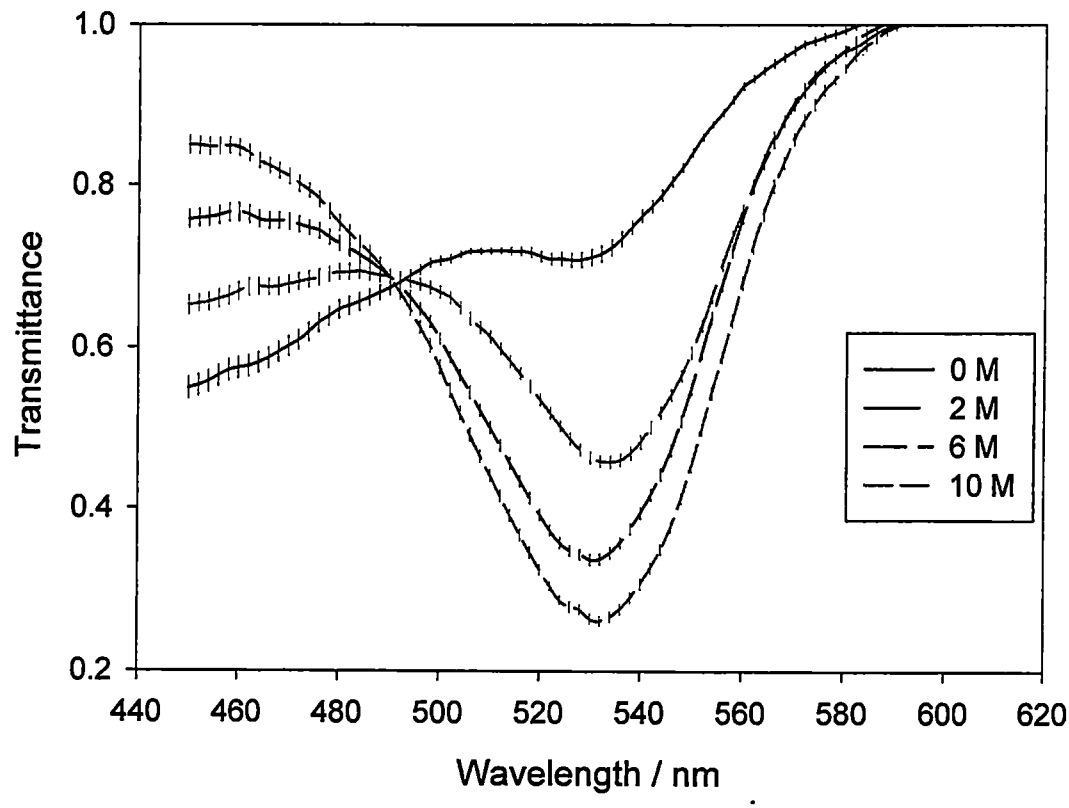

Figure 2.15. Response stability of Sensor 2 in a nine-month durability test. Sensor 2 was kept in 6 M HCl during the entire test period. The error bars are 2 σ (std. dev.).

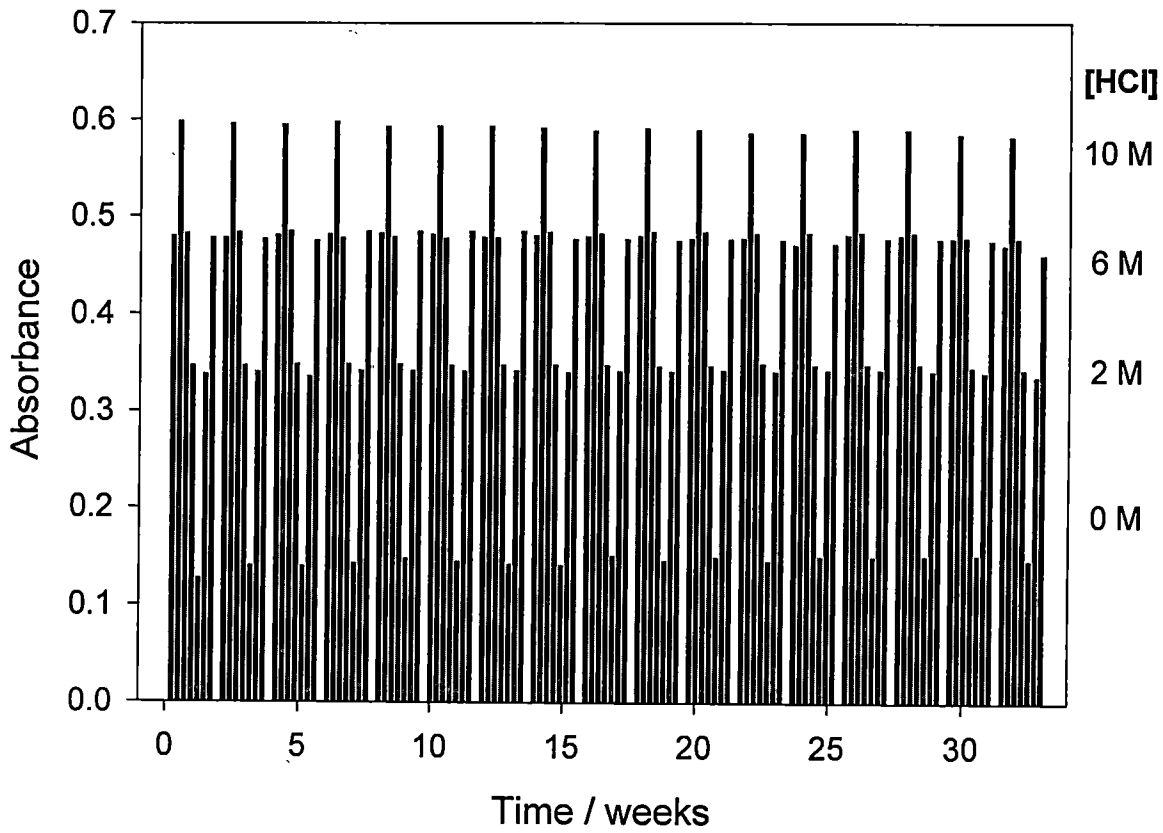

Figure 2.16. Nine-month durability test of Sensor 2. The sensor film was kept in 6 M HCl during the entire test period, and evaluated periodically.

process, and the variations in ionic strength of the acid streams need to be accounted for in the measurement of acidity.

A significant use of HCl in industry is in removing the oxide scale of iron and steel, among other metals and alloys, in a process known as pickling. In the case of iron, the concentration of HCl used is important in order to control the quality of the cleaned product. Too much acid not only removes the oxide layer, but also extensively corrodes the metal beneath the oxide layer. If the acid is not concentrated enough, the oxide layer may not be removed completely, and running the material again in an on-line process could be economically unfeasible.

One of our objectives was to develop an optical sensor that could be utilized in the pickling process to control the acid concentration on-line. The pickling acidic solution contains a mixture of both concentrated $FeCl_2$ and $FeCl_3$, as well as a large amount of particulate matter (iron particles and other debris). The high concentration of Fe^{+n}, along with particulate matter, greatly impairs the use of other acidity measurements such as automated titrators or flow injection systems. Even conventional titration is complicated by the precipitation of $Fe(OH)_n$ at low pH.

The iron pickling solutions are intensely colored. To minimize wavelength interference with our sensor system, the free optical path (the portion of the optical path in contact with the analyte solution) in the sample and reference cells (Figure 1.4a) was adjusted to be as short as possible, while keeping an adequate solution flow in the cells. The deeply colored pickling solution caused substantial wavelength interference in the 380 – 480 nm range. However, transmittance measurements outside this range were possible, and the wavelength interference on the major absorbing band of the indicator

BCP at 490 – 600 nm was minimum. Figure 2.17 shows the transmission spectra of Sensor 2 in HCl solutions containing 75 g/L of Fe^{+2} (1.34 M). These solutions were used to mimic the industrial pickling solutions. There is little interference at the lower wavelengths, and the major change observed is the apparent reduction of the sensor dynamic range. The transmittance spectra of HCl solutions containing 50 g of Fe^{+3} (0.90 M) are shown in Figure 2.18. In this case, a significant wavelength interference occurred in the 380 – 480 nm range. However, the major absorption band of the sensor was left intact, and was used to measure acidity. Again the dynamic range was shortened by the presence of the salt.

$FeCl_2$ and $FeCl_3$ are weak Lewis acids themselves, and they may contribute to the increase in the acidity of the solutions. We thus tested the response of our Sensor 2 in HCl solutions containing the neutral salt $CaCl_2$. The sensor response in these solutions was found to be similar to those of HCl containing $FeCl_2$ and $FeCl_3$. Thus, the contribution of the weak acids $FeCl_2$ and $FeCl_3$ to the solution acidity, if any, was minimum. The concentrated strong acid HCl dominated the acidity in these solutions. In other words, multimolar solutions of HCl have enough buffering power to make any acidity increase by a weak acid such as the metal chlorides negligible.

The added salt increased the ionic strength of the solutions, and thus the H^+ activity. This in turn led to the compression of the analytical range. The H^+ activity changes shifted the indicator equilibrium, and gave a smaller range of indicator response with our BCP sensor.

Figure 2.19 shows the sensor spectral changes caused by the addition of $FeCl_3$ to HCl solutions. The acid concentration, [HCl], was kept constant. The increase in

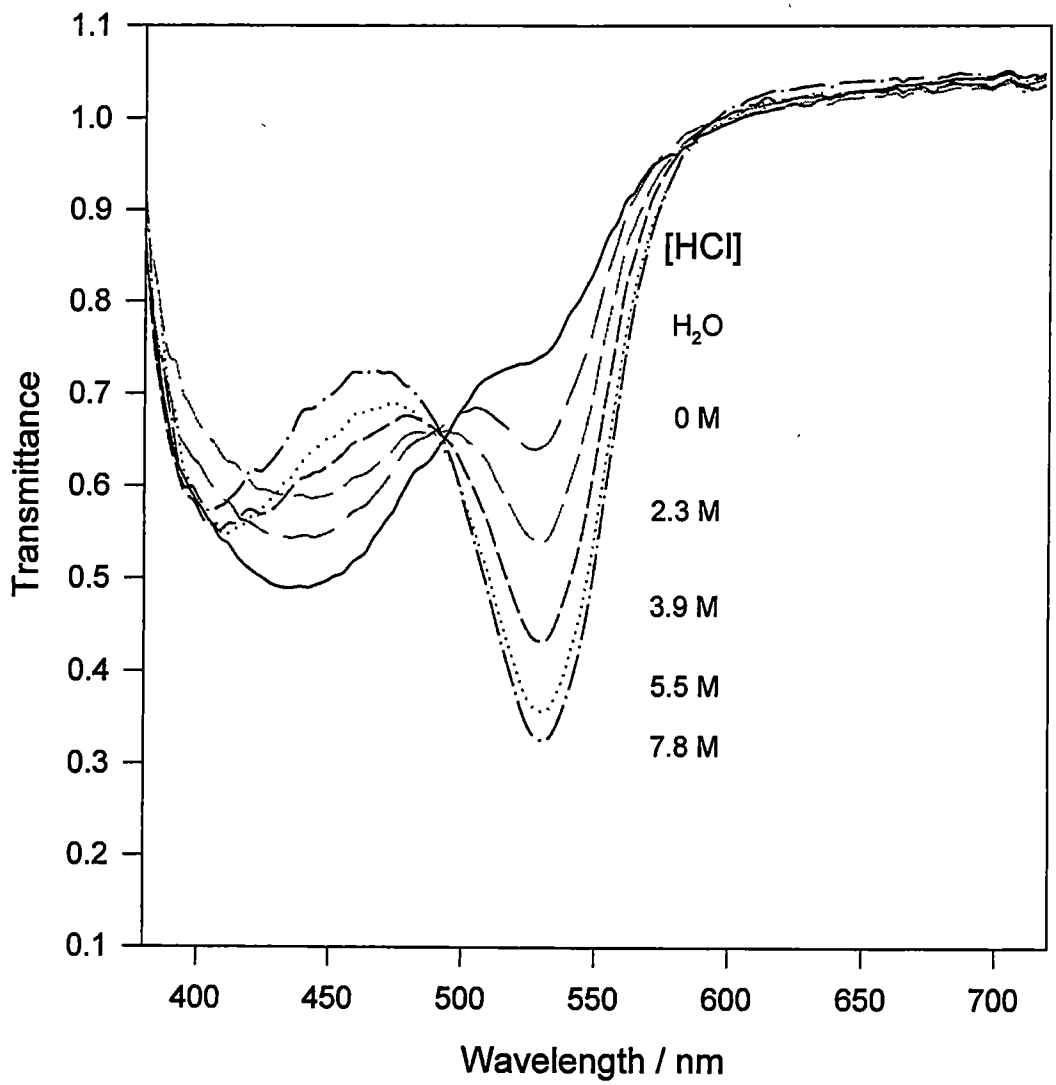

Figure 2.17. The response of Sensor 2 in $HCl/FeCl_2$ solutions (75 g/L of Fe^{+2}).

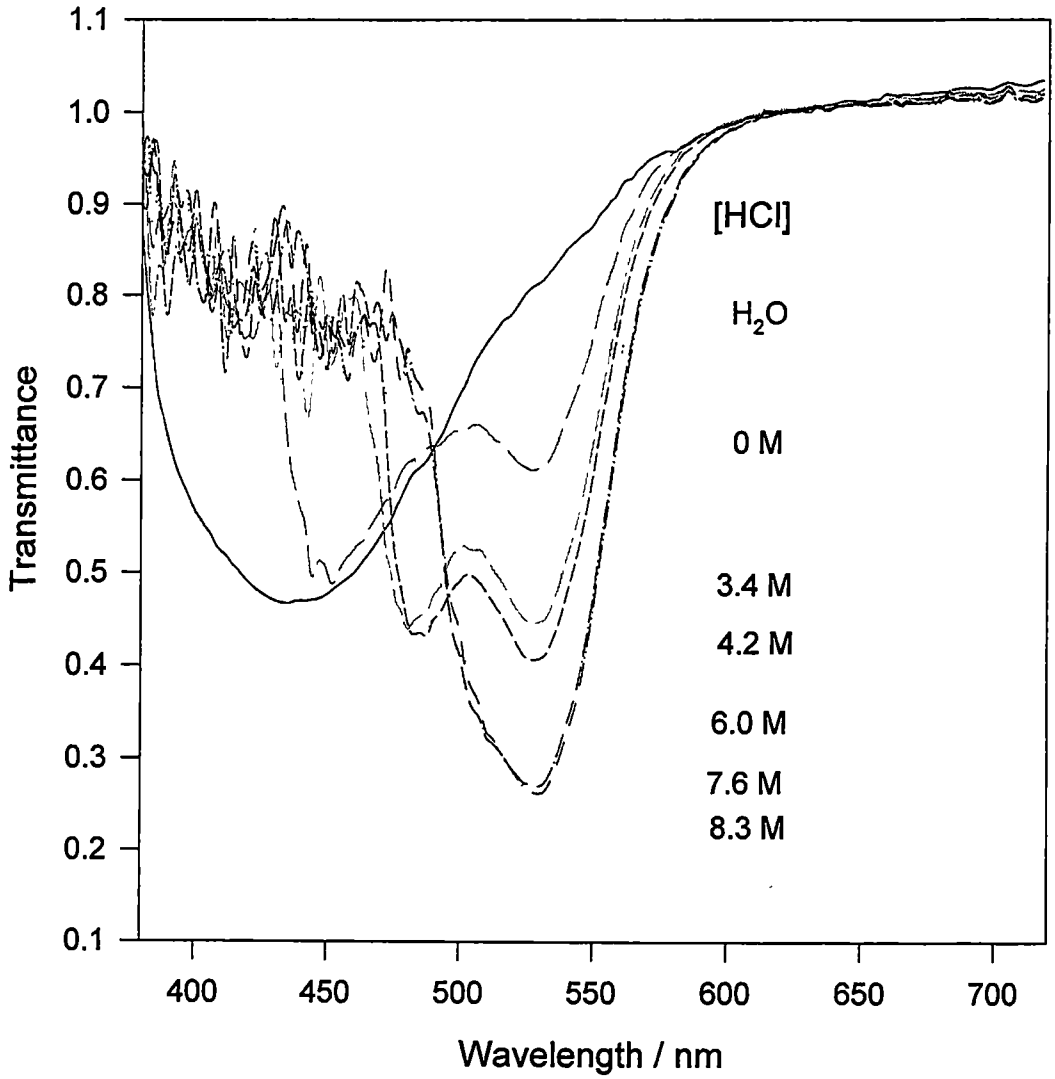

Figure 2.18. The response of Sensor 2 in $HCl/FeCl_3$ solutions (50 g/L of Fe^{+3}).

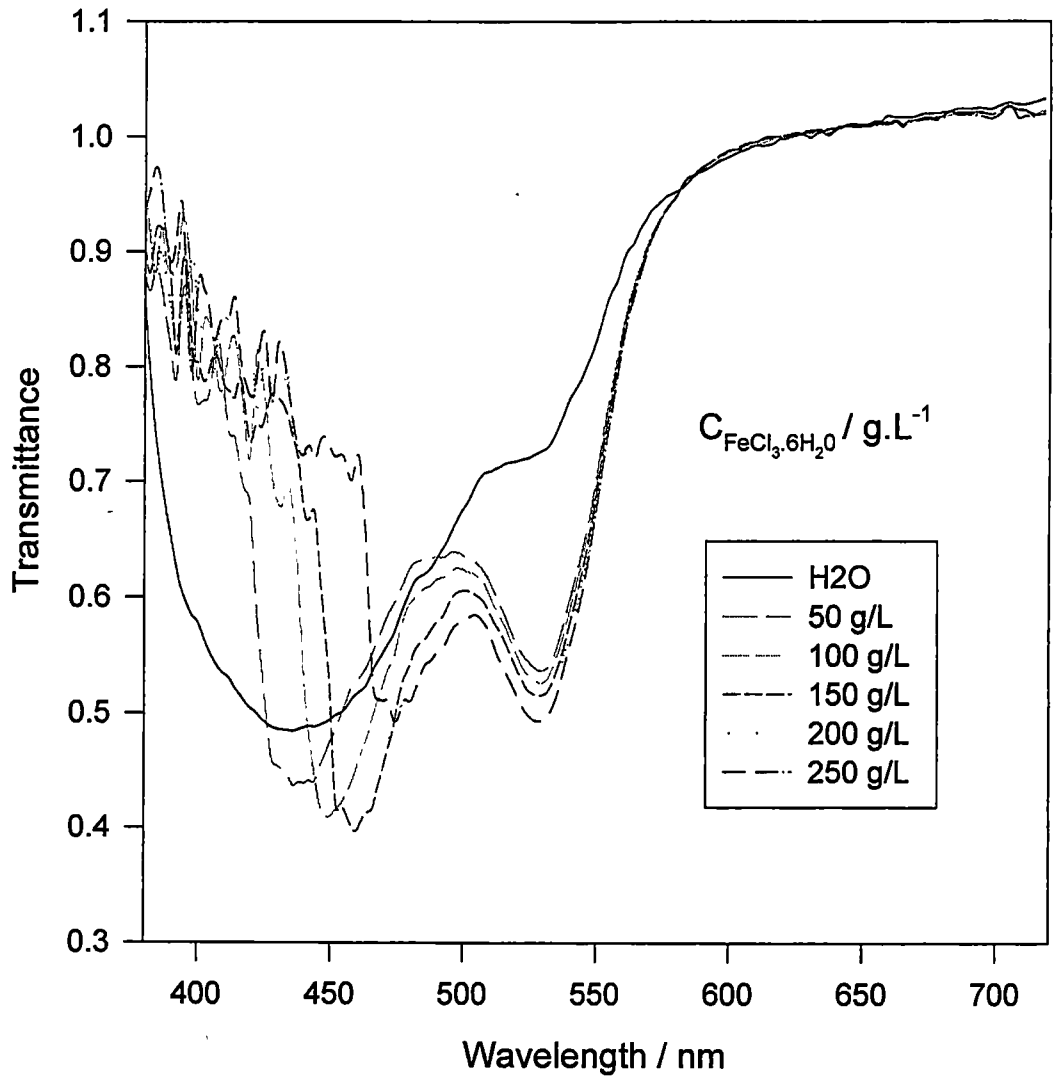

Figure 2.19. The response of Sensor 2 in HCl/$FeCl_2$ solutions ([HCl] = 2.42 M).

absorbance, A, was found to have a linear relationship with the concentration of the added salt (Figure 2.20).

The salt effect on acid activity was found to cause a very large deviation in our acidity measurement (as much as 10% of the analytical range). The ionic strength dependence is a major drawback of optical sensors, and has not been properly addressed yet. We have developed a dual-sensor approach and an algorithmic protocol to compensate the salt effect. This approach will be discussed in Chapter 4.

2.3.9 Attempted Construction of a Reflectance Probe

Many industrial processes deal with deeply colored or non-transparent solutions. In such cases, wavelength interference may become a serious problem for trasnmittance probes. Reducing the optical path can remediate the interference to a large extent. We were thus successful in analyzing deeply colored $HCl/FeCl_3$ solutions with this approach. A potentially better approach is to use diffusive reflectance probes, where high refraction index oxides (titania, zirconia) are dispersed as a sub-micrometer powder in the SiO_2 gel. The coating becomes opaque and a very good light scatterer. This tremendously enhances the collection of light absorbed by the indicator and almost none by the deeply colored environment. However, our attempts to build a reflectance cell were unsuccessful. In addition of probe leaking, inefficient light collection led to poor noise to signal ratios.

2.3.10 Measurement of Strong Acids in Organic Media

Three strong acids, HCl, HNO_3, and H_2SO_4, are widely used in organic reactions

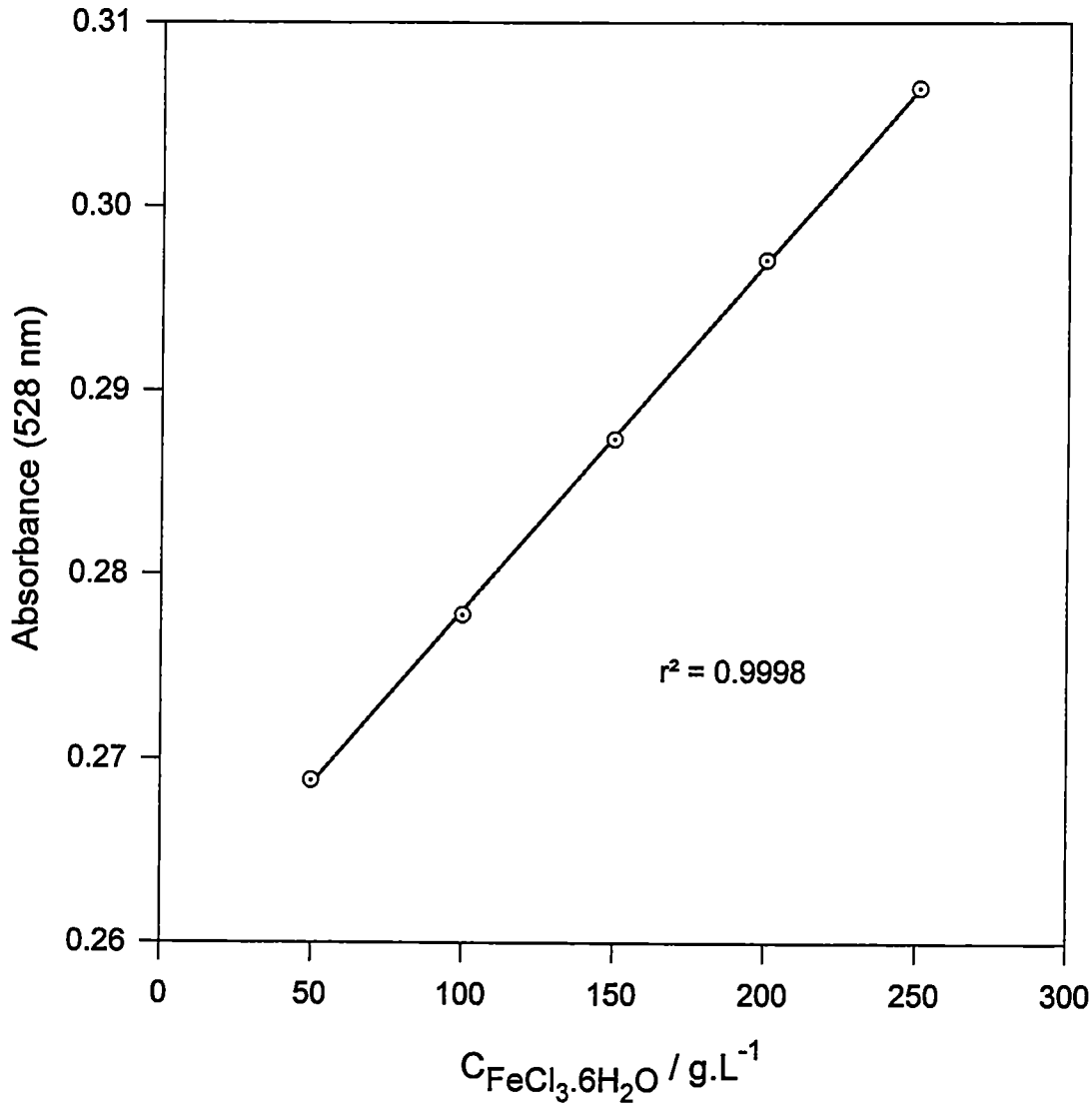

Figure 2.20. Absorbance vs. salt concentration of Sensor 2 in HCl/$FeCl_2$ solutions ([HCl] = 2.42 M).

to prepare, e.g., pharmaceuticals, gasoline, synthetic fibers, and plastics.[1] When using organic solvents containing these acids, measurement of acid concentration by optical sensors is feasible. However, three sensor parameters (response time, hysteresis, and dynamic range) are considerably affected. The hydrophilic SiO_2 matrix likely gives a much slower response (usually longer than 3 min) in organic solvents. Proton diffusion in aqueous solutions is mainly the result of the unique "proton-jump" mechanism through the hydrogen-bonded network.[38] Such mechanism leads to very fast diffusion kinetics and sensor response. In contrast, proton diffusion in organic solvents is controlled by a much slower mass transport mechanism. Hysteresis is greatly increased as well, reducing the reversibility in the sensor response. The increase in hysteresis is most likely due to the combination of poor H^+ diffusion and buffering power of the organic media. The dynamic range of the sensor was found to be shifted to much lower acid concentrations (e.g. 0 – 0.12% H_2SO_4 in benzene/acetone/water). Even though these are dilute acids in organic solvents, their relative acidity with respect to aqueous solutions is higher in these water-depleted systems. The increase in strength (decrease in the H_0 function) of acids in non-aqueous systems is responsible for the protonation of the transducer dye at much lower acid concentrations. The response of Sensor 2 in solutions of H_2SO_4/benzene/acetone/water is shown in Figure 2.21.

The BCP sensor could also be used in solutions with glacial acetic acid as the solvent. Figure 2.22 shows the sensor spectroscopic changes in H_2SO_4 solutions in glacial acetic acid. Gold and Hawes studied acidity functions in H_2SO_4/HOAc media, and analyzed the effect of H_2O on the H_0 function in organic solvents.[39] Their work (Figure 2.23) showed that the acidity increased significantly when the water content was reduced.

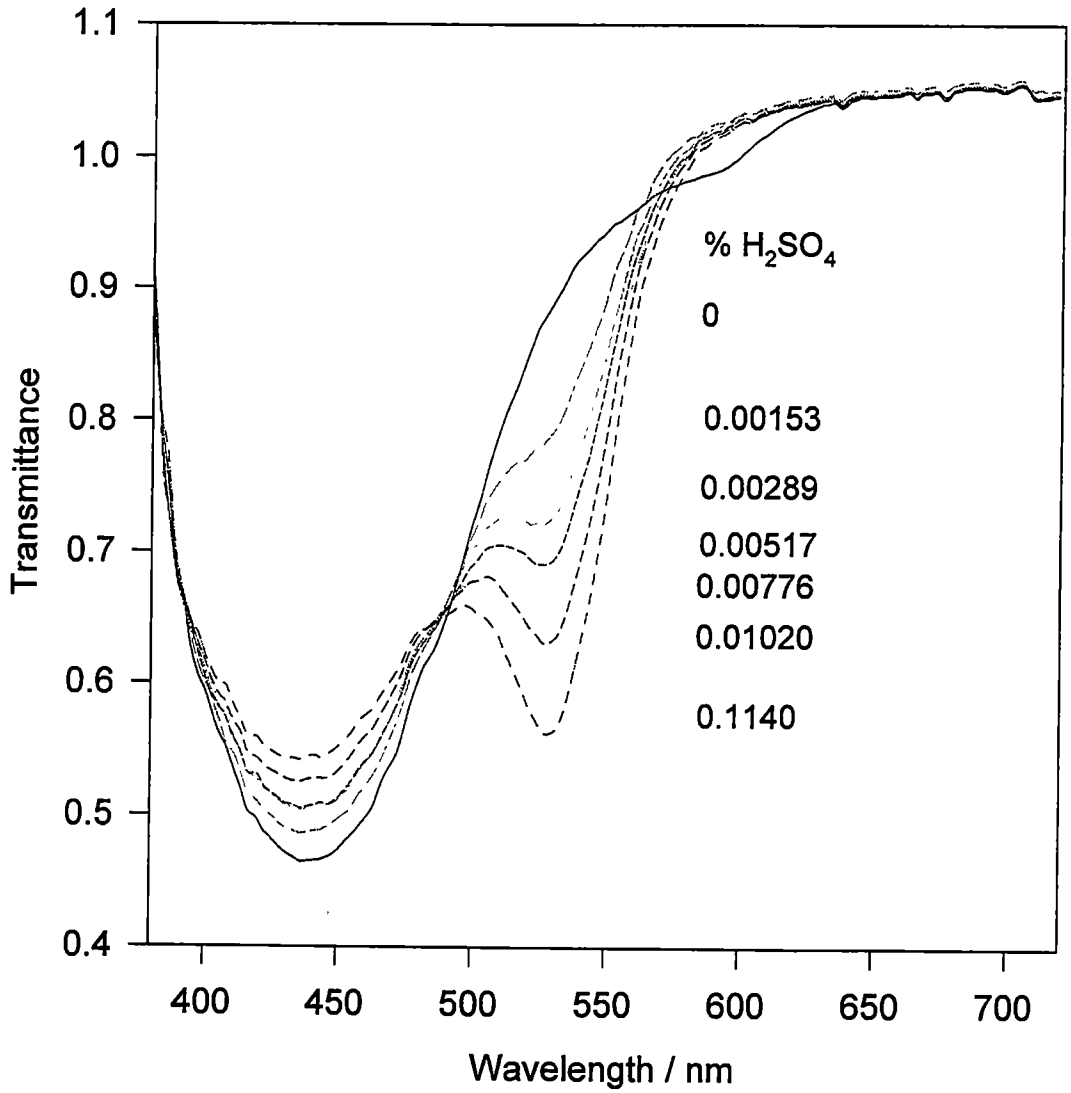

Figure 2.21. Response of Sensor 2 in solutions of H_2SO_4/benzene/acetone/water.

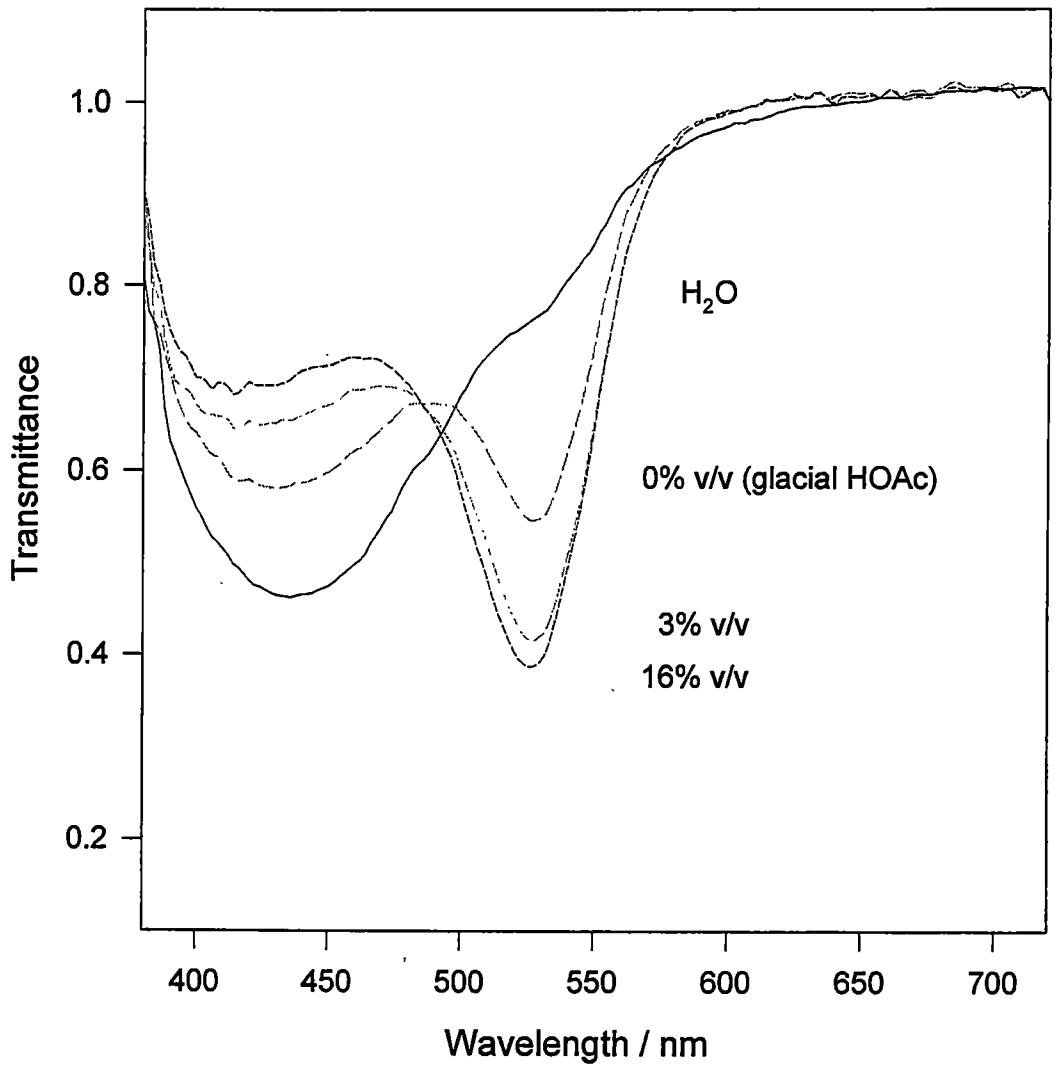

Figure 2.22. Response of Sensor 2 in solutions of H_2SO_4/HOAc.

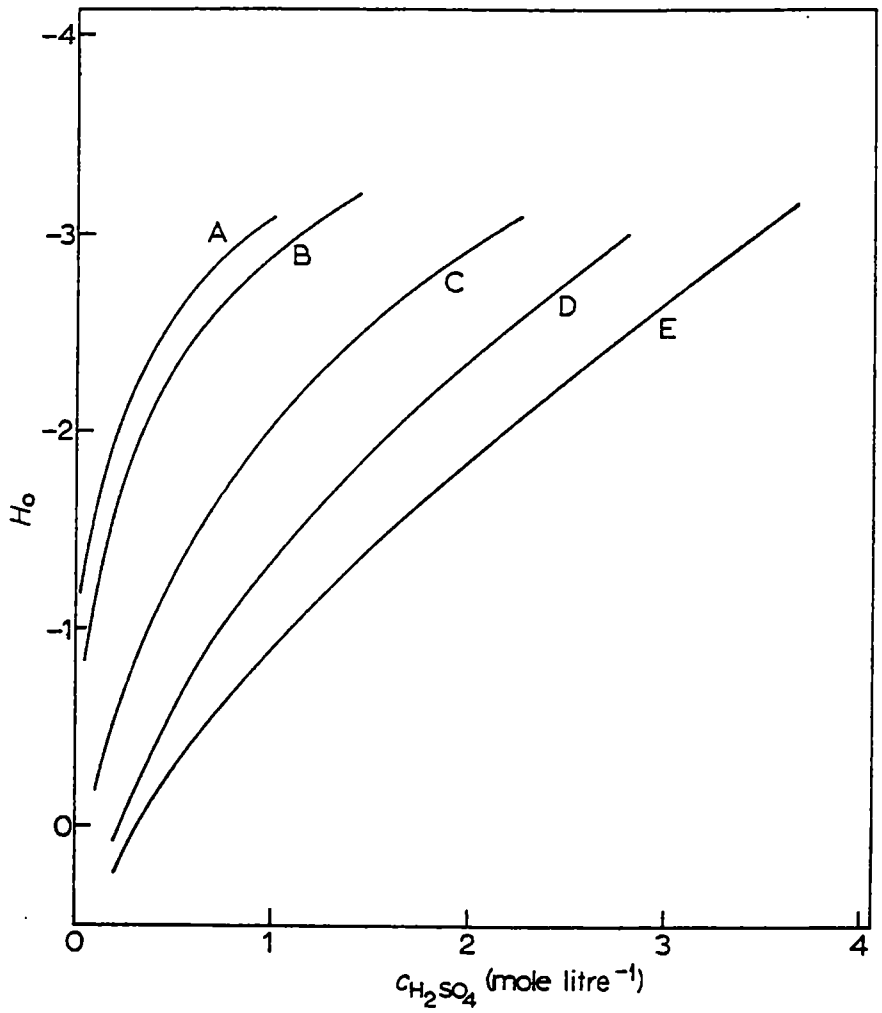

Figure 2.23. Variation of H_0 with H_2SO_4 concentration in acetic acid with small amounts of water. Curves A to E contain, respectively, 0, 1, 5, 10, and 15% H_2O. Indicator was 4-chloro-2-nitroaniline, $pK_{BH^+} = -1.03$ in water. (Adapted from ref. 39).

CHAPTER 3

Optical Sensors for the Determination of Concentrated Hydroxide

3.1 Introduction

Concentrated aqueous strong bases such as NaOH are among the largest volume chemicals manufactured in the world, and are widely used in many chemical processes.[12d,13d] However, rapid and reliable methods for their on-line determination and quality control are limited, mainly because of the corrosive nature of the concentrated alkali.[12d] Currently there is a need for reliable sensors to monitor hydroxide concentration in the range of 0.1 – 11 M (1 – 50% w/v NaOH). Such corrosive and harsh systems are widely used for acidic gas (such as H_2S, HF, HCl and SO_3) removal, paper pulp cooking liquors, and process feed reagents.[40,41] Caustic levels in these industrial systems are critical to product quality, pollution control, and equipment corrosion.

For the acid and base concentrations around neutral pH (pH = 3 to 11), a variety of optical sensors have been developed, including those based on different supports and dye immobilization techniques.[2d,15,26,42] Special emphasis was placed on sensors for invasive physiological pH determination.[42,43] However, for the more mundane pH measurements (in the range of pH = 2 to 12), the better established electrochemical sensors are more accurate than optical sensors, since the former have a direct relationship with proton *activity*, whereas optical parameters such as absorbance or emission intensity are a function of concentration of species involved in an acid-base equilibrium.[44] When working with very concentrated solutions or with organic solvents, however,

electrochemical sensors are not in general reliable, and optical sensors can fare better. In addition, the typical glass electrodes used to measure pH will produce a large positive error in alkali hydroxide solutions (pH > 12), or alkaline solutions containing high concentrations of Groups 1 and 2 metal ions,[19] greatly limiting their use in concentrated basic solutions.

Other methods such as on-line titration, flow injection analysis (FIA), measurement of refraction index and density, and near-infrared spectroscopy (NIRS)[41,45,46] have limitations. On-line titrators are often complex and maintenance-intensive; FIA requires sampling of solution; refraction index and density measurements are only accurate for clean caustic solutions with a specific composition at a constant temperature; low resolution and severe spectral overlap in NIRS limit its use in caustic measurement, although these problems can be minimized by using multivariate calibration methods.[40,41] To our knowledge, a renewable reagent-based fiber-optic sensor has so far been the best reported example of an on-line sensor for hydroxide.[40] Its operation relies on the steady-state diffusion of OH^- ions through a hollow membrane, where the OH^- ions are mixed with a continuously pumped indicator solution and monitored spectroscopically. Optical sensors have been developed by immobilizing pH-indicators on cellulose thin films over a polyester support, and they are successful for concentrations up to pH = 13.[47,48] Another detector was prepared based on the length of stain that a known volume of a OH^- solution produces on a cellulose membrane support containing a pH indicator.[49] Cellulose, a very hydrophilic polymer, offers fast diffusion kinetics, but it is easily degradable in more concentrated base solutions. Conductivity sensors are still *en vogue* for alkali determination in kraft liquors for the paper and

cellulose industry.[50] However, the non-selective nature of the measurement process limits its usability, despite the fact that such sensors can be made very rugged to survive this corrosive environment. Another sensor using the luminescence of europium-phenanthridinium complexes has been reported. The luminescence is pH dependent in the range 1.8 – 6.3, and in addition, the N-methylated ligand can react reversibly with OH^-, quenching the europium luminescence between pH = 11 – 13.[51,52]

In the current work, we developed optical sensors for concentrated basic media. Special indicators are immobilized into a metal-oxide matrix, and alkalinity changes are monitored spectroscopically. The hydrophilic nature of inorganic metal-oxides and their chemical stability in concentrated hydroxide make them attractive as support materials for sensors. We describe here durable base sensors prepared using blends of organic polymers and mixed metal-oxides for on-line high alkalinity measurements.

3.2 Experimental Section

Visible spectra were recorded using the portable spectroscopic system described in Chapter 1. Since base solutions can absorb a considerable amount of air-borne CO_2, and hence be partially neutralized, the sample set was prepared fresh from dilutions of an 11 M NaOH stock solution. The sample set was then standardized by titration with potassium hydrogen phthalate to the phenolphthalein end point, and used in a few days. All chemicals (Aldrich, Sigma, Scientific Polymer Products, and Mallinckrodt) were used as received. Thiazole Yellow GGM (also known as Thiazole Yellow, Thiazole Yellow G or Titan Yellow) was obtained from Eastman-Kodak, and its purity was considered appropriate by TLC analysis. Organic solvents were dried according to standard

laboratory purification techniques.[53] Brunauer-Emmett-Teller (BET) surface area and pore size distribution measurements were conducted on a Quantachrome Corporation Nova-1000 Gas Sorption Analyzer.

The sensors were prepared by casting the surface of Pyrex glass slides with an organic/inorganic polymer blend *via* a spin coating process (1650 rpm). Prior to casting, the Pyrex glass surface was roughened and washed with KOH - 2-propanol solution. The surfaces were then scrubbed and rinsed with water, propanol, acetone, and deionized water. The glass slides were mounted in a Teflon cell (Figure 1.4b, Chapter 1), leaving a 0.7 mm space along the optical path for contact with the flowing liquid sample. Transmittance measurements were taken with a regular glass slide without any coating as a blank. Blank glass slides that were coated with the composite material without indicators were found to give results identical to those of uncoated glass slides. Reflectance measurements were referenced against coated slides containing no dye.

3.2.1 Preparation of the SiO_2/ZrO_2-PSMMA Sensor (Sensor 7) [PSMMA: poly(styrene methylmethacrylate) copolymer 70:30, mw = 270 kd]

I. Stock solution of SiO_2/ZrO_2: In an oven-dried vial was dissolved 950 mg of $Zr(OBu^n)_4$ (80% in Bu^nOH) in 500 μL of dry EtOH. In a second vial, 200 μL of $Si(OMe)_4$ was mixed homogeneously with 400 μL of dry MeOH and 67.0 μL of 0.01 M HCl. After 120 s the $Si(OMe)_4$ solution was quickly added to the $Zr(OBu^n)_4$ solution at once with vigorous stirring. The system became very viscous for a short interval (1 to 5 s) and liquefied afterwards to form a clear, homogeneous solution. Any slight excess of

water caused formation of a poorly cross-linked gel, which eventually liquefied under vigorous mixing (such solutions can still be used). The sol-gel solution was stirred for 16 h.

II. Mixing with PSMMA: Thiazole Yellow GGM (28 mg) was dissolved in 200 μL of dry DMF and 150 μL of dry THF in a small vial. To this solution, 240 mg of a 35.3% w/w PSMMA/THF solution (based on THF weight) was added, producing a homogeneous system. The SiO_2/ZrO_2 stock solution (300 μL) was then added with stirring, and after 2 min the solution was spin-coated (1650 rpm) onto a glass slide. The sensor film was left to cure at room temperature in air. After one day the film was heated to 45 °C for five days.

3.2.2 Preparation of the SiO_2/ZrO_2-Nafion Sensor (Sensor 8)

Thiazole Yellow GGM (21 mg) was dissolved in 100 μL of dry DMF and 150 μL of dry MeOH in a small vial with stirring. Nafion (a 5% dispersion of nafion polymer in an alcoholic mixture containing 10% w/w of H_2O, 182 mg), 10.0 μL of H_2O and 5.0 μL of 1.0 M HCl were added with stirring. $Si(OMe)_4$ (200 μL) was then added to this solution, and the mixture was stirred for 9 min. At this point, 315 μL of $Zr(OBu^n)_4$ (80% in Bu^nOH) was quickly added at once with vigorous stirring. The system became very viscous for a short interval (1 to 5 s) and liquefied afterwards to form a clear, homogeneous solution. After 10 min this solution was spin-coated onto a glass surface. The sensor film was left to cure in air at room temperature. After one day at ambient conditions the film was heated to 45 °C for five days.

3.2.3 Preparation of the SiO_2/ZrO_2-Nafion-PSMMA Sensor (Sensor 9)

The SiO_2/ZrO_2-Nafion solution (300 μL) prepared by the method above (Sensor 8) was added under vigorous stirring to a mixture of 17 mg of Thiazole Yellow GGM, 100 μL of dry DMF, 100 μL of dry THF, and 230 mg of a 35.3% w/w PSMMA/THF solution. After 60 min the solution was spin-coated (1650 rpm) onto a glass slide. The sensor film was left to cure at room temperature in air. After one day the film was heated to 45 °C for five days.

3.2.4 Preparation of SiO_2/ZrO_2 with a Chelating Agent (Sensor 10)

Sulfonazo III (3.2 mg) was dissolved in 140 μL of MeOH. Acetylacetone (27.5 μL, 0.267 mmol) and $Si(OMe)_4$ (40 μL, 0.27 mmol) were added and the solution was stirred in a closed vial until the dye was dissolved. Then $Zr(OBu^n)_4$ (80% in Bu^nOH) (125 μL, 0.27 mmol) was added and stirred for 30 s to give a clear solution. H_2O (40 μL, 2.22 mmol) was added to the system and no precipitation of ZrO_2 was observed. After 50 min, the clear solution was spin-coated (1650 rpm) onto a glass slide. The sensor film was left to cure at room temperature in air. After five days the film was heated to 50 °C for seven days.

Other SiO_2/ZrO_2 ratios (2 : 1, 3 : 2, 2 : 1) as well as adding different amounts of acid (0.01 M HCl) as a catalyst were tested. None of these approaches led to improvement in their durability in concentrated hydroxide.

3.2.5 Preparation of ZrO_2 with $(CF_3)_2CO{\cdot}3H_2O$ (Sensor 11)

Thiazole Yellow GGM (28.8 mg) was dissolved in 230 μL of dry EtOH. Sub-micrometer TiO_2 powder (Du Pont hydrophilic grade, 81.1 mg) was added, and uniformly dispersed under vigorous stirring. To this mixture, $(CF_3)_2CO{\cdot}3H_2O$ (70 mg, 0.50 mmol) and $Zr(OBu^n)_4$ (80% in Bu^nOH) (350 μL, 0.77 mmol) were added and stirred. A clear solution formed and, after 30 min, it was spin-coated (1650 rpm) onto a glass slide. The sensor film was left to cure at room temperature in air. After one day the film was heated to 50 °C for four days.

3.2.6 Preparation of SiO_2/ZrO_2 with Micelle Templating (Sensor 12)

Cetyltrimethylammonium bromide (60 mg, 0.16 mmol) was dissolved in 290 μL of dry EtOH and HCl (0.01 N, 25 μL). To this solution, Alizarin Yellow (10 mg) and $Si(OMe)_4$ (100 μL, 0.68 mmol) were added and stirred in a closed vial. After 5 min, $Zr(OBu^n)_4$ (80% in Bu^nOH) (315 μL, 0.68 mmol) was added and vigorously stirred. The system became very viscous for a short interval (1 to 5 s) and liquefied afterwards to form a clear, homogeneous solution. After 60 min, the clear solution was spin-coated (1650 rpm) onto a glass slide. The sensor film was left to cure at room temperature in air. After one day the film was heated to 50 °C for five days.

3.2.7 Preparation of SiO_2/ZrO_2 with Emulsion Templating (Sensor 13)

A modification of the procedure in ref. 56c was adopted in the current preparation.

Emulsion preparation: PEG-PPG-PEG (a triblock copolymer of polyethylenegylcol-polypropyleneglycol-polyethyleneglycol, 200 mg) dissolved in 10.0 mL of formamide was added slowly with stirring 10.0 mL of isooctane (containing 1% w/w silicone oil). The mixture was vigorously agitated for 5 min to give Emulsion 1. After decantating overnight, the top portion (cream) was separated as Emulsion 2.

Metal-oxide synthesis: Acetylacetone (65 μL, 0.63 mmol) was added to $Zr(OBu^n)_4$ (80% in Bu^nOH) (295 μL, 0.64 mmol) and 425 μL of formamide, forming two phases. $Si(OMe)_4$ (92.5 μL, 0.63 mmol), H_2O (50 μL, 2.8 mmol), and HCl (0.01 N, 30 μL, 1.7 mmol) were added and the solution was stirred in a closed vial for 3 min. In order to extract the alcohol by-product, the formamide solution was transferred to an extraction funnel containing 5 mL of hexanes and thoroughly mixed before separation of the two phases. Bromocresol Purple (80 mg) was dissolved in 500 μL of the formamide phase, and 400 μL of the isooctane/formamide emulsion (Emulsion 2) was added and quickly mixed. The final emulsion was stable and viscous. After 10 min, the emulsion was spin-coated (1650 rpm) onto a glass slide. The sensor film was left to cure at room temperature in air. After three days the film was heated to 50 °C for another two days.

3.2.8 Preparation of SiO_2/ZrO_2 with a TiO_2 Reflective Coating (Sensors 14 - 15)

Thiazole Yellow GGM (11 mg) was dissolved in 300 μL of dry EtOH. HCl (0.01 M, 67.0 μL) and $Si(OMe)_4$ (100 μL) were added and the solution was stirred in a closed vial for 6 min, after which 315 μL of $Zr(OBu^n)_4$ (80% in Bu^nOH) was quickly added at once with vigorous stirring. The system became very viscous for a short interval (1 to 5 s) and liquefied afterwards to form a clear, homogeneous solution. After 20 min, 50 mg

of sub-micrometer TiO_2 powder (Du Pont hydrophilic grade) was added, and uniformly dispersed under vigorous stirring. After 40 min, the solution was spin-coated (1650 rpm) onto a glass slide. The sensor film was left to cure at room temperature in air. After one day the film was heated to 50 °C for seven days to give Sensor 14. Sensor 15 was prepared similarly with 11 mg of Alizarin Yellow instead of Thiazole Yellow GGM.

3.2.9 Conditioning of the Films

The sensor element was cooled down to 23 °C and then immersed in water for two days, until no appreciable leaching of the dye was detected spectrometrically.

3.3 Results and Discussion

Two major obstacles for the sensor development were the selection of high p*K*a dyes chemically stable in concentrated OH^- and the preparation of a durable support with fast transport properties. Among other requirements, an ideal dye should have an appropriate p*K*a (13 – 18), a large dynamic spectral range, and be chemically stable to OH^- attack and oxidation. The porosity of the thin-films is also crucial to prevent dye leaching and allow fast and reversible mass transfer of the analyte (OH^-). Sensors can be built to work in either transmittance or reflectance modes.

In the current study, we developed SiO_2/ZrO_2-polymer blend composites as sensor supports. The mixed oxide SiO_2/ZrO_2 provided a hydroxide-stable matrix. The addition of a hydroxide-stable polymer PSMMA or Nafion in the matrix either reduced indicator leaching and increased the sensor film mechanical stability in a SiO_2/ZrO_2-PSMMA composite, or enhanced OH^- diffusion and sensor response in a SiO_2/ZrO_2-

Nafion composite. In the current work, a mechanically stable film does not swell, peel-off or break apart in the analyte (OH^-) environment.

3.3.1 The Metal-Oxide Support

The properties of the support largely define the kinetics of analyte diffusion, and hence, the response time. Finding supports that can withstand caustic solutions is a particularly challenging task, and in most cases, chemically stable supports are also associated with slow response time.

During our studies, several materials for the support were investigated. Our initial focus was given to metal and metalloid oxides due to their known high hydrophilicity. Simple SiO_2 is not a good candidate, as it is quickly consumed in concentrated OH^- solution.[54] Our studies, as well as others,[54] have shown that metal-oxides such as MO_2 (M = Ti, Zr) or mixed metal-oxides MO_2/SiO_2 are reasonably stable in highly caustic media, and can be prepared via sol-gel processes from their respective alkoxide precursors, $M(OR)_4$ and $Si(OR)_4$, according to the following general polymerization reactions:

$$M(OR)_4 + 2\,H_2O \xrightarrow{H^+} M(OH)_4 + 4\,ROH \qquad \text{(hydrolysis)}$$

$$M(OH)_4 + M(OH)_4 \longrightarrow (HO)_3M\text{-}O\text{-}M(OH)_3 + H_2O \qquad \text{(condensation)}$$

M = Si, Ti, Zr; R = Me, Et, Bu^n

The sensor probe consists of an appropriate organic indicator doped in a thin film of these metal oxides. The thin film is prepared by hydrolyzing a solution of a high p*K*a indicator and $M(OR)_4/Si(OR)_4$, and spin-coating the resulting inorganic sol-gels onto a glass substrate. Our studies of several transparent metal-oxides (ZrO_2, TiO_2, SiO_2/ZrO_2, SiO_2/TiO_2) showed that the mixed system SiO_2/ZrO_2 has better performance. The hydrolysis of $M(OR)_4$ is much faster than that of $Si(OR)_4$, and as a consequence, the hydrolysis rates of $Si(OR)_4$ and $M(OR)_4$ need to be adjusted to give homogeneous mixed-oxides (with no micro segregation of the two oxide phases). The best protocol to prepare hydroxide-stable SiO_2/ZrO_2 involves pre-hydrolysis of $Si(OMe)_4$ followed by addition of $Zr(OBu^n)_4$. Thus, the much faster hydrolysis of $Zr(OBu^n)_4$ is stoichiometrically controlled by the amount of available $Si(OH)_4$. $Si(OMe)_4$ reacts with H_2O, leaving a water-depleted system. Control of the amount of water in the system is fundamental in order to avoid fast hydrolysis of $Zr(OBu^n)_4$ and precipitation of ZrO_2. For this reason the system must be kept closed at all times. If the final solution is too viscous, a small volume of dry solvent (100 μL of dry MeOH or THF) can be added. A scheme describing this procedure is shown in Figure 3.1. Several other techniques, including the use of chelating agents to slow Zr alkoxide hydrolysis,[55] were tested but later abandoned, as the resulting materials were found to have poor chemical stability in concentrated alkali. The hydrolysis rate of $Zr(OBu^n)_4$ slowed down considerably when the central atom was coordinated to a chelating agent, such as acetylacetone (Hacac). The acac-coordinated zirconium alkoxide had a hydrolysis rate similar to that of $Si(OR)_4$. This slowed hydrolysis made it possible to prepare a homogeneous mixed-oxide by the

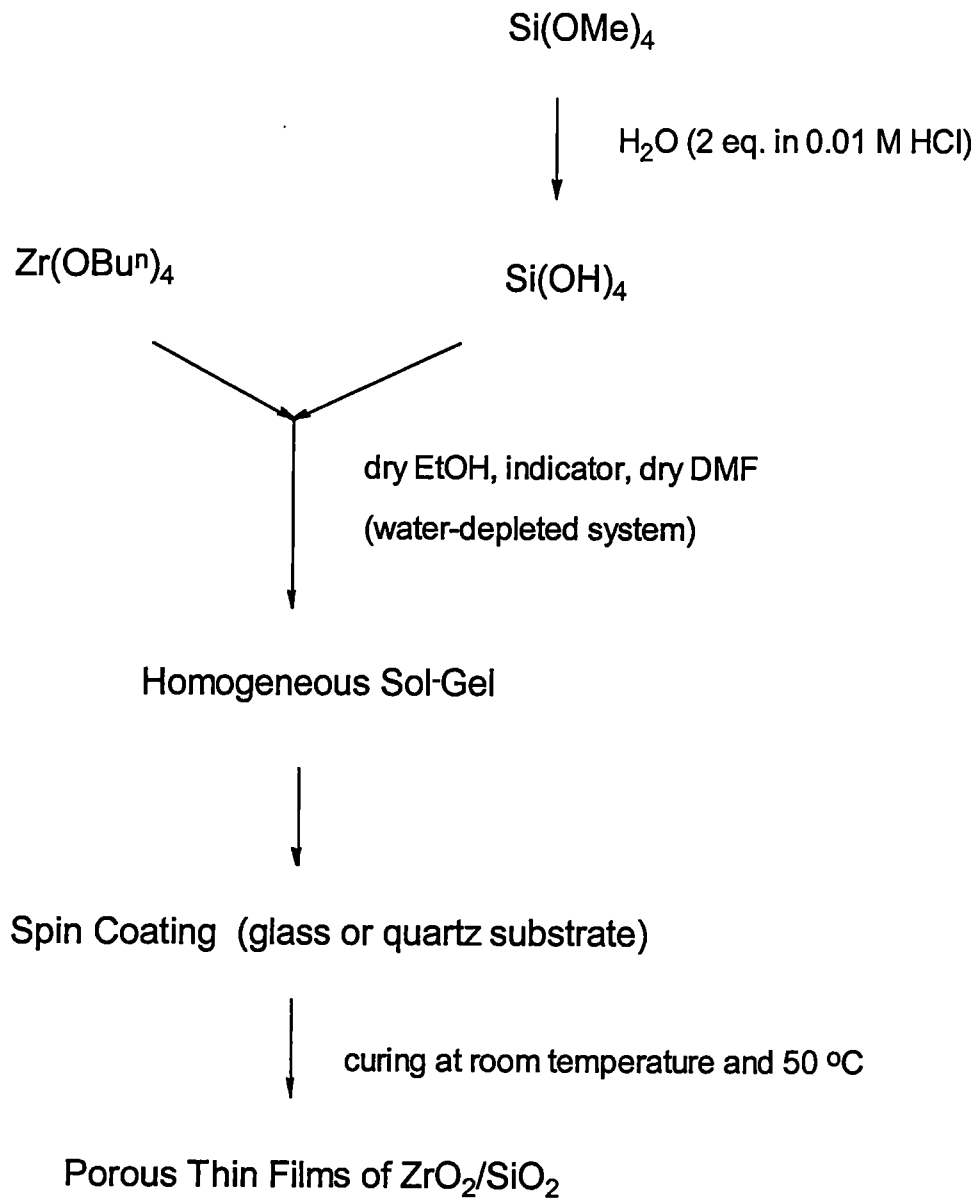

Figure 3.1. Preparation of SiO_2/ZrO_2 with pre-hydrolysis of $Si(OMe)_4$.

sol-gel process (Sensor 10). A scheme of the preparation steps using a chelating agent is shown in Figure 3.2.

Sol-gel preparation of ZrO_2 could also be achieved by controlled hydrolysis of $Zr(OBu^n)_4$; the hydrated hexafluoroacetone $(CF_3)_2CO{\cdot}3H_2O$, which exists as the geminal diol $[(CF_3)_2C(OH)_2{\cdot}2H_2O]$, was added to $Zr(OBu^n)_4$ in $HOBu^n$, and H_2O was slowly released from this hydrated diol[56a] to hydrolyze $Zr(OBu^n)_4$ to give Sensor 11 (Figure 3.3).

These mixed-oxides were found to have pore sizes too small for fast OH^- diffusion. For this reason, techniques to increase the film porosity and thus the mass transport of OH^- were explored. The techniques that were explored in the current study included micelle templating (Sensor 12),[56b] emulsion templating (Sensor 13),[56c] and doping with sub-micrometer TiO_2 powder as a filler (Sensors 14 - 15). In the latter case, the TiO_2 powder primarily served as a reflective coating for reflectance sensors, as it has a high refractive index (2.5, compared to 1.4 for amorphous SiO_2). In addition, we found that the diffusion of OH^- increased significantly in these TiO_2 powder-doped sensors. Sensor 13 prepared by emulsion templating indeed showed fast response, but did not survive in 11 M NaOH. Likewise, micelle templating, used to make Sensor 12, only met partial success. Cetyltrimethylammonium bromide and dodecylamine, a cationic and a neutral surfactant respectively, improved significantly the diffusion rate of hydroxide in the support. However, the films of Sensor 12 easily degraded in 11 M NaOH (usually in a few days). Several surfactant concentrations were tested, and the best range was between 0.14 and 0.20 M, which was well above the critical micelle concentration. Anionic surfactants did not produce any remarkable changes in the sensor response time. The curing temperature was also found to influence porosity. In general, lower

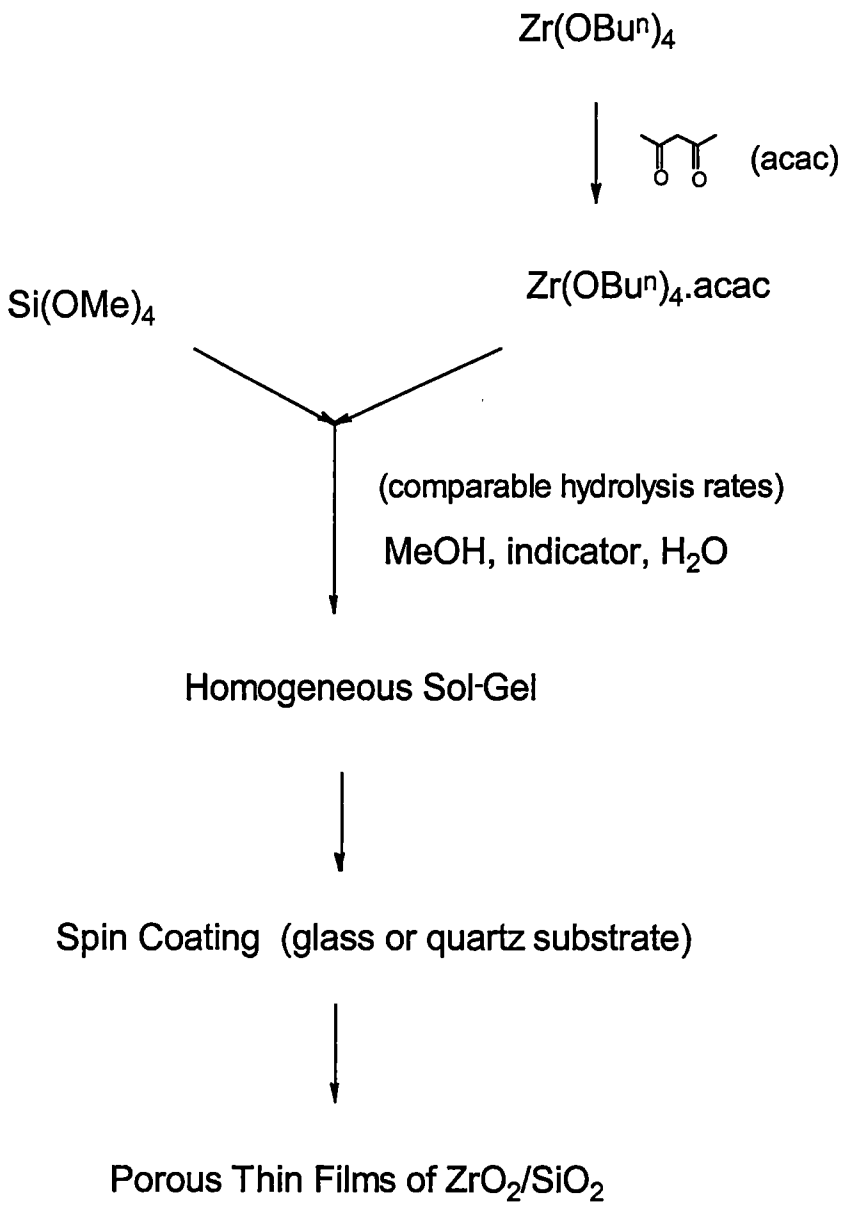

Figure 3.2. Preparation of SiO_2/ZrO_2 with the use of a chelating agent to reduce the hydrolysis rate of $Zr(OBu^n)_4$.

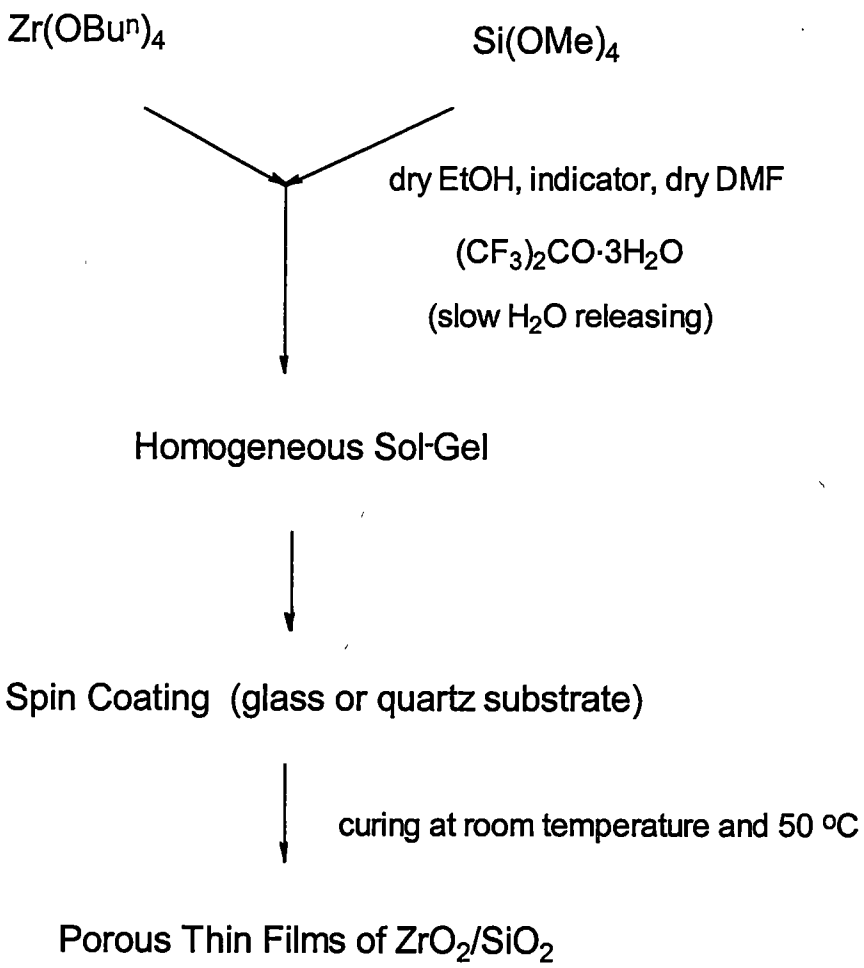

Figure 3.3. Preparation of SiO_2/ZrO_2 with the use of $(CF_3)_2CO{\cdot}3H_2O$ as a slow H_2O-releasing agent.

temperature curing (25 °C) gave films with faster response times than higher temperatures (50 and 100 °C). However, these films degraded faster.

Our studies on oxide-only sensor films showed that they had either long response time or severe indicator leaching. We then turned to SiO_2/ZrO_2-organic polymer composites as sensor supports.

3.3.2 The Composite Support

To reduce the response time, we developed blends of hydroxide-stable polymers and hydrophilic SiO_2/ZrO_2 to form composite sensor films. A major challenge in the blending process was to achieve compatibility between the two phases and hence, the choice of solvents was critic. The presence of a small amount of water or a very polar solvent may cause phase-separation of the current composite system.

$Si(OMe)_4$ was quickly hydrolyzed in the presence of an acid and, when added to $Zr(OBu^n)_4$, formed a gel that lost viscosity upon stirring. This water-depleted system was mixed with a THF solution of PSMMA, and the final solution was spin-coated onto a glass substrate. The indicator was doped in the organic/inorganic composite, showing a fairly large response to hydroxide concentration changes. The polymer phase produced a shift in the indicator p*K*a to lower values, whereas the pure metal-oxide phase did not (*vide infra*).

Another class of composites was prepared with Nafion and SiO_2/ZrO_2. Nafion is a poly(tetrafluoroethylene)polyphenylene ether sulfonate resin. Response time was found to decrease significantly by addition of this hydrophilic perfluorinated resin to the composite film. A colloidal dispersion of this resin in a H_2O/alcohol mixture is

commercially available, and was used to prepare a composite with SiO_2/ZrO_2. Complete dehydration of the H_2O-rich Nafion solution was necessary to avoid phase separation during blending, and was achieved by reacting it first with $Si(OMe)_4$ under acidic conditions. Then, either $Zr(OBu^n)_4$ alone or $Zr(OBu^n)_4$ and a PSMMA/THF solution were added, followed by spin-coating onto glass substrates, to give Sensor 8 or 9. A scheme describing this procedure is shown in Figure 3.4.

Blending these organic/inorganic polymers could only be accomplished in the right solvent system. Anhydrous conditions were necessary to avoid phase separation. In the Thiazole Yellow GGM-based sensors, N,N'-dimethylformamide, DMF, was used only to enhance the solubility of the dye; other dyes were incorporated in this inorganic/organic polymer composite by the use of different solvent mixtures in the preparation.

Both dye-doped non-porous SiO_2/ZrO_2 oxide films and hydrophobic organic polymers have long response times to OH^-, up to several hours. On the other hand, the composite films had response times that varied from 5 to 50 s. Hysteresis, being inherently associated with response time, also decreased appreciably. In general, organic polymers increase the physical integrity of the composite films. However, their films tend to have much lower affinity for the glass substrate. If the films have a large organic polymer content (> 80% total weight of precursors), they are less transparent and tend to peel off easily from the substrate. Several hydroxide-stable organic polymers such as polyvinyl butyral, poly-1,4-phenylene ethersulfone, polyvinyl acetate, polystyrene sulfonate, and hydroxypropylcellulose were also tested. They were found unsuitable due to either low transparency, lack of long-term durability, poor mechanical properties,

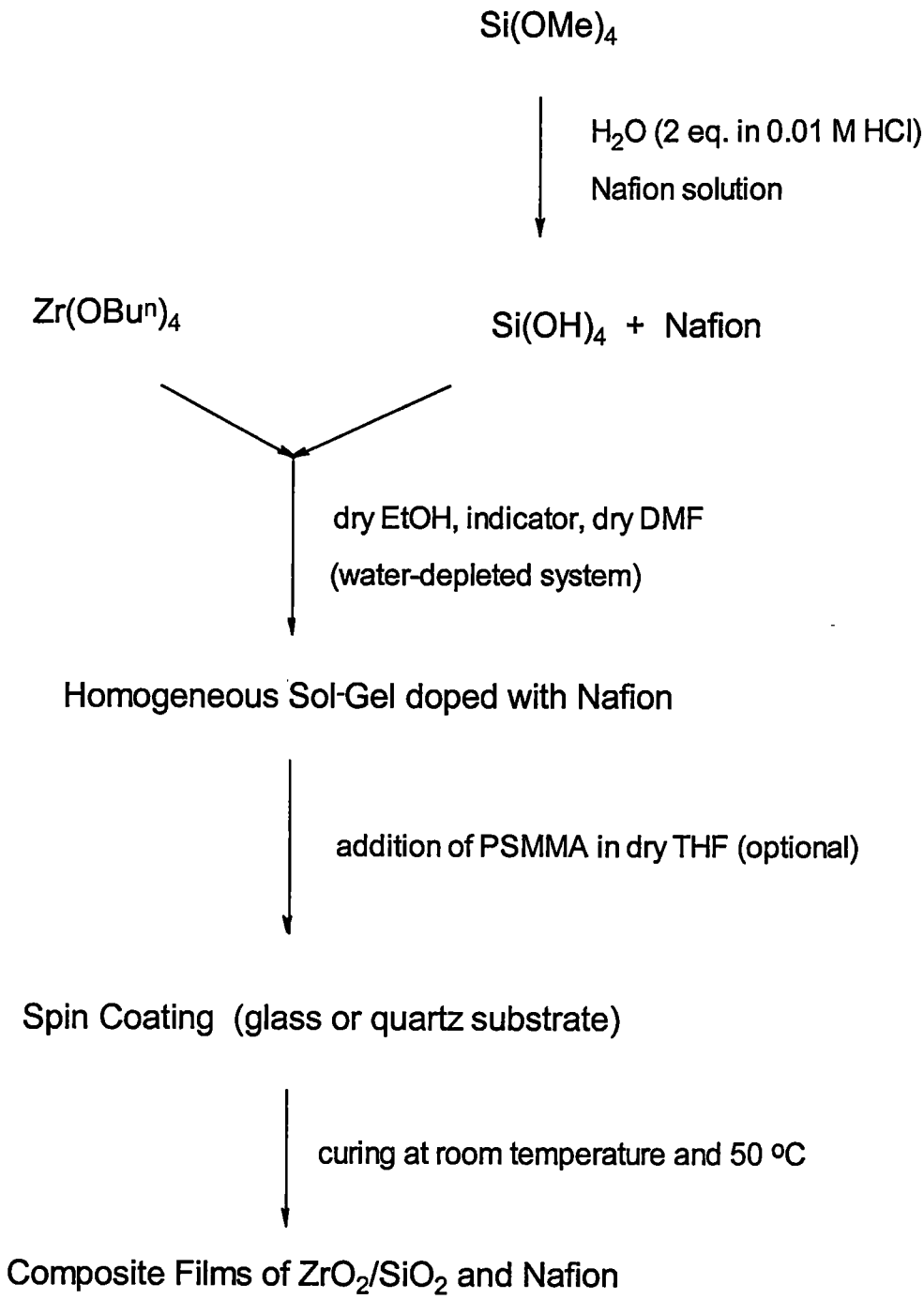

Figure 3.4. Preparation of a composite SiO_2/ZrO_2-organic polymer sensor.

and/or slow OH^--diffusion kinetics. PMMA (polymethylmetacrylate) and PBA (polybutylacrylate) were found to be much more stable, showing degradation only after long exposure to 45% NaOH, and were not used further.

The most stable film with least indicator leaching was obtained with PSMMA in Sensor 7. The Nafion composite in Sensor 8, on the other hand, showed fast OH^- diffusion and sensor response. The composite containing both PSMMA and Nafion in Sensor 9 retained the properties of both PSMMA and Nafion composites.

The scanning electron micrographs (SEM) of the different sensor films are shown in Figure 3.5. There was no micro-segregation of the SiO_2 and ZrO_2 phases as seen in Figure 3.5a, although extensive cracking in this oxide-only film was observed. The organic/inorganic polymer composite in Sensor 9 (Figure 3.5c) was found to be homogeneous as well. The holes in this film are likely the result of solvent evaporation in the sol-gel formation. It is evident from Figures 3.5a and 3.5c that adding the organic polymer blend in Sensor 9 made profound changes in the film morphology. In the case of the reflectance probe (Figure 3.5b), colloidal TiO_2 is distributed evenly in the SiO_2/ZrO_2 phase.

The Brunauer-Emmett-Teller (BET) surface area of the sensor materials was estimated by nitrogen adsorption-desorption isotherms. Due to their limited mass, we could not directly determine the porosity of the films by the BET method. Instead the porosity of similarly prepared bulk materials was measured. The composition of the bulk materials is identical to the films, and the principal difference is the former has a longer solvent evaporation rate. The surface area of the bulk material varied from 280 to 350 m^2/g with an average pore size of 35 – 45 Å.

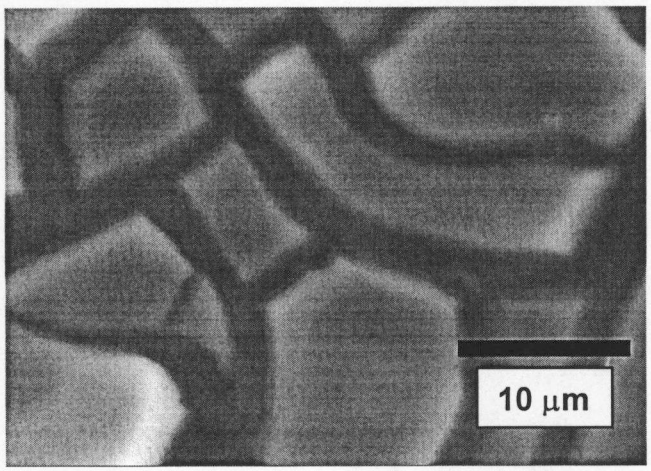

(a)

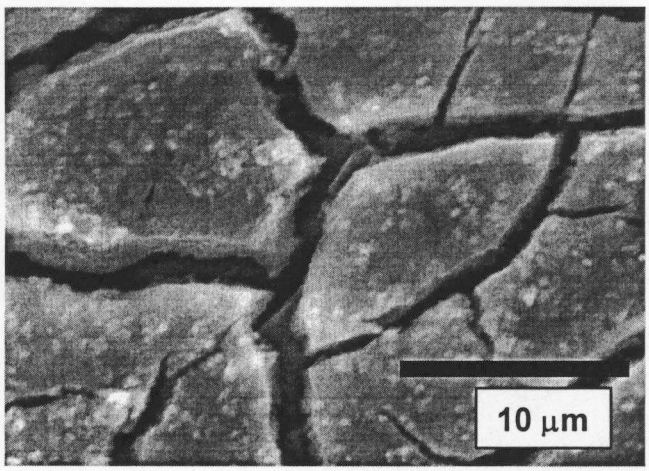

(b)

Figure 3.5. SEM of the surface of the sensor films: (a) a SiO_2/ZrO_2 sensor; (b) a SiO_2/ZrO_2 sensor doped with TiO_2 powder (Sensor 14); (c) a SiO_2/ZrO_2-PSMMA-Nafion composite sensor (Sensor 9).

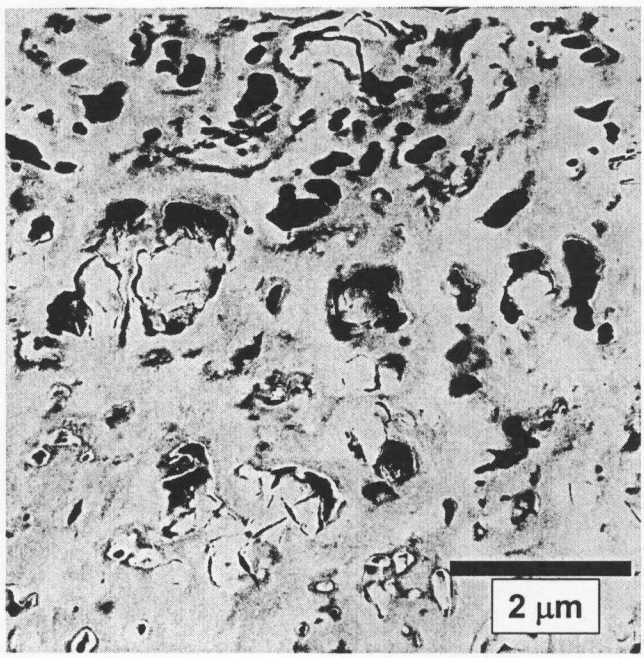

(c)

Figure 3.5. (Continued)

Our work also indicated that the solvent evaporation rate during film preparation is perhaps responsible for large variations in the sensor properties (e.g., response time and hysteresis). This effect was investigated with the use of different evaporation conditions. Either fast evaporation (during spin-coating) or very slow (in a solvent-saturated atmosphere) evaporation were found to give films with longer response times. For the composite sensors (Sensors 1, 2 and 6), the film thickness was determined by profilometry measurements and found to range from 3.5 to 4.7 μm. The films did not visibly deteriorate after repeated use.

3.3.3 The Transducer Dyes

Literature on base indicators (pH > 13) is scarce, and the selection of dyes is a key issue. Among the properties that an ideal dye should have are appropriate p*K*a (13 – 18), large dynamic spectral range, and chemical stability to OH^- attack and oxidation. Our studies showed that, in the presence of concentrated OH^-, O_2 in air can oxidize many dyes, leading to their decomposition. A literature survey[57] led us to conduct tests on over one hundred dyes with high p*K*a. We found that even the indicators that were used to build basicity functions,[58a] such as substituted diphenylamines and anilines, show decomposition in concentrated sodium hydroxide from a few minutes to hours. Among those that meet the above criteria for stable base indicators are Alizarin Yellow, Thiazole Yellow GGM, Calcion, Arsenazo III, Azoviolet, and Chromothrope 2B (see Appendix A for a listing of the indicators that were tested and found to degrade in concentrated hydroxide).

The dissociation constant of Thiazole Yellow GGM was observed to shift when the indicator was doped in the composite solid supports. In the composites, the organic polymer phase significantly lowered the indicator p*K*a value, and the oxide phase only marginally affected the p*K*a. The absorption spectrum of a Thiazole Yellow GGM sensor in NaOH solutions consists of two absorbance maxima separated by a well-defined isosbestic point. This strongly supports the existence of only two different protonated forms of the dye (Figure 3.6) in the equilibrium shown in Eq. 3.1a.

$$HInd + OH^- = Ind^- + H_2O \qquad (K) \qquad \text{(Eq. 3.1a)}$$

$$K = \frac{\{Ind^-\} \cdot a_w}{\{HInd\}\{OH^-\}} \qquad \text{(Eq. 3.1b)}$$

$$pKw - pKa = \log\left(\frac{\{Ind^-\} \cdot a_w}{\{HInd\}\{OH^-\}}\right) = \log\left(\frac{[Ind^-]}{[HInd][OH^-]} \cdot \frac{\gamma_{Ind^-} \cdot a_w}{\gamma_{HInd} \cdot \gamma_{OH^-}}\right) \qquad \text{(Eq. 3.2)}$$

where {S} is the activity of species S, [S] is its molar concentration, and f_S is its activity coefficient.

The activity coefficients γ_{Ind^-} and γ_{HInd} for Thiazole Yellow in concentrated electrolytes are inherently difficult to evaluate. Thus the thermodynamic dissociation constant,[59] *K*a, of the indicator Thiazole Yellow was estimated by determining [OH^-] at the half ionization of the indicator. A basicity function, H_-, for a series of known indicators in aqueous NaOH (Eq. 3.3) had been previously determined,[58b] and was used

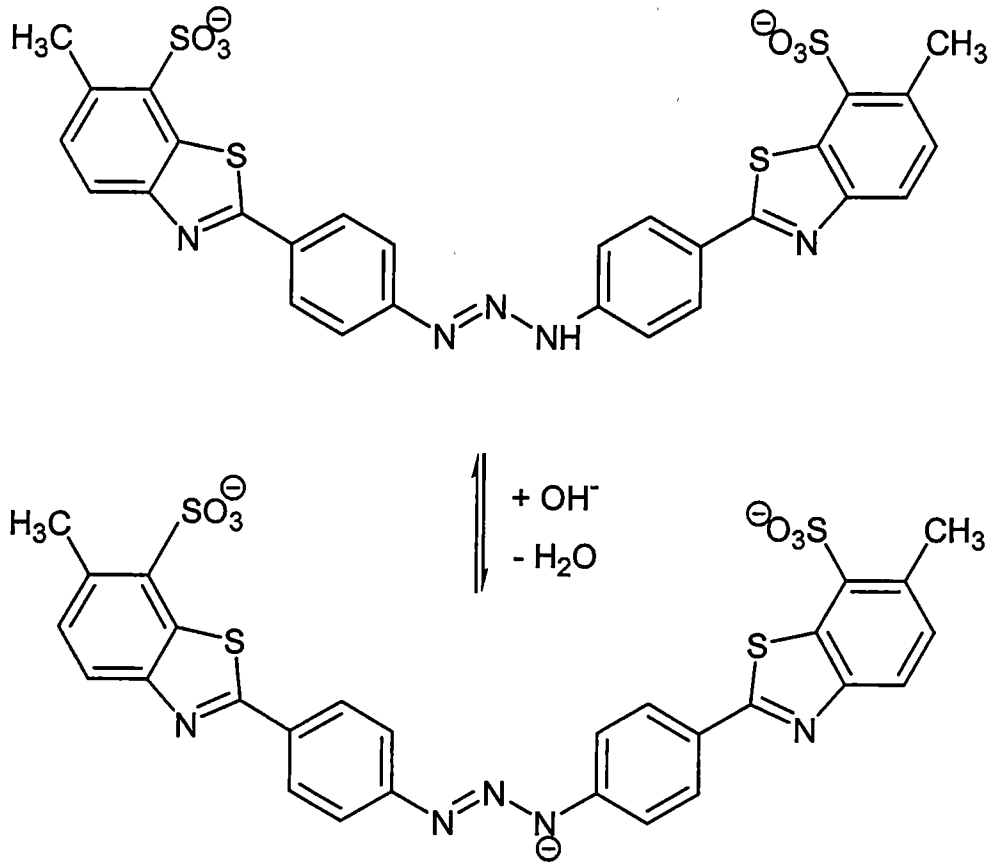

Figure 3.6. Equilibrium involving the protonated and deprotonated forms of Thiazole Yellow GGM.

in the current study to estimate *K*a of Thiazole Yellow.

$$H_ = \mathrm{p}Kw + \log[OH^-] - \log\left(\frac{\gamma_{B^-} \cdot a_w}{\gamma_{HB} \cdot \gamma_{OH^-}}\right) \qquad \text{(Eq. 3.3)}$$

At half ionization, [HInd] = [Ind$^-$] and p*K*a = $H_$, as long as the activity coefficient ratio for the indicators used in the basicity function, f_B/f_{HB}, is close enough to the ratio f_{Ind}/f_{HInd} for the indicator Thiazole Yellow.[8]

The indicator half ionization point was determined spectrometrically. Table 3.1 lists the [NaOH] at half ionization, $[NaOH]_{\alpha = 0.5}$, and thermodynamic (*K*a) dissociation constants of Thiazole Yellow GGM, calculated for different sensors.

3.3.4 Response of the Sensor Films in Concentrated NaOH

Typical transmission spectra (Figure 3.7) of a SiO_2/ZrO_2-PSMMA Thiazole Yellow GGM sensor (Sensor 7) in NaOH solutions (1 to 32% w/v) show two absorbance maxima at 412 and 524 nm, respectively, along with a well defined isosbestic point. This strongly supports the existence of only two different protonated forms of the dye in equilibrium. The longer wavelength showed greater analytical sensitivity, and data collected were divided by the absorbance at the isosbestic wavelength to compensate for any correlated variations in light power or detection. A typical calibration plot in hydroxide solutions is shown in Figure 3.8.

The response reversibility of the sensor was also tested by exposing it to solutions

Table 3.1 Thermodynamic Dissociation Constants for Thiazole Yellow GGM in Different Supports*

Sensor	$[NaOH]_{\alpha = 0.5}$ / (mol/L)	p*Ka*
SiO_2/ZrO_2-Nafion (Sensor 8)	0.64 ± 0.11	13.84 ± 0.07
SiO_2/ZrO_2-Nafion-PSSMA (Sensor 9)	1.03 ± 0.12	14.06 ± 0.05
SiO_2/ZrO_2-PSSMA (Sensor 7)	1.12 ± 0.06	14.09 ± 0.02
SiO_2 (Control)	4.48 ± 0.48	14.95 ± 0.10

* The errors are standard deviations.

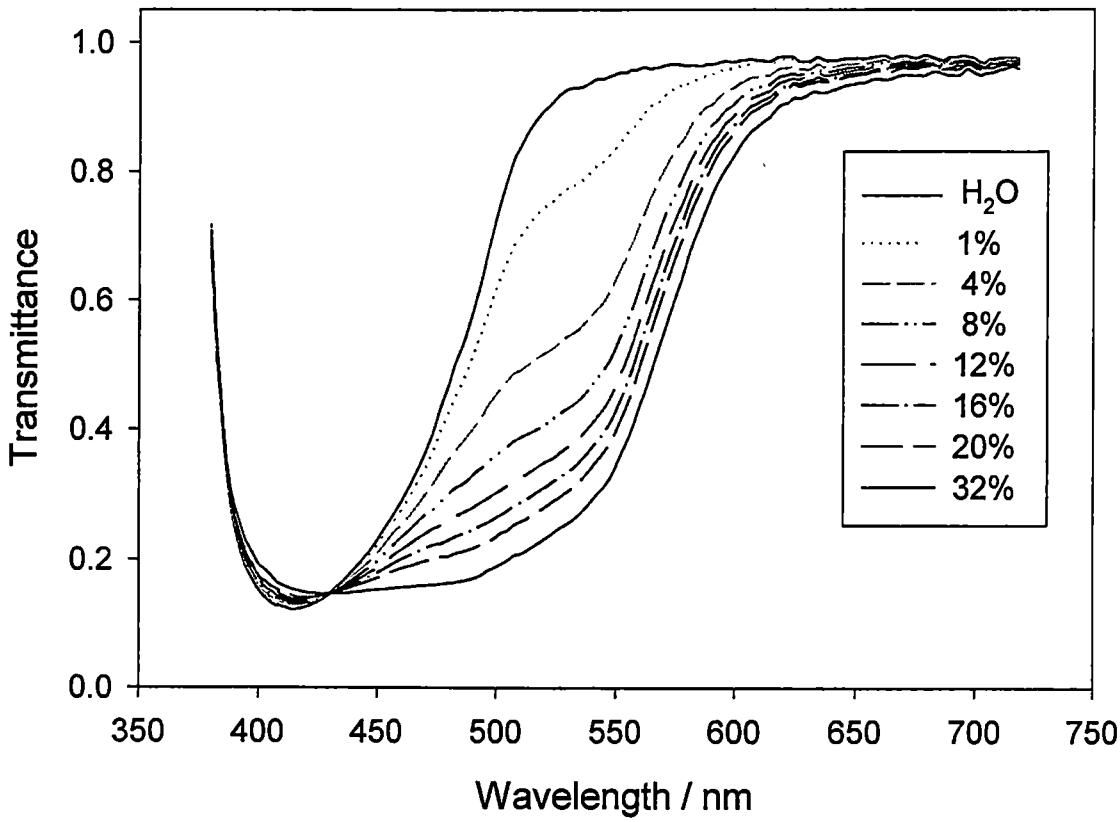

Figure 3.7. Typical transmittance spectra of Sensor 7 in NaOH solutions (concentrations in % w/v).

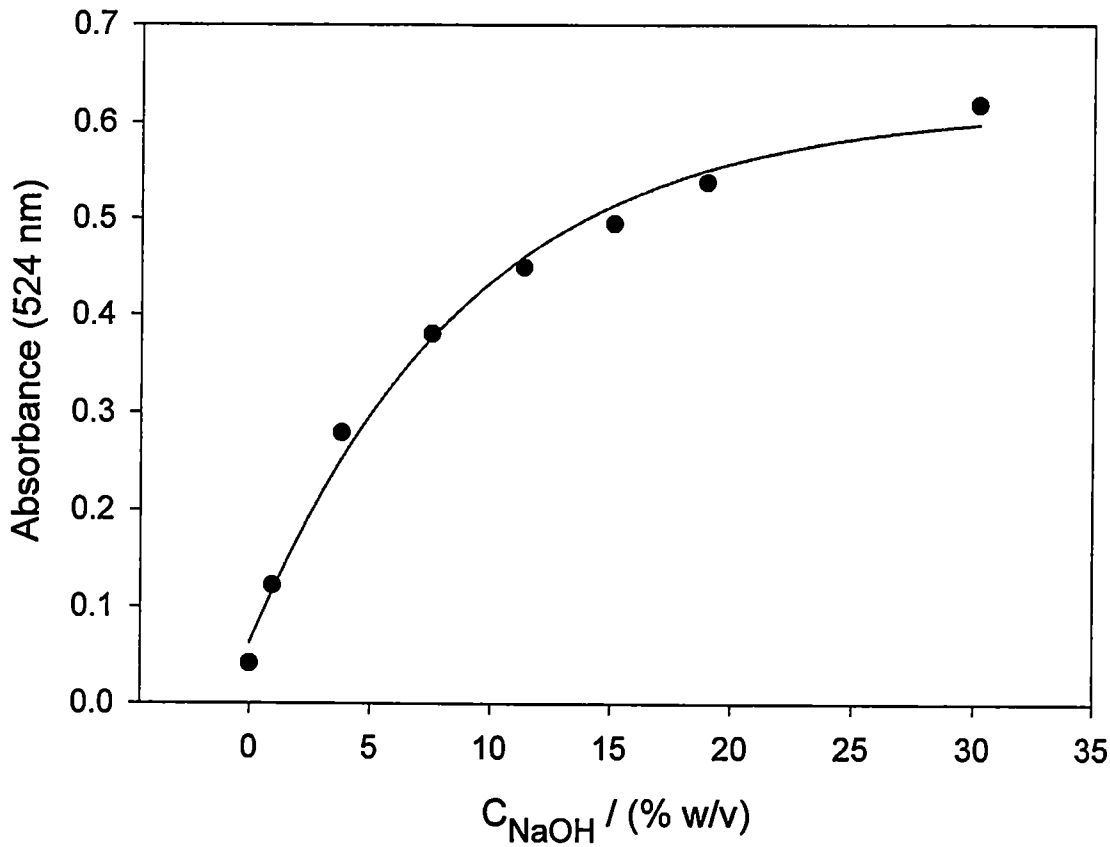

Figure 3.8. Calibration curve of Sensor 7 in NaOH solutions.

of NaOH (H_2O, 1, 4 and 15% w/v) in cycles where the sensor faced incremental and decremental changes in alkali concentration (Figure 3.9). An excellent response time in both directions (5 s) was obtained, and the sensor film showed little hysteresis (width < 2%). The precision of the sensor has a standard deviation of less than 2.3% (n = 9), and is stable for weeks (*vide infra*).

3.3.5 Response Time

The response kinetics for the sensors is shown in Figure 3.10. The sensors were subject to a concentration change from H_2O to 12% w/v NaOH. The SiO_2/ZrO_2-Nafion composites (Sensor 8) had the fastest response, achieving 90% of total signal change in 5 s. SiO_2/ZrO_2-Nafion-PSMMA (Sensor 9) and SiO_2/ZrO_2-PSMMA (Sensor 7) give 90% of total signal change in 15 and 50 s, respectively. Kinetics for the response change when the sensors were rewashed with H_2O yielded similar results (Figure 3.11), showing that the sensors are reversible.

The increase in PSSMA content clearly leads to longer response times, most likely due to its hydrophobicity. However it provides a better mechanical integrity and indicator immobilization to the sensor. The effect of the PSMMA composition on the response time was investigated by evaluating the response kinetics for sensors prepared with the same precursors in complementing fractions. The amount of PSMMA was found to have a pronounced effect on response time. As shown in Figure 3.12, the plot of the logarithm of 90% response time vs. the relative PSMMA composition is a straight line. Short response times are desirable for the reduction of lag time and hysteresis, and consequently, analytical error. A more comprehensive discussion of hysteresis is given

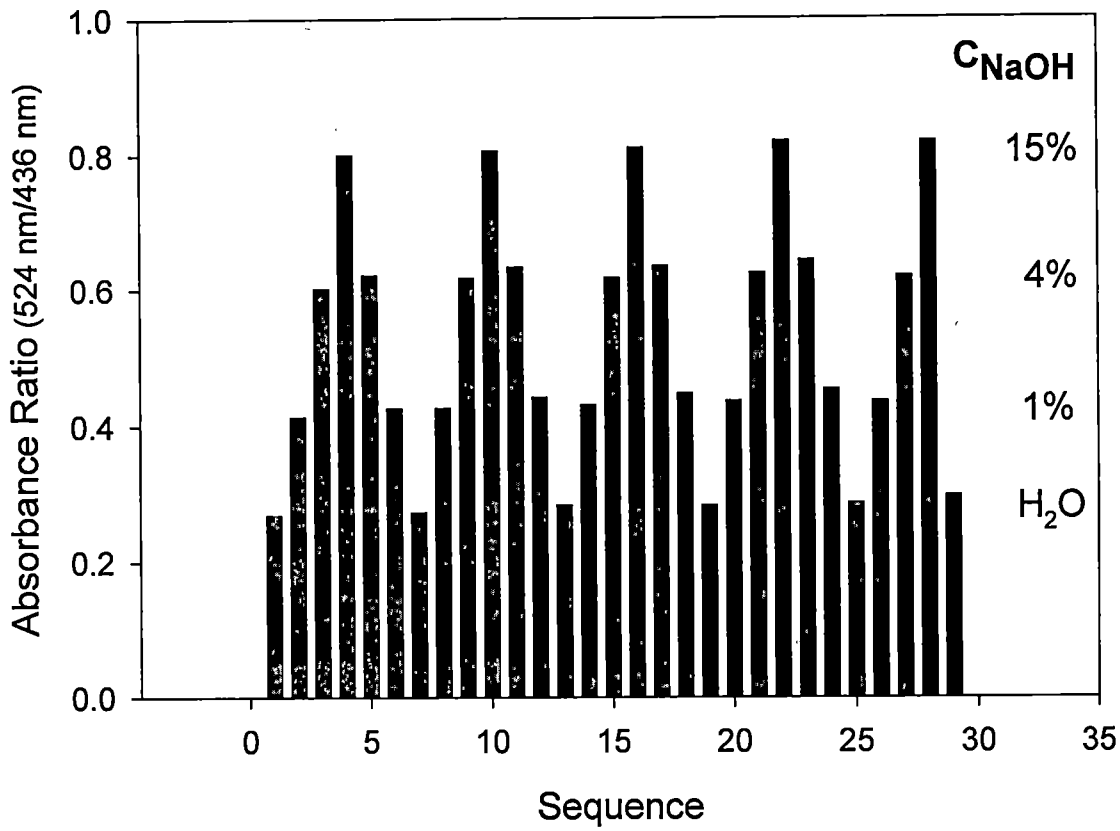

Figure 3.9. Response reproducibility of Sensor 8 in NaOH solutions (concentrations in % w/v).

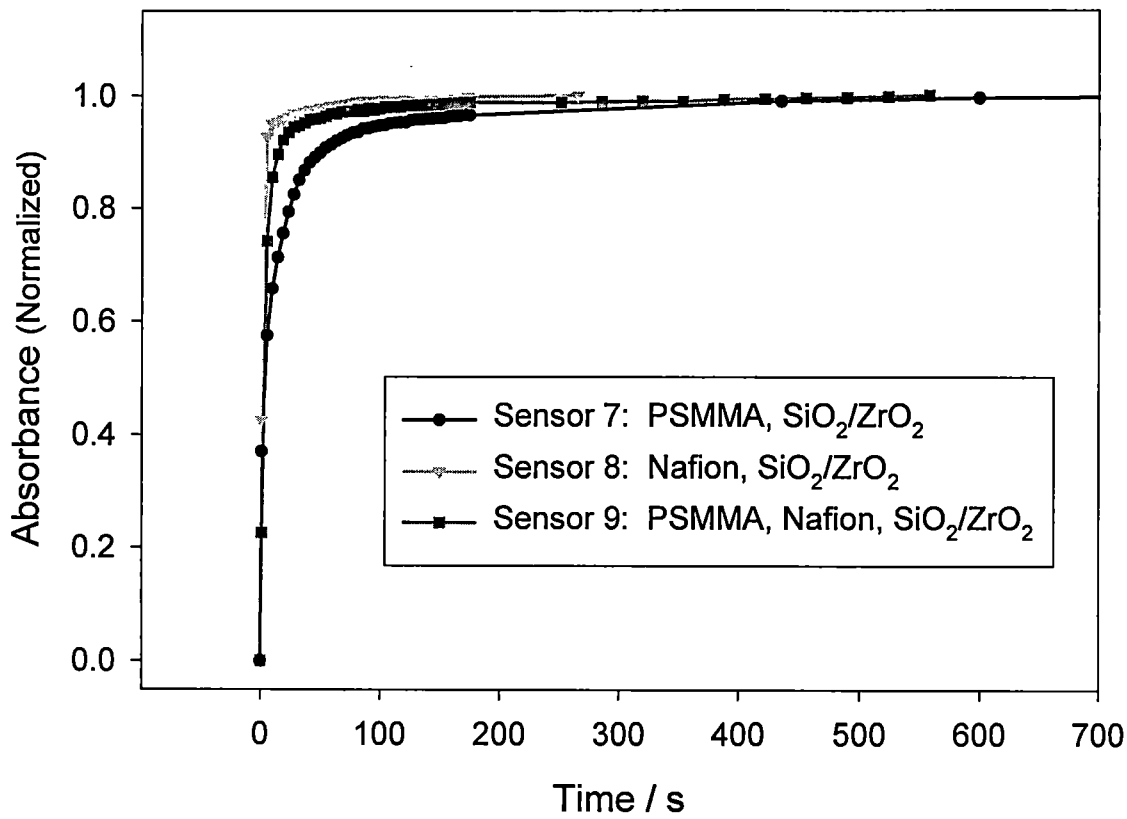

Figure 3.10. Response kinetics of Sensors 7 – 9 under a positive concentration gradient, from H_2O to 12% w/v NaOH.

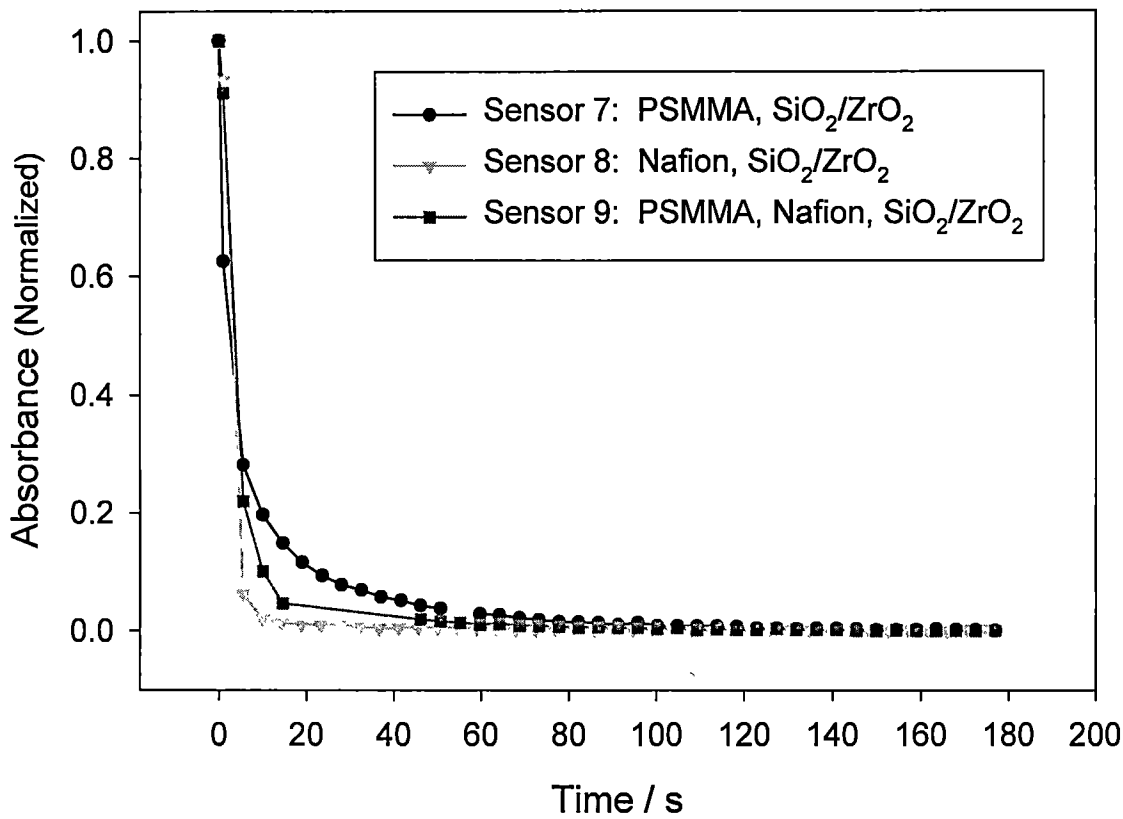

Figure 3.11. Response kinetics of Sensors 7 – 9 under a negative concentration gradient, from 12% w/v NaOH to H_2O.

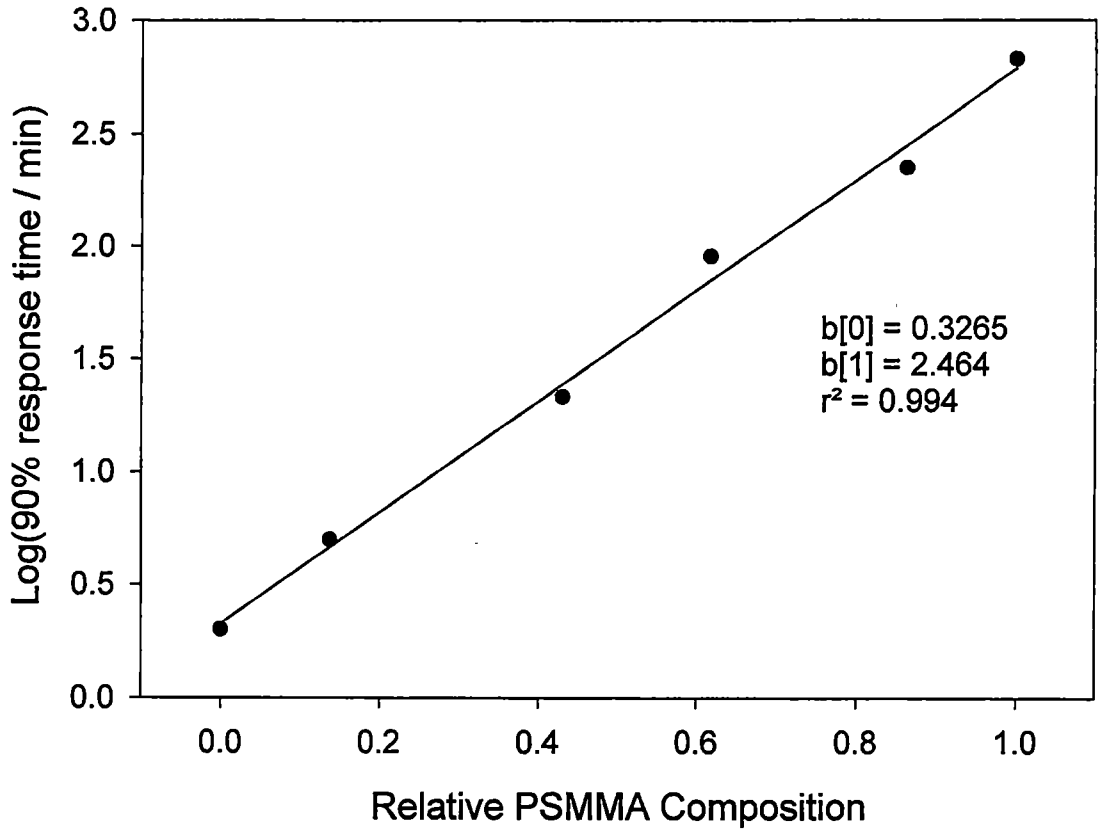

Figure 3.12. Exponential dependence of the response time and PSMMA composition of Sensor 7. Response times were calculated using sensor absorbance changes from 12% w/v NaOH to H_2O.

in Chapter 5.

3.3.6 Long-Term Stability of the Sensors

The long-term stabilities of Sensors 7 – 9 were evaluated for a period of 30 days (Figures 3.13, 3.14, and 3.15, respectively). The sensors were kept in 4 M NaOH in the entire period, except during measurements when they were exposed to 8 M NaOH and their absorbance recorded. The absorbance at 524 nm showed standard deviations of 3.3%, 4.7%, and 3.0% of the total signals for Sensors 7, 8, and 9, respectively. However, dividing the data collected at 524 nm by the transmittance at the isosbestic wavelength (Figure 3.16), to compensate for any correlated variations in light power or detection, improves the overall stability of the signal (standard deviation = 1.6% for Sensor 8).

3.3.7 Reflectance vs. Transmittance Sensors

Reflectance measurements are usually free of the occasional wavelength interference from the analyte matrix. However, variations in the refractive index of the concentrated alkali solutions cause different amounts of light scattering, leading to signal losses need to be accounted for. In other words, these refractive index variations are responsible for a noticeable baseline shift. Submicrometer TiO_2 powder was used as filler to improve porosity and the scattering properties of the platforms to give Sensor 14 (see Figure 3.5b for its SEM). Hydrophilic grades performed the best, as they were more easily dispersed than other grades. Typical graphs of the response of TiO_2 filler-reflectance sensors with Thiazole Yellow (Sensor 14) and Alizarin Yellow (Sensor 15) as

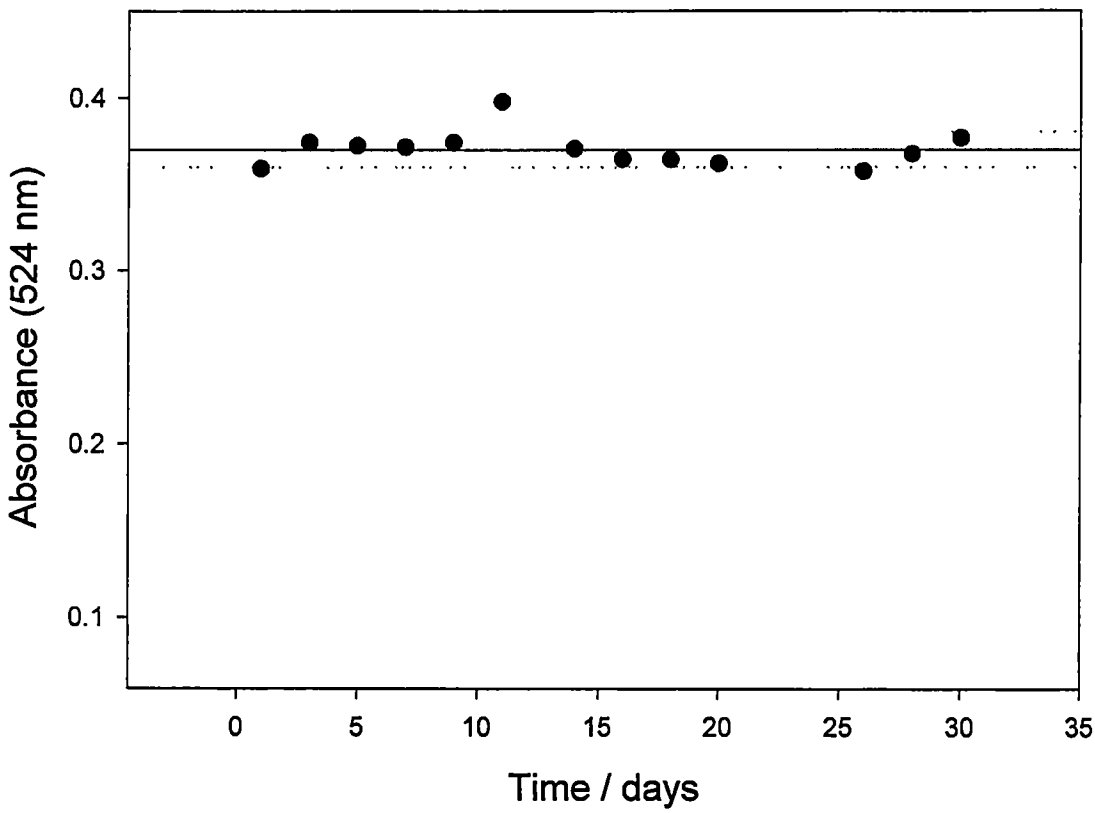

Figure 3.13. Long-term stability test of Sensor 7.

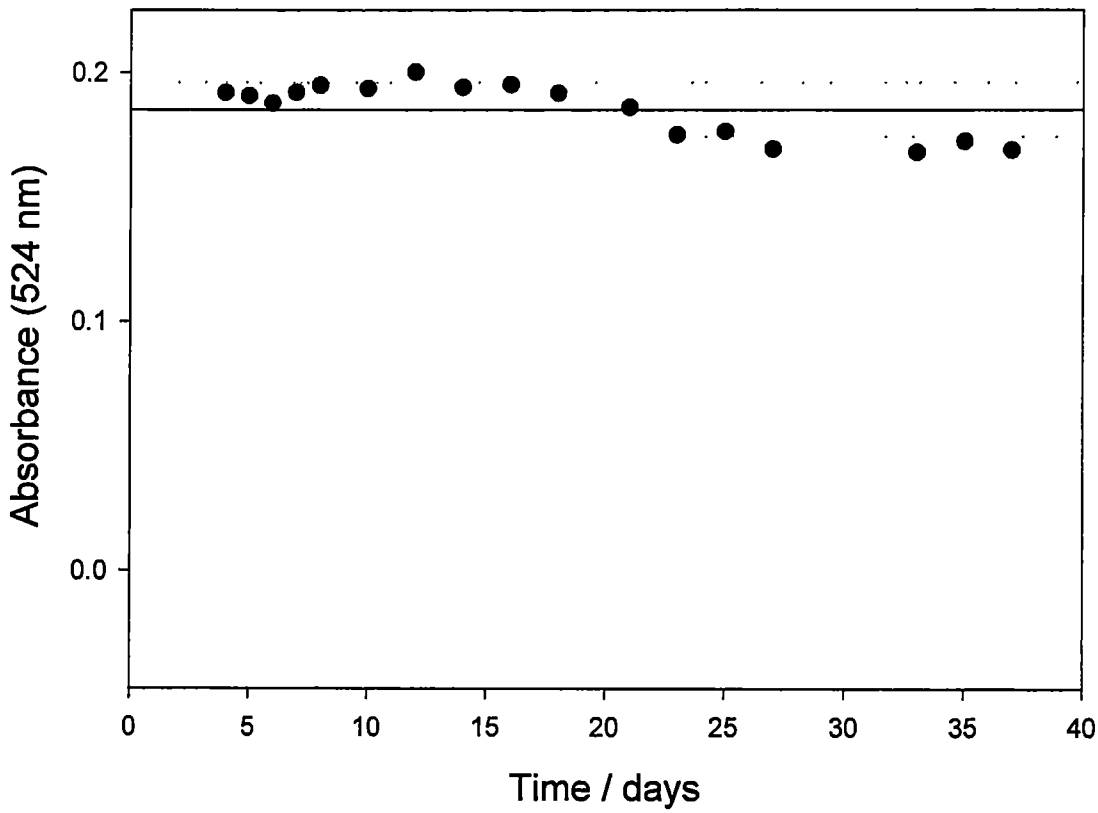

Figure 3.14. Long-term stability test of Sensor 8.

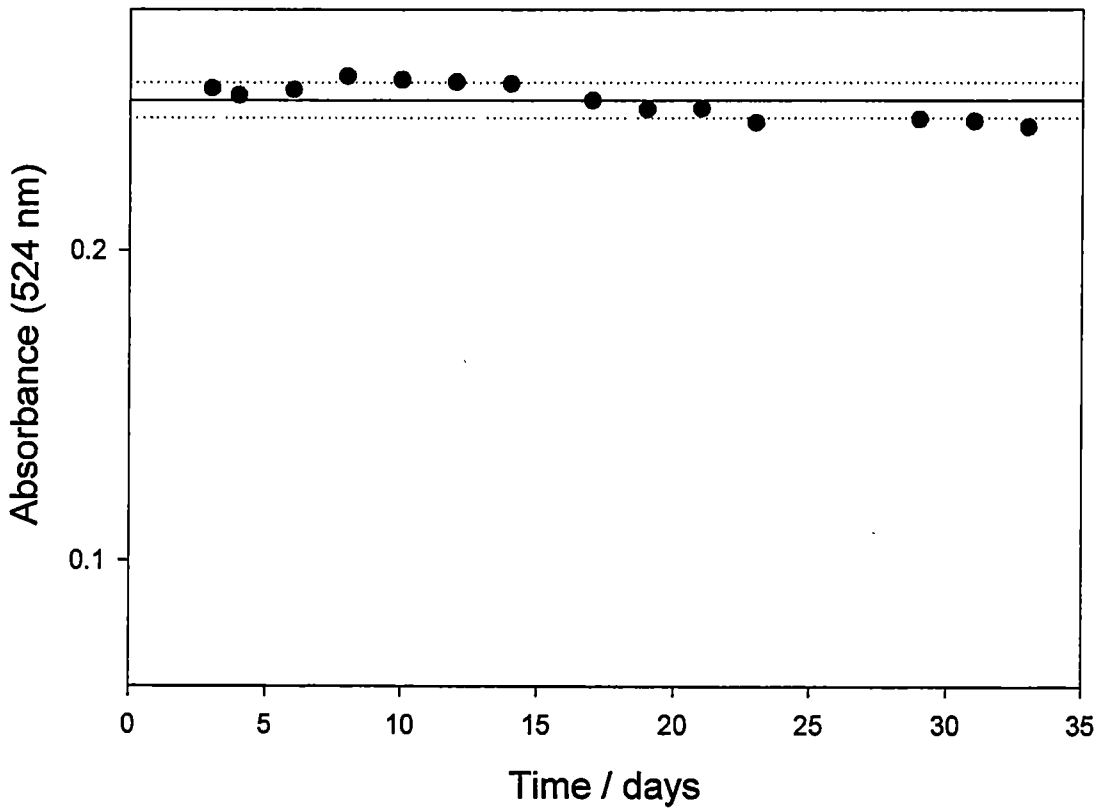

Figure 3.15. Long-term stability test of Sensor 9.

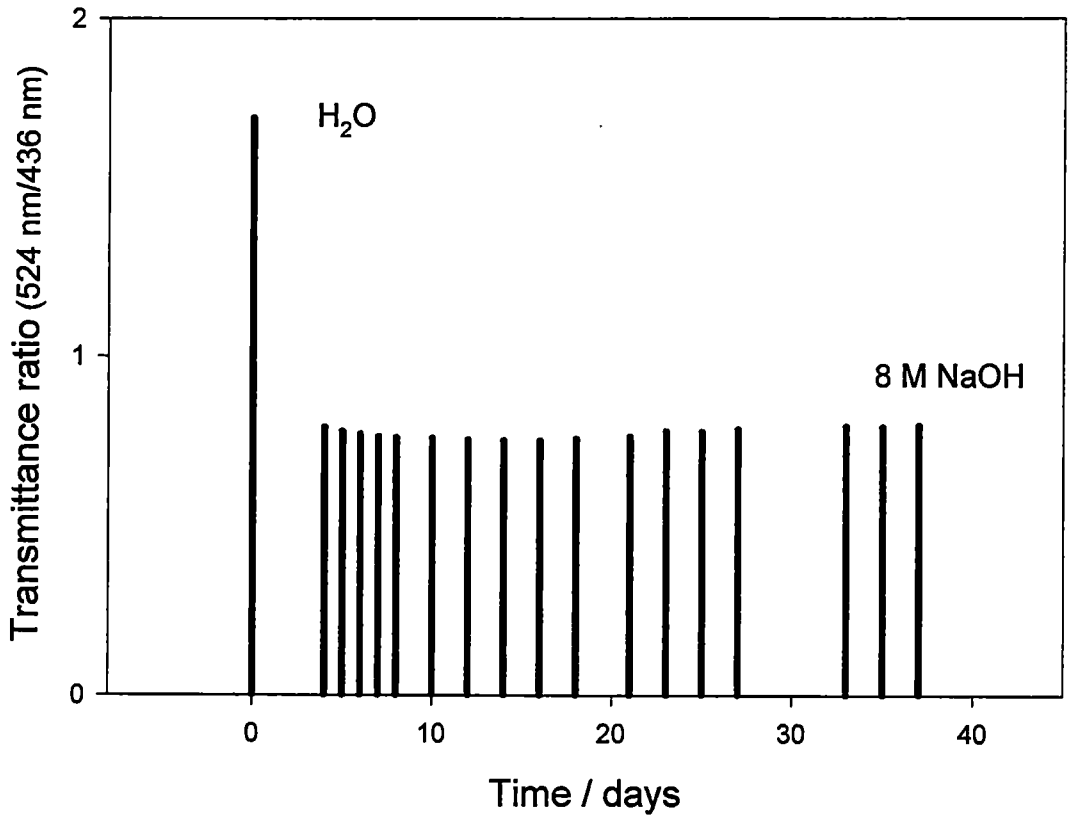

Figure 3.16. Long-term stability test of Sensor 8. Response was corrected by dividing the transmittance at λ_{max} by $\lambda_{isosbestic}$.

transducers are shown in Figures 3.17 and 3.18, respectively. The spectrometer error is also increased in comparison to transmittance measurements to ±0.15% (absorbance).

3.3.8 Effect of Ionic Strength

Alkali is often used in the presence of other salts. Since the dissociation constant of an indicator is a function of ionic strength, the presence of the salt is known to affect the ionic strength and thus the indicator response. In the H_2S scrubbing process, NaOH is used to neutralize the acid and sequester the toxic and odoriferous sulfide in the solution in order to reduce air pollution. In the scrubbing bath, the NaOH concentration diminishes as the product Na_2S is formed. To conduct a preliminary analysis of the influence of Na_2S on the sensor response, solutions of varying Na_2S and fixed NaOH at 2 M were prepared and measured by an Alizarin Yellow SiO_2/ZrO_2 sensor. The sensor absorbance has a linear dependence on the salt concentration (Figure 3.19). Na_2S is a weak base as well as a salt. Thus, two factors may give rise to the observed changes: the basicity increase by the weak base Na_2S and the ionic strength change by Na_2S.
An attempt was made to produce a sensor with negligible ionic strength dependence, and provide a better immobilization of the indicator in the polymer phase. Even at low pH, the deprotonated form of the indicator is predominant, and formation of an ionic pair with a cationic surfactant can significantly reduce the indicator solubility. In addition, the increase in electrical potential in the vicinity of the indicator by the doped surfactant could make the sensor less susceptible to signal alterations due to changes in ionic strength, an idea that has been successfully explored by Wolfbeis.[60] A sensor based on this idea was thus prepared containing Thiazole Yellow GGM and a stoichiometric

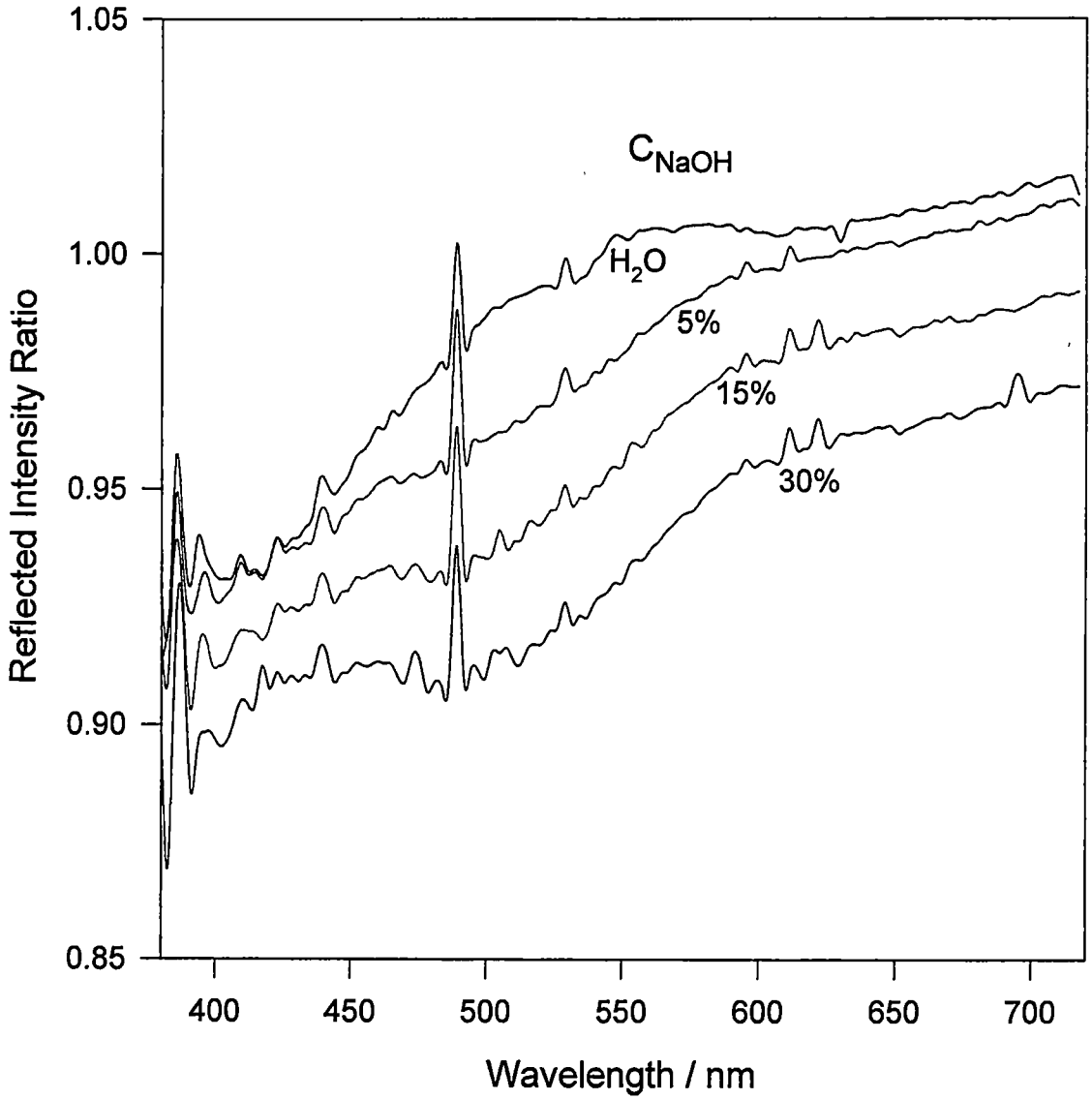

Figure 3.17. Typical reflectance spectra of Thiazole Yellow GGM-doped Sensor 14 in NaOH solutions (concentrations in % w/v).

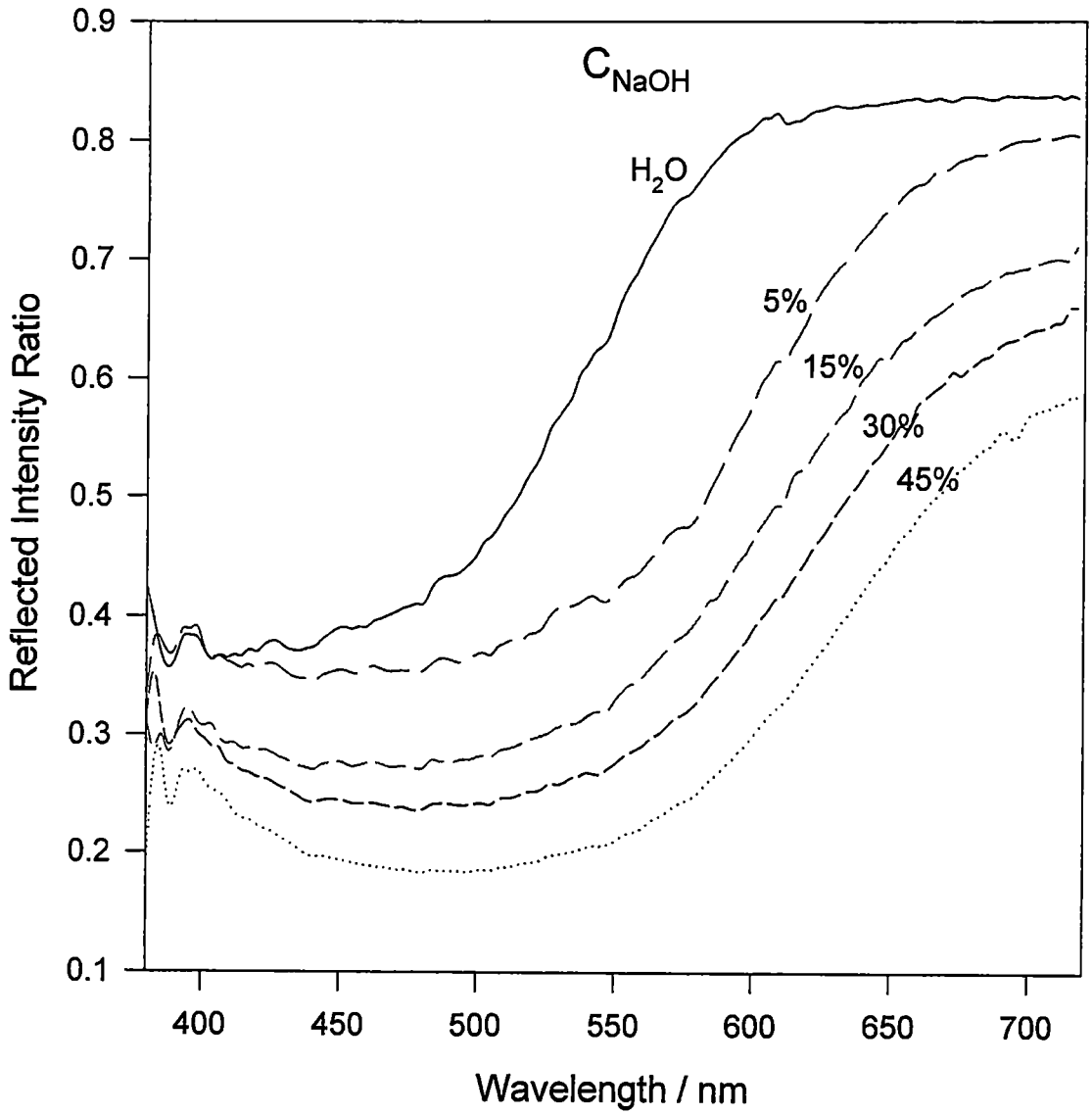

Figure 3.18. Typical reflectance spectra of Alizarin Yellow-doped Sensor 15 in NaOH solutions (concentrations in % w/v).

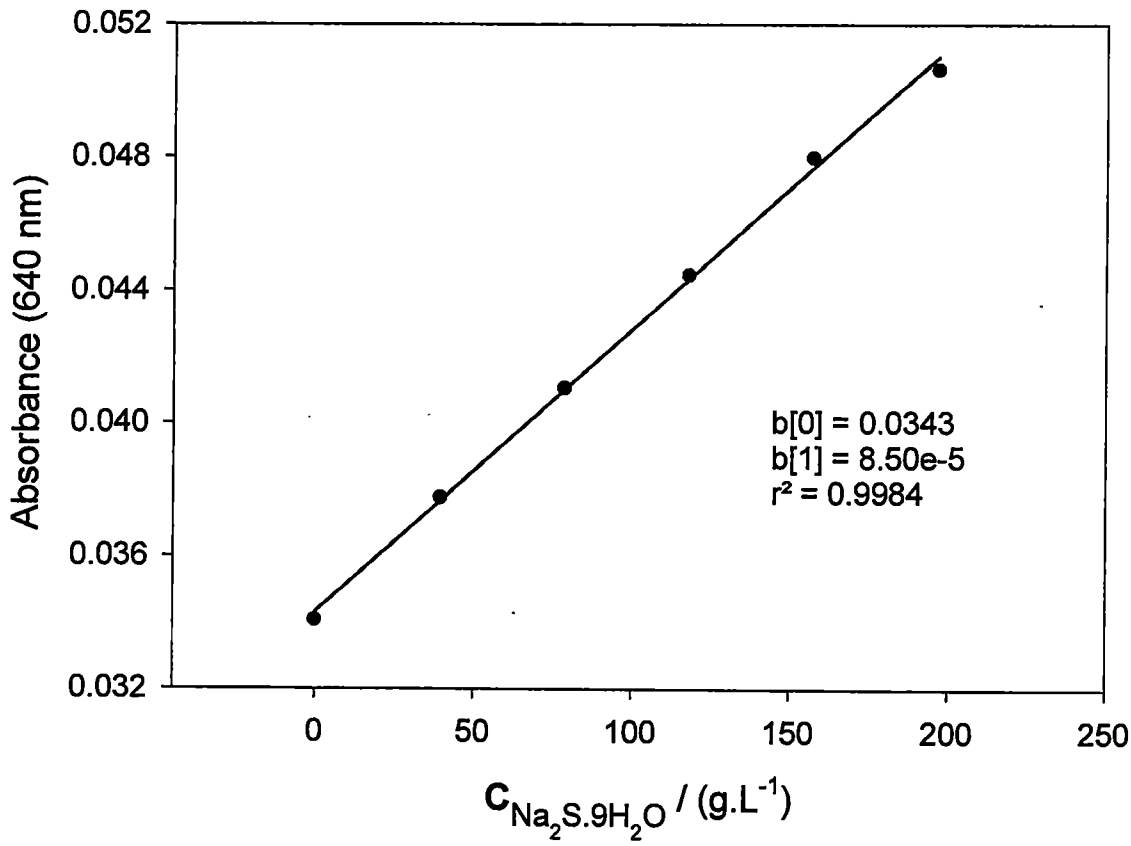

Figure 3.19. Effect of ionic strength: sensor response vs. Na_2S concentration. NaOH concentration was fixed at 2 M.

amount of a cationic surfactant. The p*K*a of the indicator shifted dramatically down, and the sensor produced color changes at pH < 12, making it inapplicable for concentrated hydroxide measurement.

Salt effects were also observed in the measurements using our acid sensors (Chapter 4). A successful dual-sensor approach was developed to accurately measure acidity in the presence of salts. This subject is discussed in Chapter 4.

CHAPTER 4

Optical Sensors and the Salt Effect: A Dual-Transducer Approach to Acidity Determination in Salt-Containing Concentrated Strong Acids

4.1 Introduction

Optical sensors are of intense current interest due in part to the recent development of low cost opto-electronics and optical fibers. Optical sensors are now used to measure analytes in multi-component systems. In such systems, it is desirable to measure each component accurately and minimize or compensate interference from others.

In general, the response of optical sensors that are based on indicator equilibria as the transducing mechanism, is significantly affected by changes in ionic strength *I*. Variations in ionic strength shift the indicator equilibrium in an optical sensor, and thus change the optical parameters such as indicator absorbance. As Rilbe aptly put, "it varies with the milieu in which the protolyte dwells."[59] Furthermore, these changes in the optical parameters caused by ionic strength are often indistinguishable from signal changes caused by the analyte.

Edmonds and coworkers have shown that an increase in ionic strength from 0.01 to 3.00 M can shift the p*K*a' value by as much as 1.23 units.[61] If no correction for ionic strength is made, the ionic strength of the sample has to be kept constant during calibration and pH measurements. Optiz and Lubbers have developed an approach

employing a dual pH fluorescence indicator system that is based on indicators with different relationships between p*K*a and ionic strength.[62] These relationships yielded two independent equations to measure both the ionic strength and pH.[2d] However, such relationships are highly non-linear, thus limiting the use of regression analysis. In addition, this approach using pH fluorescence indicators was suitable for low-medium ionic strength (0.1 – 1 M) and near neutral pH (6.5 – 7.5).

In another approach developed by Wolfbeis, a combination of sensors was used to measure both pH and ionic strength, through two independent pH measurements.[63] The method was based on covalent immobilization of a dye onto porous glass supports with distinct surface chemistries. In one sensor, the environment around the indicator was non-charged, whereas in the other sensor, a highly charged environment surrounded the indicator. The charged environment made the indicator chemical equilibrium less susceptible to further changes in ionic strength. In other words, the sensor was desensitized to changes in salt concentration.

A sensor array has been recently reported using a multi-coated sensor surface integrated with a CCD (charge coupled device) detector to simultaneously determine the concentrations of different analytes (pH, Ca^{+2}, Ce^{+3}, and fructose).[64] In this approach, there is a non-specific transducer for each analyte, and a set of independent equations containing an equal number of variables are solved to yield the concentrations of the analytes. Although not stated in this paper, effects of, e.g., temperature and ionic strength could also, *a priori*, be treated by increasing the number of independent equations, i.e., transducers.

Another approach to ionic strength measurement based on an optical reflection interference filter coated on a swelling polymer has been reported, where the degree of swelling is a function of ionic strength.[65]

These reported approaches to correct ionic strength in optical sensing were designed for the pH region and solutions of low-medium ionic strength.[62-65] Some of the approaches are based the Debye-Hückel theory, and thus valid for low ionic strength.[62-63]

Concentrated strong acids such as HCl, which are among the largest volume chemicals manufactured in the world, are widely used in many chemical processes.[12a,13a] However, rapid and reliable methods for their on-line determination and quality control are limited, as discussed in Chapter 2. Concentrated strong acids such as HCl are often used in the presence of other chemicals (salts), and the ionic strength changes by these salts further complicate the acidity measurement. We have developed a fast and reversible acid sensor (Chapter 2) for highly acidic solutions ($[H^+] = 1 - 11$ M), capable of measuring HCl concentrations in, e.g., industrial pickling solutions containing large amounts of $FeCl_2/FeCl_3$. Although we could minimize the wavelength interference by the strongly absorbing $FeCl_3$, the change in ionic strength by $FeCl_3$ was found to be a considerable source of analytical error and had to be addressed to give the accurate acidity in such systems. The salt concentrations used in these systems far surpass the limits of the Debye-Hückel approximation and thus the previous approaches.[61,62,64,65] This prompted us to develop a new approach to accurately measure acid and salt concentrations in salt-containing, highly acidic solutions. Using transducers that have a different dependence on I, the signal array can be deconvoluted to give information on the true acid concentration and the ionic strength deviation. The dual transducer approach

requires a decomposition algorithm that utilizes the combination of different sensors. To enhance the signal decomposition capability, we used a combination of sensors with very distinct ionic strength dependencies. In addition, sensors with dynamic intervals that are complementary and superimposing enhance the measurement precision when monitoring solutions with a large range of acid concentration.

We describe here a novel linear relationship between $\left(\partial A/\partial C_{salt}\right)_{C_{acid}}$ and $\left(dA/dC_{acid}\right)_{C_{salt}=0}$ and a dual-transducer approach based on this relationship to obtain the acid and salt concentrations in salt-containing concentrated strong acids. This new approach has been used to measure acid and salt concentrations in solutions with a salt contribution of up to 4.5 M to ionic strength.

4.2 Experimental Section

Visible spectra were recorded using the spectroscopic system described in Chapter 1. Solutions of HCl and HCl/$CaCl_2$ were prepared by gravimetric dilution and titrated with NaOH standards to the phenolphthalein end point. All chemicals (Aldrich, Sigma, Scientific Polymer Products, and Mallinckrodt) were used as received. $CaCl_2.2H_2O$ was kept at 45 °C for one week prior to its use. Organic solvents were dried according to standard laboratory purification techniques.[53] Sensor 2 (Bromocresol Purple), Sensor 3 (Fastgreen FCF), Sensor 4 (Bromocresol Green), and Sensor 5 (Acid Blue 147) in Chapter 2 were used in the current studies. Data analysis was conducted with Sigma Plot (SPSS Inc., 233 S. Wacker Drive, 11th Floor, Chicago, IL 60606-6307;

http://www.spss.com) and Matlab (The MathWorks, Inc., 3 Apple Hill Drive, Natick, MA 01760-2098; http://www.mathworks.com) programs.

Conductance measurements were obtained using a YSI model 35 conductimeter, with an in-house assembled electrode cell. The cell electrodes consisted of two parallel Pt foil squares (0.25 cm^2) separated by 1.0 cm. The cell constant was calibrated with standard KCl solutions and determined to be 0.785 ± 0.003 cm^{-1}.

4.2.1 Preparation of Sensor 16

Neutral Red (12 mg) was dissolved in a mixture of HCl (100 μL, 0.01 N), dry MeOH (40 μL), and 158 mg of Nafion solution (a 5% dispersion of Nafion polymer in an alcoholic mixture containing 10% w/w of H_2O), with stirring. $Si(OMe)_4$ (300 μL) was then added and the mixture was stirred for 46 h. At this point, the solution was coated onto a glass surface through a spin coating process (1650 rpm). The sensor films were left to cure in air at room temperature. After one day at ambient conditions the films were heated to 45 °C for five days to give Sensor 16.

4.2.2 Measurement Procedure

The sensor element, an indicator-doped film coated onto a glass slide, was mounted in a Teflon cell, leaving a 0.7 mm space along the optical path for contact with the flowing liquid sample.

4.3 Results and Discussion

4.3.1 The Transducing Mechanism

There are two issues to be considered in acidity measurement in salt-containing concentrated strong acids: how proton activity varies in concentrated acid, an issue already addressed by the Hammett indicator acidity functions, and how proton activity is affected by ionic strength. The latter has been approached, to a small extent, in the study of the acidity functions of some indicators.[66,67]

The transducing mechanism of the sensor depends on the acid-base equilibrium (Eq. 4.1) of an indicator that is positively charged in concentrated acid.

$$HInd^+ + H_2O = Ind + H_3O^+ \qquad (Ka) \qquad \text{(Eq. 4.1)}$$

$$Ka = \frac{\{H_3O^+\}\{Ind\}}{\{HInd^+\}} \qquad \text{(Eq. 4.2)}$$

where {S} is the activity of species S.

*K*a, the thermodynamic dissociation constant in terms of activities, is independent of ionic strength or solvent. However, since individual activities cannot be independently measured (Chapter 1, Section 1.4), the stoichiometric dissociation constant, *K*a" (also known as the mass-action constant), is often used for convenience. In such a case, *K*a" is no longer a true constant, but will be dependent on the solution ionic strength and dielectric constant.

$$Ka'' = \frac{[H_3O^+][Ind]}{[HInd^+]} = \frac{C_{acid}[Ind]}{[HInd^+]} \qquad (C_{acid} = [H_3O^+]) \qquad \text{(Eq. 4.3)}$$

For dilute electrolyte solutions, the variations in p*K*a" can be correlated with *I*, the solution ionic strength ($I = 0.5 \sum c_i.z_i^2$; c_i = concentration of species i; z_i = valence of species i) through a simple relationship that depends on the number and type of charged species produced by the indicator protic equilibrium. For dilute solutions (< 0.1 M), the effect of *I* on the dissociation constants can be estimated for the different types of charged indicators, as shown below:[34c]

$$HInd^+ \rightleftharpoons H^+ + Ind \qquad pKa' = pKa'' + 0.5 \cdot I^{1/2} \qquad \text{(Eq. 4.4)}$$

$$HInd \rightleftharpoons H^+ + Ind^- \qquad pKa' = pKa'' - 0.5 \cdot I^{1/2} \qquad \text{(Eq. 4.5)}$$

$$Hind^- \rightleftharpoons H^+ + Ind^{2-} \qquad pKa' = pKa'' + 1.5 \cdot I^{1/2} \qquad \text{(Eq. 4.6)}$$

As a consequence, indicators that have neutral or zwitterionic forms in the protic equilibrium have a minimal dependence on ionic strength.

For more concentrated electrolytes (*I* < 0.5 M), the changes in p*K*a" due to ionic strength can be expressed by the following Debye-Hückel equation:[62]

$$pKa = pKa'' + (2\nu + 1) \cdot \left[\frac{C \cdot \sqrt{I}}{B \cdot d \cdot \sqrt{I}} \right] \qquad \text{(Eq. 4.7)}$$

where ν is the valence, C is a temperature-dependent constant, and B and d are molecular parameters.

Solutions with higher ionic strength ($I > 0.5$ M) cannot be adequately treated with the Debye-Hückel approximation, and empirical relationships are often used instead.

The molar concentration of a chemical species S, denoted by [S], can be correlated to its activity through the expression $\{S\} = f[S]$, where f is the activity coefficient for species S. Thus, $Ka = \gamma Ka''$ where γ is the activity coefficient ratio of the species involved in the equilibrium, and a function of ionic strength I. Because ionic strength changes Ka'', and shifts the equilibrium in Eq. 4.1, it changes optical parameters such as absorbance A that measure, e.g., $[HInd^+]$. The variations in the optical signal due to ionic strength changes cannot thus be isolated from those caused by the analyte H^+. In other words, ionic strength is potentially a considerable source of error if not accounted for. The activity coefficients are generally smaller than unity in dilute solutions, but as the ionic concentration increases, they approach a minimum and rise sharply afterwards.[59] Thus the pH scale appears greatly expanded for solutions of concentrated strong acids, a fact very noticeable in any Hammett indicator acidity function.

Although the acid concentration in the range of 1 – 11 M changes by more than one order of magnitude, the proton activity in fact varies by about 3.5 orders of magnitude (in the case of HCl). This is a unique behavior of concentrated acid solutions explored by Hammett six decades ago.[10]

$Ind_T = [HInd^+] + [Ind]$ $\quad\quad$ Ind_T = total concentration of the indicator

A, the absorbance, is proportional to the concentration of the protonated form of the indicator: $A = \kappa[\mathrm{HInd}^+]$. Thus the plot of A vs. C_{acid} is theoretically a nonlinear function shown in Eq. 4.8.

$$A = \frac{\kappa \cdot \mathrm{Ind}_T \cdot [\mathrm{H}^+]}{Ka'' + [\mathrm{H}^+]} = \frac{\kappa \cdot \mathrm{Ind}_T \cdot C_{acid}}{Ka'' + C_{acid}} \qquad \text{(Eq. 4.8)}$$

Since the Hammett indicator acidity function H_0 is defined as $H_0 = \mathrm{p}Ka - \log([\mathrm{HInd}^+]/[\mathrm{Ind}]) = -\log(\gamma C_{acid})$,[11,66a] Eq. 4.8 can be converted into Eq. 4.9. In other words, when the activities are considered, the plot of A vs. acidity (10^{-H_0}) is different from that of A vs. C_{acid}.

$$A = \frac{\kappa \cdot \mathrm{Ind}_T \cdot \gamma 10^{-H_0}}{Ka'' + \gamma 10^{-H_0}} = \frac{\kappa \cdot \mathrm{Ind}_T \cdot 10^{-H_0}}{Ka + 10^{-H_0}} \qquad \text{(Eq. 4.9)}$$

Thus an optical sensor that bases its transducing mechanism on a chemical (indicator) equilibrium may show a nonlinear relationship between its analytical signal and analyte concentration, as is the case (Eq. 4.8) of acid indicators. In addition, when ionic strength is included in high acidity measurements, Eq. 4.9 gives the theoretical relationship between A and the Hammett indicator acidity function H_0. For our Bromocresol Purple (BCP) sensor (Sensor 2), the experimental plots of A vs. C_{acid}, and A vs. 10^{-H_0} are shown in Figures 4.1 and 4.2, respectively.

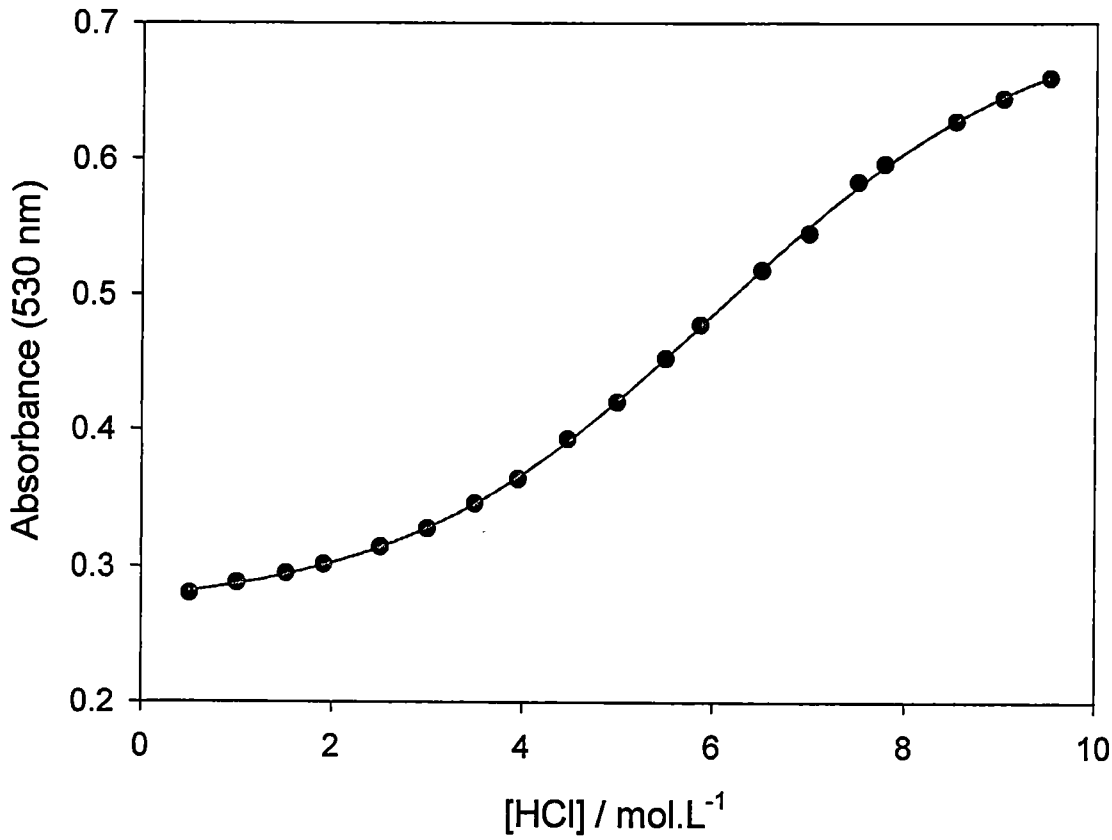

Figure 4.1. Calibration plot of *A* vs. [HCl] for Bromocresol Purple Sensor 2.

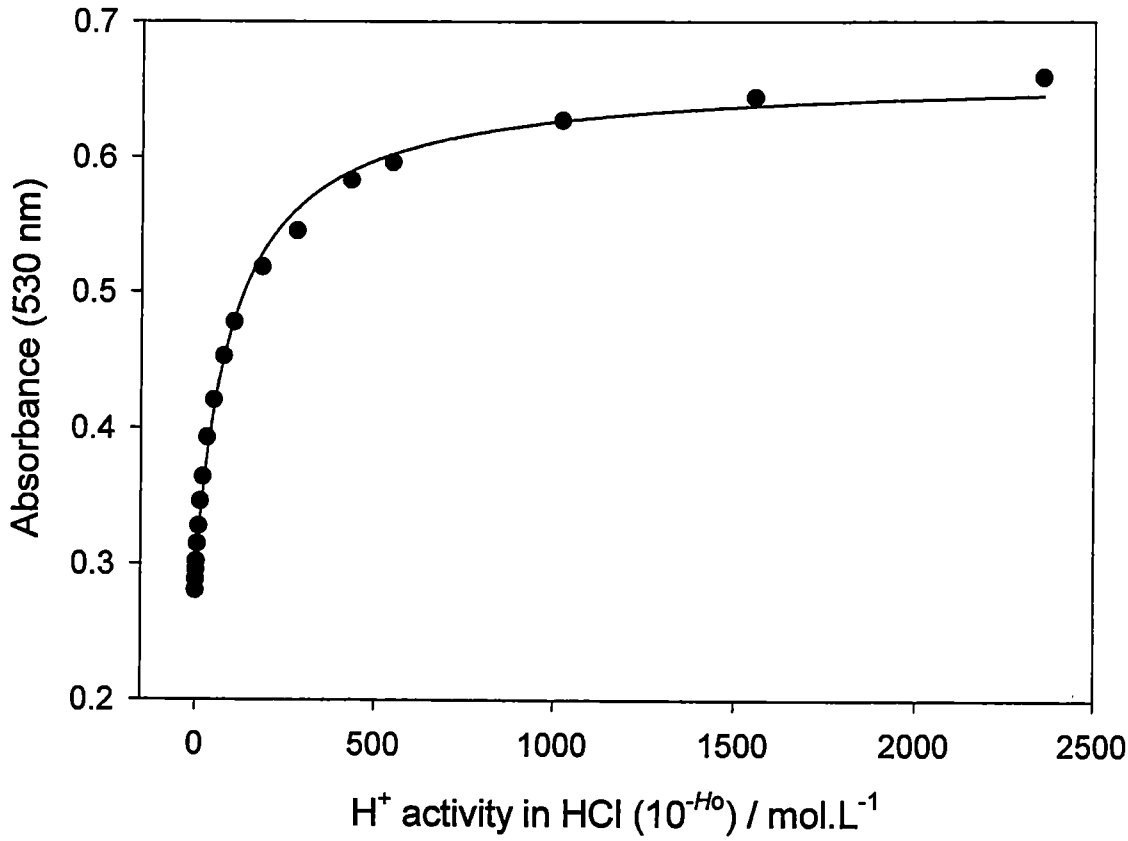

Figure 4.2. Theoretical plot of A vs. 10^{-H_0} for Sensor 2. H_0 is a Hammett acidity function for HCl.

The non-linear relationship between analytical signal and analyte concentration in optical sensors contrasts with the more common linear (or logarithmic) relationship found in other transducing mechanisms. For example, electrochemical sensors rely on a logarithmic relationship between electrode potential and hydrogen ion activity: $E = E^{\circ} + E_j + RT \cdot \ln\{H^+\}$. E is a direct function of hydrogen ion activity $\{H^+\}$ through the diffusion potential of H^+ ions, which does not depend on the ionic strength. In addition, only the junction potential, E_j, which has a small contribution to E, has a dependence on ionic strength.[44] Thus ionic strength has a much smaller effect on electrochemical pH measurements than on the indicators in optical sensors. This is the underlying reason why pH optical sensors are less accurate than their electrochemical counterparts in the normal pH range, a subject already explored by Janata.[44] However, in concentrated acid or base solutions at the extreme pH, electrochemical measurements are not reliable, and currently there is no reliable approach to acidity measurements in salt-containing concentrated strong acids.

4.3.2 The Salt-Effect

We observed that when a large amount of a neutral salt (e.g. $CaCl_2$) was added to an acid solution of a fixed concentration, the absorbance of the sensor monitoring the acid concentration varied proportionally to the amount of the added salt. Such responses for Fastgreen FCF and Bromocresol Green sensors (Sensors 3 - 4) are shown in Figures 4.3 and 4.4, respectively.

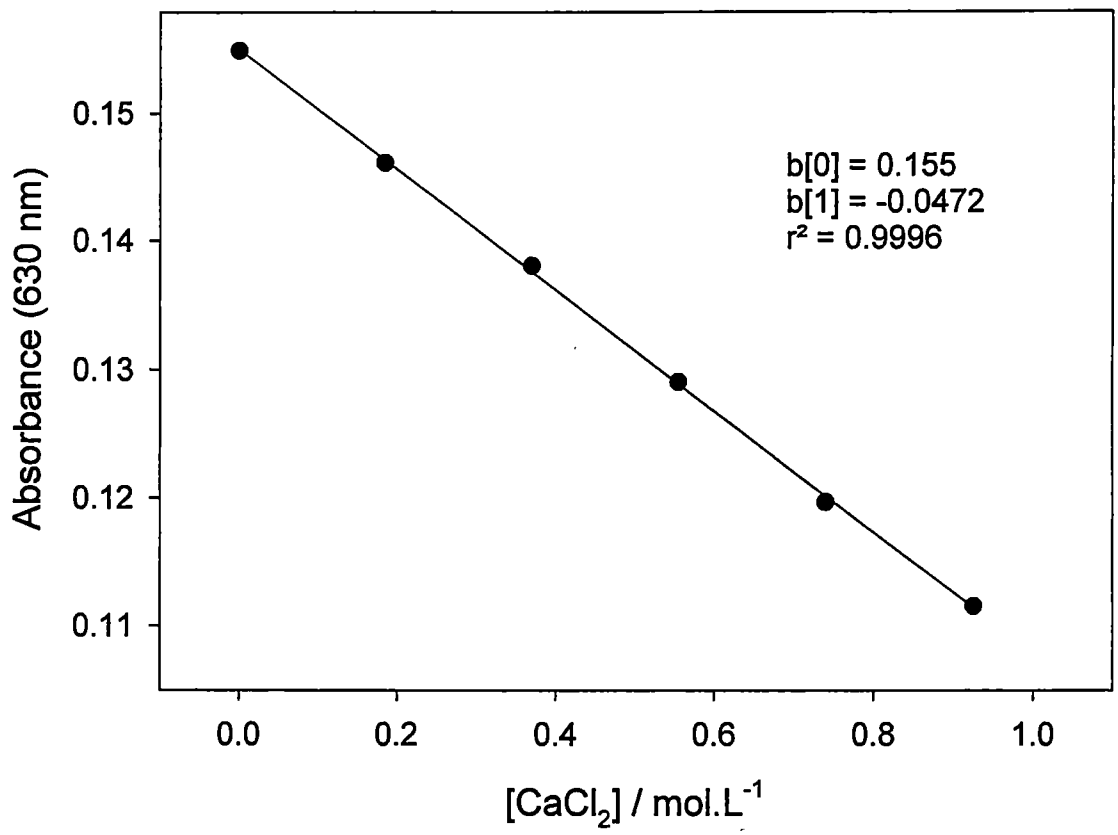

Figure 4.3. Response of Fastgreen FCF Sensor 3 in $CaCl_2$/HCl solutions ([HCl] = 2.42 M).

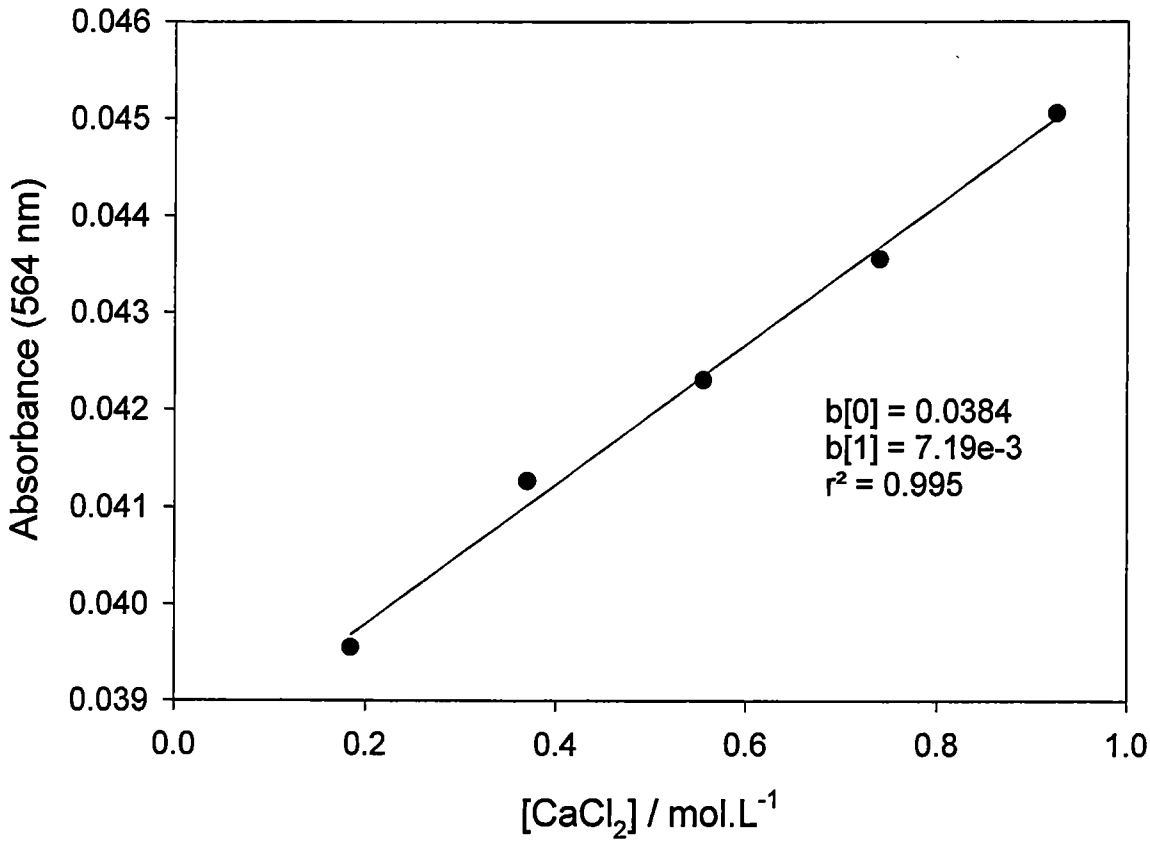

Figure 4.4. Response of Bromocresol Green Sensor 4 in $CaCl_2$/HCl solutions ([HCl] = 2.42 M).

4.3.3 Dual Optical Transducer Approach

Figures 4.5, 4.6, and 4.7 show 3-dimensional experimental plots of A vs. C_{acid} and C_{salt} ($CaCl_2$) for three different sensors: Bromocresol Purple Sensor 2, Acid Blue 147 Sensor 5, and Neutral Red Sensor 16, respectively. We found that the slope of A vs. C_{salt} at a given acid concentration, $\left(\partial A/\partial C_{salt}\right)_{C_{acid}}$, was proportional to the respective tangent of the A vs. C_{acid} plot for a salt-free acid solution, $\left(dA/dC_{acid}\right)_{C_{salt}=0}$. This was later confirmed by the linear relationship observed between the calculated slopes of A vs. C_{salt} plots and the first derivatives of A vs. C_{acid} curves. The linear plots depicting this differential relationship for the three sensors are shown in Figures 4.8, 4.9, and 4.10. These observations led to a new relationship, shown in Eq. 4.10.

$$\left(\partial A/\partial C_{salt}\right)_{C_{acid}} = \beta \cdot \left(dA/dC_{acid}\right)_{C_{salt}=0} \qquad \text{(Eq. 4.10)}$$

This novel relationship forms the basis to estimate acid (C_{acid}) and salt concentration (C_{salt}) in a salt-containing concentrated strong acid.

For each of the three sensors in salt-free ($C_{salt}=0$) acid solutions, the plot of A vs. C_{acid} such as Figure 4.1 for Sensor 2, could be fitted by an empirical sigmoid curve in Eq. 4.11. We found that the high acid concentrations C_{acid} do not allow the experimental data to fit the theoretical equation in Eq. 4.8.

$$A = A^{\circ} + \frac{a}{1 + e^{(b - C_{acid})/c}} \qquad A^{\circ}, a, b \text{ and } c \text{ are constants} \qquad \text{(Eq. 4.11)}$$

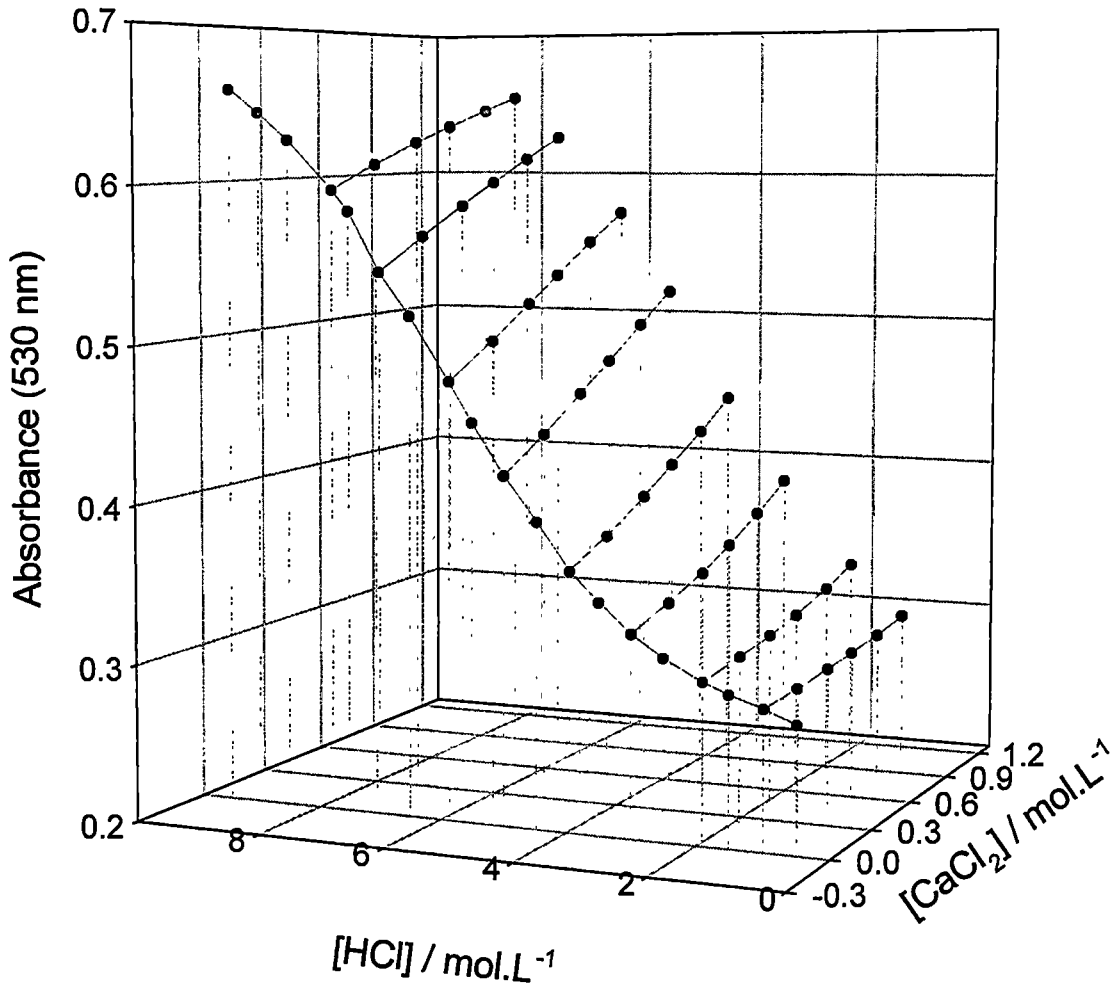

Figure 4.5. Response of Bromocresol Purple Sensor 2 in $CaCl_2$/HCl solutions.

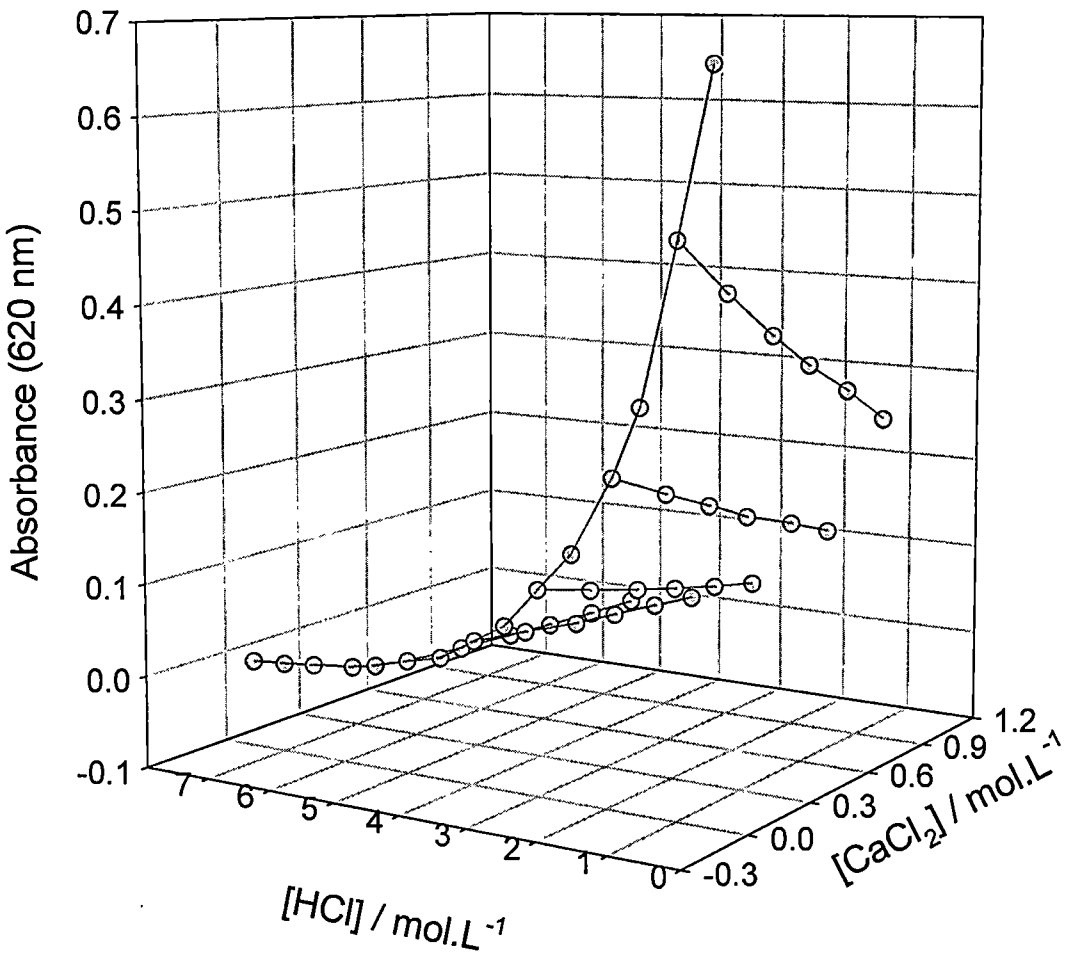

Figure 4.6. Response of Acid Blue 147 Sensor 5 in $CaCl_2$/HCl solutions.

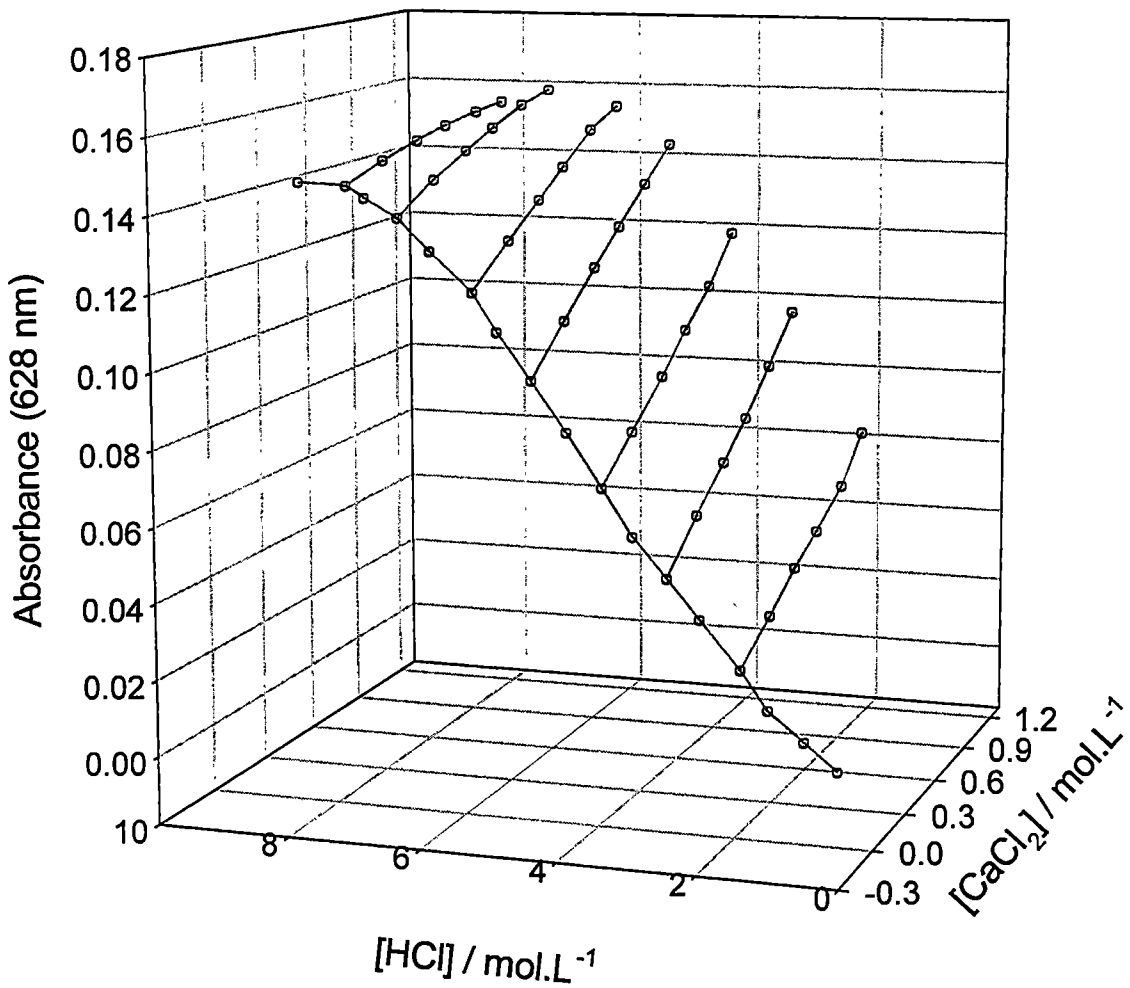

Figure 4.7. Response of Neutral Red Sensor 16 in $CaCl_2$/HCl solutions.

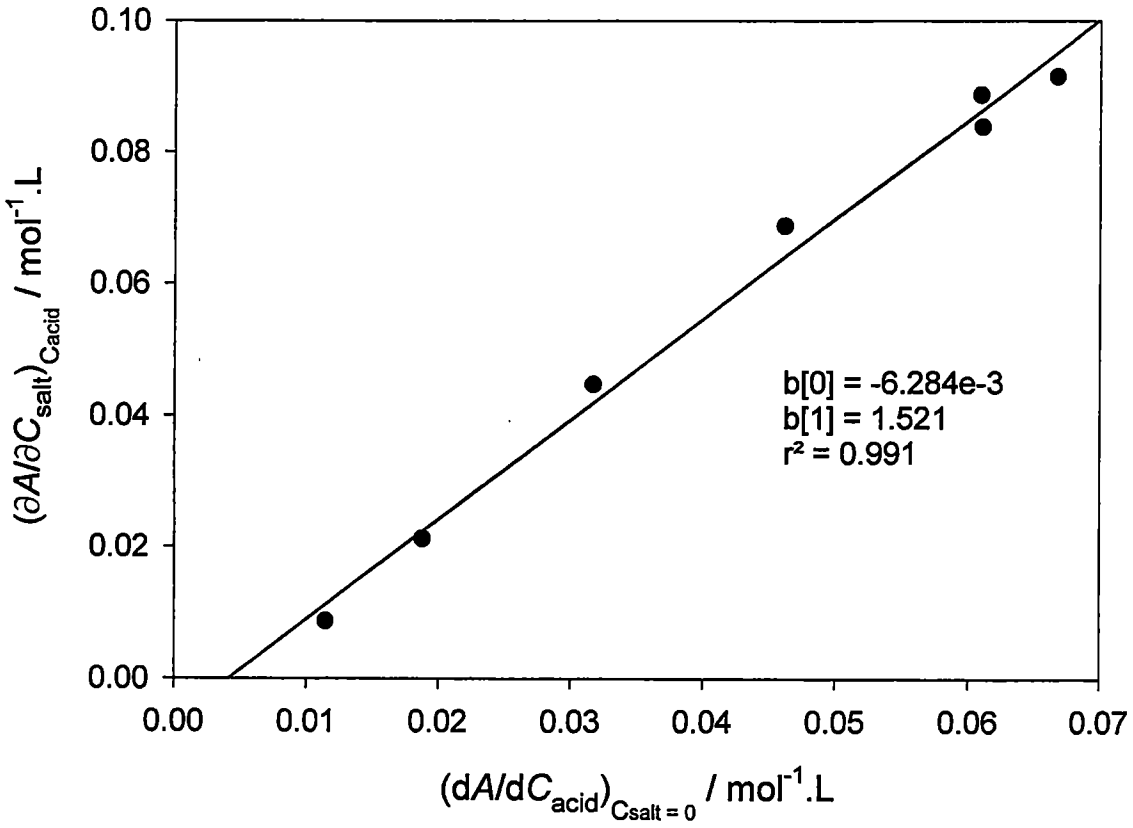

Figure 4.8. Plot of $\left(dA/dC_{acid}\right)_{C_{salt}=0}$ vs. $\left(\partial A/\partial C_{salt}\right)_{C_{acid}}$. A is the absorbance of Sensor 2 in $CaCl_2$/HCl solutions.

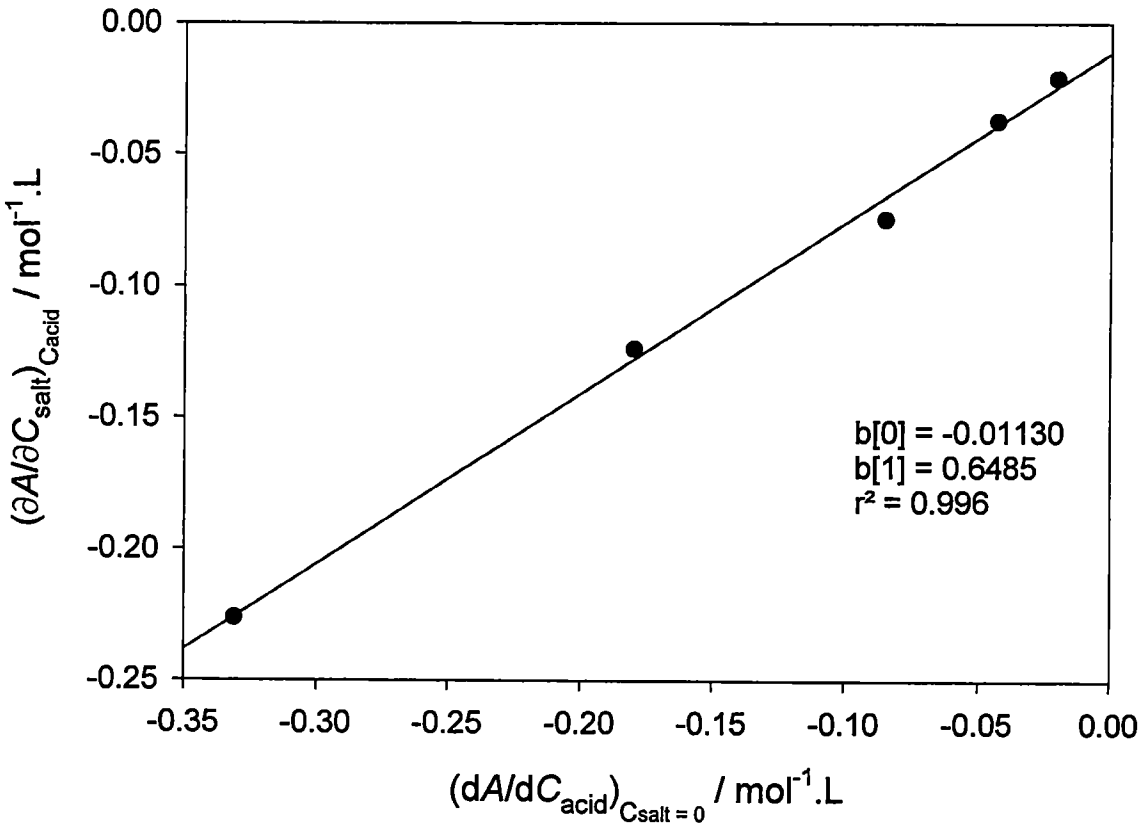

Figure 4.9. Plot of $\left(dA/dC_{acid}\right)_{C_{salt}=0}$ vs. $\left(\partial A/\partial C_{salt}\right)_{C_{acid}}$. A is the absorbance of Sensor 5 in $CaCl_2$/HCl solutions.

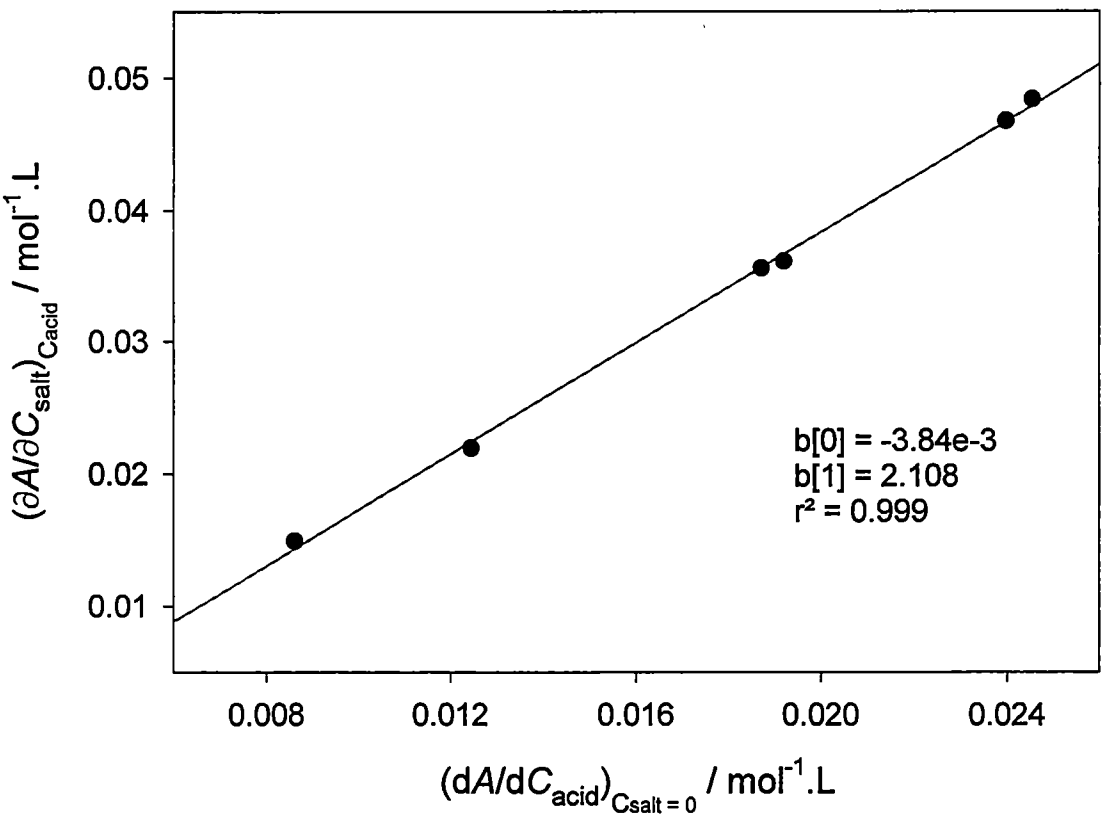

Figure 4.10. Plot of $\left(dA/dC_{acid}\right)_{C_{salt}=0}$ vs. $\left(\partial A/\partial C_{salt}\right)_{C_{acid}}$. A is the absorbance of Sensor 16 in $CaCl_2$/HCl solutions.

$$\left(dA/dC_{acid}\right)_{C_{salt}=0} = \frac{a \cdot e^{(b - C_{acid})/c}}{c[1 + e^{(b - C_{acid})/c}]^2} \qquad \text{(Eq. 4.12)}$$

The addition of a salt will lead to an increase in absorbance by ΔA, which, in our systems, is proportional to the salt concentration C_{salt}:

$$\Delta A = \left(\partial A/\partial C_{salt}\right)_{C_{acid}} \cdot C_{salt} \qquad \text{(Eq. 4.13)}$$

$\left(\partial A/\partial C_{salt}\right)_{C_{acid}}$, a constant at a given C_{acid} in our systems, was found to vary with C_{acid}. The total absorbance A^{tot} is thus:

$$A^{tot} = A + \Delta A = A^{\circ} + \frac{a}{1 + e^{(b - C_{acid})/c}} + \left(\partial A/\partial C_{salt}\right)_{C_{acid}} \cdot C_{salt} \qquad \text{(Eq. 4.14)}$$

Using the novel relationship (Eq. 4.10) observed in the current study, $\left(\partial A/\partial C_{salt}\right)_{C_{acid}}$ can be replaced by $\beta\left(dA/dC_{acid}\right)_{C_{salt}=0}$ to give Eq. 4.15

$$A^{tot} = A + \Delta A = A^{\circ} + \frac{a}{1 + e^{(b - C_{acid})/c}} + \beta \cdot \left(\partial A/\partial C_{acid}\right)_{C_{salt}=0} \cdot C_{salt}$$

$$= A^{\circ} + \frac{a}{1 + e^{(b - C_{acid})/c}} + \beta \cdot \frac{a \cdot e^{(b - C_{acid})/c}}{c[1 + e^{(b - C_{acid})/c}]^2} \cdot C_{salt}$$

or using $z(C_{acid}) = e^{(b - C_{acid})/c}$

$$A^{tot} = A^{\circ} + \frac{a}{1 + z(C_{acid})} + \beta \cdot \frac{a \cdot z(C_{acid})}{c \cdot [1 + z(C_{acid})]^2} \cdot C_{salt} \qquad \text{(Eq. 4.15)}$$

By using at least two different (and thus independent) transducers, represented by the subscripts 1 and 2, the following two equations and two variables (C_{acid} and C_{salt}) are obtained:

$$A_1^{tot} = A_1^{\circ} + \frac{a_1}{1 + z_1(C_{acid})} + \beta_1 \cdot \frac{a_1 \cdot z_1(C_{acid})}{c_1 \cdot [1 + z_1(C_{acid})]^2} \cdot C_{salt} \qquad \text{(Eq. 4.16)}$$

$$A_2^{tot} = A_2^{\circ} + \frac{a_2}{1 + z_2(C_{acid})} + \beta_2 \cdot \frac{a_2 \cdot z_2(C_{acid})}{c_2 \cdot [1 + z_2(C_{acid})]^2} \cdot C_{salt} \qquad \text{(Eq. 4.17)}$$

The solutions to this set of highly non-linear equations could be obtained through a series of iterations. A program (Appendix B) was written in Matlab to calculate C_{acid} and C_{salt} for given A_1^{tot} and A_2^{tot}.

An initial C_{acid}(est) was obtained from A vs. C_{acid} curve for the salt-free HCl. Due to the salt contribution to A, the initial C_{acid}(est) was larger than the actual C_{acid}. The program then changed C_{acid}(est) in small decremental steps to calculate C_{acid}(est) and C_{salt}(est). Thus, for a given A^{tot} of each sensor, the iteration program yields a curve of C_{acid}(est) vs. C_{salt}(est). The interception of the two independent curves for two sensors gives C_{acid} and C_{salt}. The use of Sensors 2 and 16 for C_{acid} and C_{salt} determination in a $CaCl_2$-containing HCl solution is given in Figure 4.11.

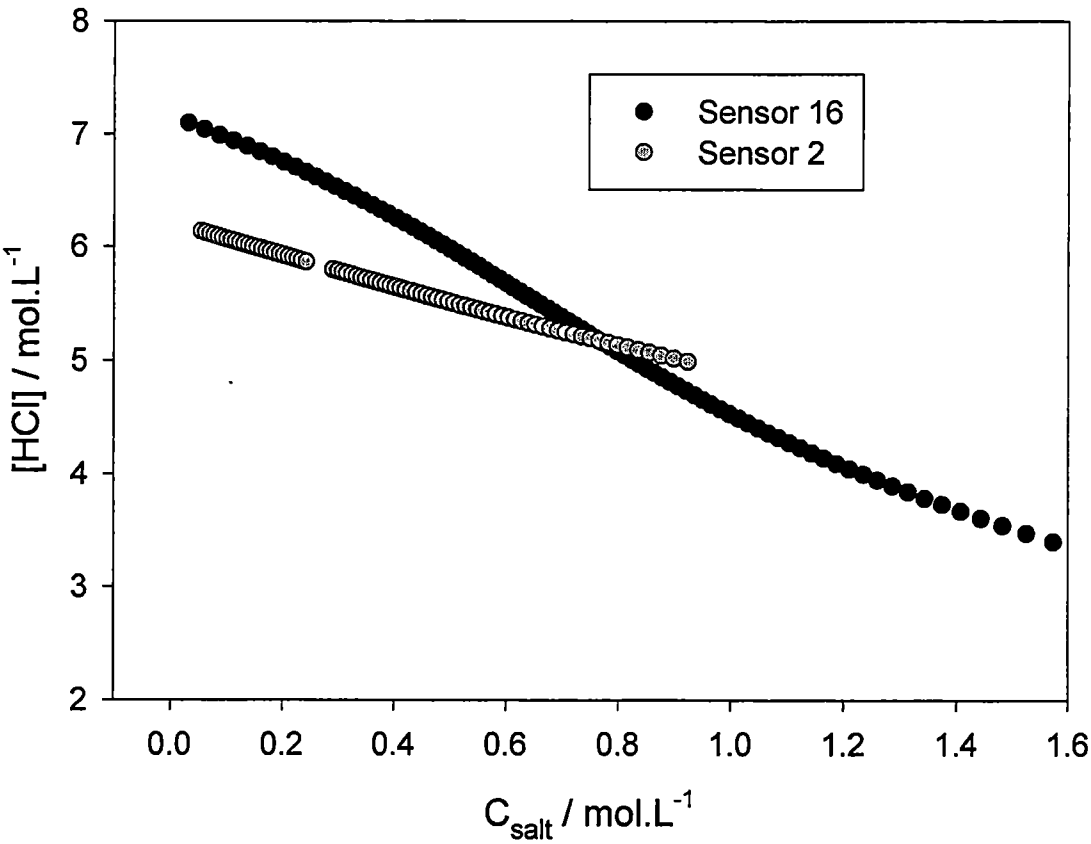

Figure 4.11. Plots of computed (C_{salt}, [HCl]) pairs for given absorbance readings from Sensors 2 and 16.

Figure 4.12 shows the error in acidity determination for 5 M HCl solutions containing $CaCl_2$. Without correction for the ionic strength, both Sensors 2 and 16 produced significant errors in the presence of a salt. These errors can be as large as 60% (Figure 4.12). The use of the current dual-transducer approach led to a significant drop in the error to < 4%. In addition, this approach yielded the salt concentrations C_{salt}(calc'd) with errors between 2 – 10% (Figure 4.13).

4.3.4 Indicator Absorbance and Acidity Function

Previous studies identified an empirical linear relationship between C_{salt} and the Hammett acidity function H_0 for both dilute and concentrated acid solutions (Figure 4.14).[11,66-68] It was surprising that the increase in acid strength (H_0) is correlated so simply to the increase in salt concentration, an observation that "must be fortuitous and caused by compensation of two or more effects" according to Högfeldt.[68a] It has long been proposed that the increase in acidity due to the presence of a neutral salt is caused by the decrease in a_w, the water activity. The water activity decreases when H_2O is removed from the bulk solution to solvate ions.[68b]

The current work showed a linear relationship between C_{salt} and ΔA in Eq. 4.13. As shown here, such relationship could be transformed to a linear relationship between H_0 and C_{salt}. Furthermore, the observed linear relationship between $\left(\partial A/\partial C_{salt}\right)_{C_{acid}}$ and $\left(dA/dC_{acid}\right)_{C_{salt}=0}$ in Eq. 4.10 could be used to derive the empirical linear dependence of H_0 on C_{salt} reported earlier.[11,67,68]

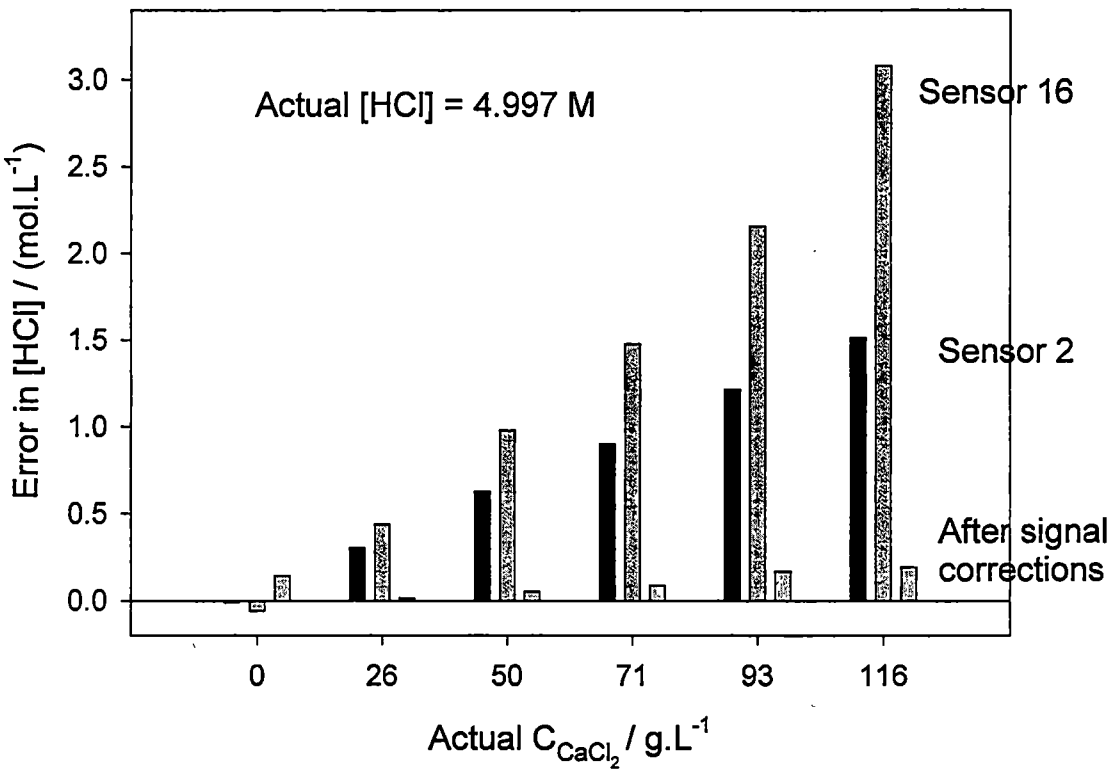

Figure 4.12. Comparison of errors in [HCl] measurements using Sensors 2 and 16, in the presence of $CaCl_2$, before and after the corrections.

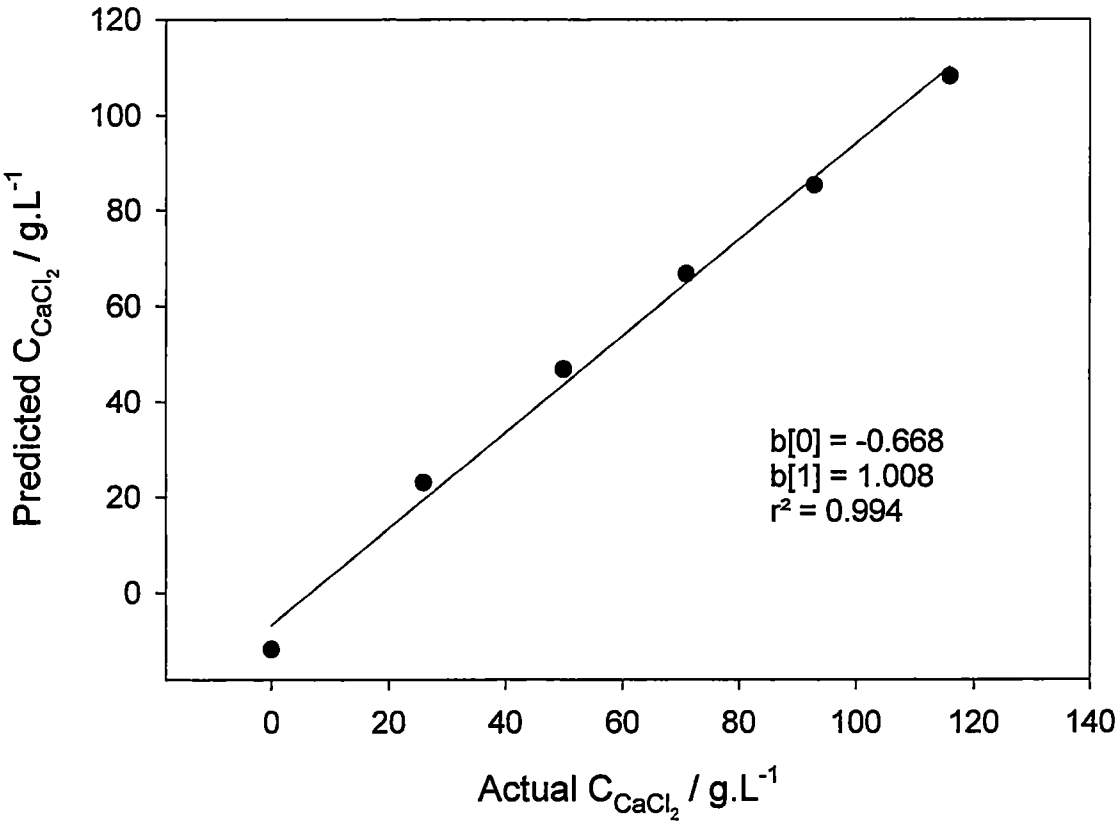

Figure 4.13. Validation plot of predicted vs. actual $CaCl_2$ concentrations in $HCl/CaCl_2$ solutions. Predicted values were computed by a signal deconvolution algorithm using data from Sensors 2 and 16.

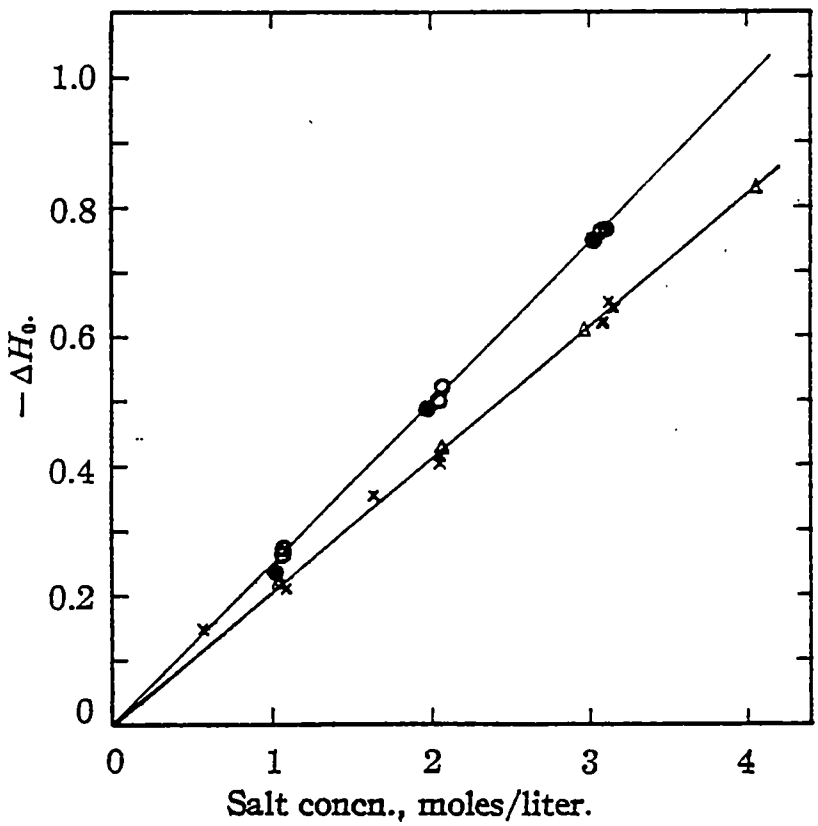

Figure 4.14. Effect of NaCl on ionization of indicators from ref. 67: •, diphenylamine in 0.05 M HCl; o, diphenylamine in 0.1 M HCl; Δ, p-nitroaniline in 0.1 M HCl; ×, 2,4-dichloroaniline in 0.01 M HCl.

In Eq. 4.9, Ka, the thermodynamic constant, is independent of ionic strength, and H_0 is the only variable. Taking the derivatives of Eq. 4.9 gives

$$\left(\frac{\partial A}{\partial C_{salt}}\right)_{C_{acid}} = \frac{\kappa \cdot \mathrm{Ind}_T \cdot Ka}{(Ka + 10^{-H_0})^2}\left(\frac{\partial(10^{-H_0})}{\partial C_{salt}}\right)_{C_{acid}} = \frac{-\kappa \cdot \mathrm{Ind}_T \cdot Ka \cdot (10^{-H_0}) \ln 10}{(Ka + 10^{-H_0})^2}\left(\frac{\partial H_0}{\partial C_{salt}}\right)_{C_{acid}}$$

$$\left(\frac{dA}{dC_{acid}}\right)_{C_{salt}=0} = \frac{\kappa \cdot \mathrm{Ind}_T \cdot Ka}{(Ka + 10^{-H_0})^2}\left(\frac{d(10^{-H_0})}{dC_{acid}}\right)_{C_{salt}=0}$$

$$= \frac{-\kappa \cdot \mathrm{Ind}_T \cdot Ka \cdot (10^{-H_0}) \ln 10}{(Ka + 10^{-H_0})^2}\left(\frac{dH_0}{dC_{acid}}\right)_{C_{salt}=0}$$

Thus the linear relationship between $\left(\partial A/\partial C_{salt}\right)_{C_{acid}}$ and $\left(dA/dC_{acid}\right)_{C_{salt}=0}$ in Eq. 4.10 leads to

$$\left(\frac{\partial H_0}{\partial C_{salt}}\right)_{C_{acid}} = \beta \cdot \left(\frac{dH_0}{dC_{acid}}\right)_{C_{salt}=0} \qquad \text{(Eq. 4.18)}$$

For salt-free acid systems, $\left(\frac{dH_0}{dC_{acid}}\right)_{C_{salt}=0}$ is a function of C_{acid} only, thus

$$\left(\frac{\partial H_0}{\partial C_{salt}}\right)_{C_{acid}} = \beta \cdot \left(\frac{dH_0}{dC_{acid}}\right)_{C_{salt}=0} = g(C_{acid}) \qquad \text{(Eq. 4.19)}$$

Eq. 4.19 indicates that, at a given C_{acid}, the derivative $\left(\frac{\partial H_0}{\partial C_{salt}}\right)_{C_{acid}}$ is a constant. In other words, there is a linear relationship between H_0 and C_{salt} at constant C_{acid}. The novel linear relationship in the current study (Eq. 4.10) thus leads to the empirical relationship in Eq. 4.20, which has been reported in the literature.[11,66,67]

$$(\Delta H_0)_{C_{acid}} = g(C_{acid}) \cdot (\Delta C_{salt})_{C_{acid}} \qquad \text{(Eq. 4.20)}$$

To our knowledge, there has been no report to link $\left(\partial H_0 / \partial C_{salt}\right)_{C_{acid}}$ with $\left(\frac{dH_0}{dC_{acid}}\right)_{C_{salt}=0}$, or to obtain any more fundamental relationship from the empirical relationship in Eq. 4.20. In the cases of the three indicators studied in the current work, the novel relationship in Eq. 4.10 (and in Eq. 4.18) is perhaps a more fundamental relationship that can lead to, e.g., the empirical relationship in Eq. 4.20.

4.3.5 Evaluation of Conductivity as a Secondary Concentration Transducer

Conductivity measurements of salt solutions in HCl showed a linear relationship between the solution conductivity and the salt concentration (Figure 4.15). We have studied the conductance of a solution and its feasibility as a secondary transducer. The plot of conductance vs. different concentrations of HCl, as well as HCl/$CaCl_2$ solutions is given in Figure 4.16. There was a clear linear dependence between the salt concentration and conductance, as shown by the straight lines in Figure 4.16. However, the function [HCl] vs. conductance (represented by • in Figure 4.16) was not monotonic. In other

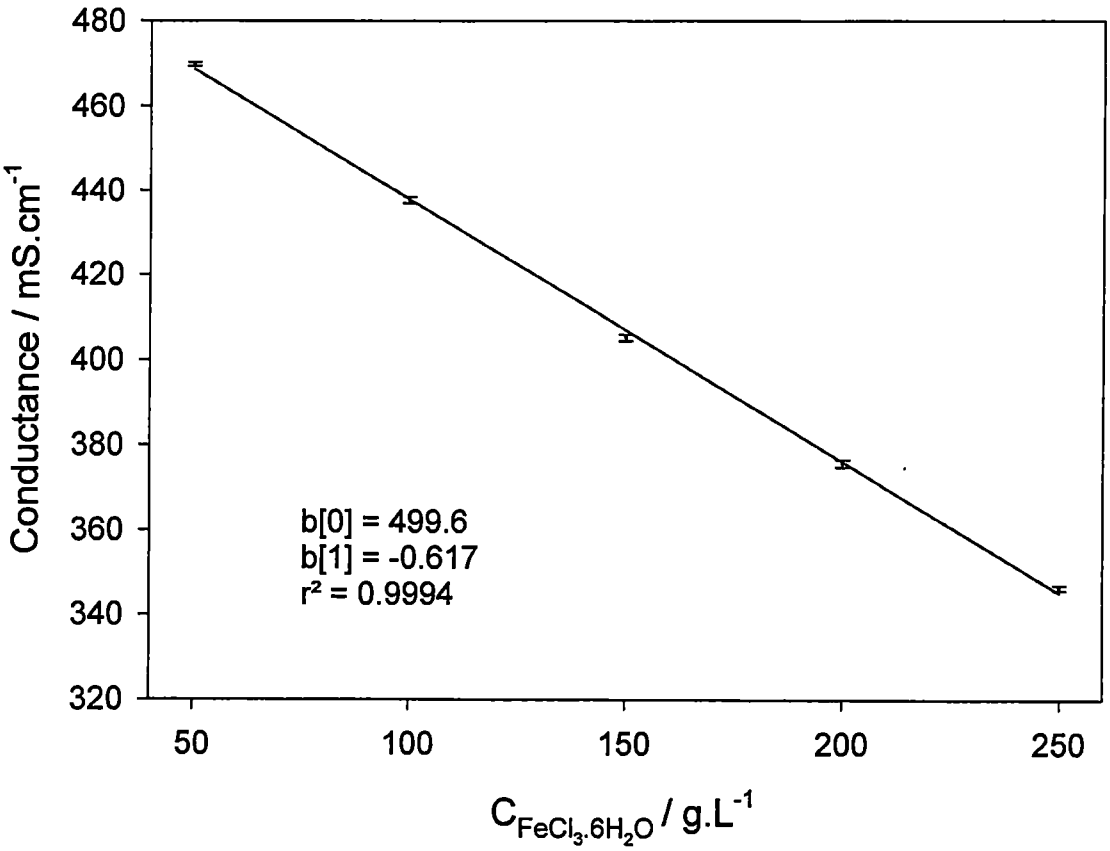

Figure 4.15. Conductance of $FeCl_3$/HCl solutions as a function of $FeCl_3$ concentration ([HCl] = 2.42 M).

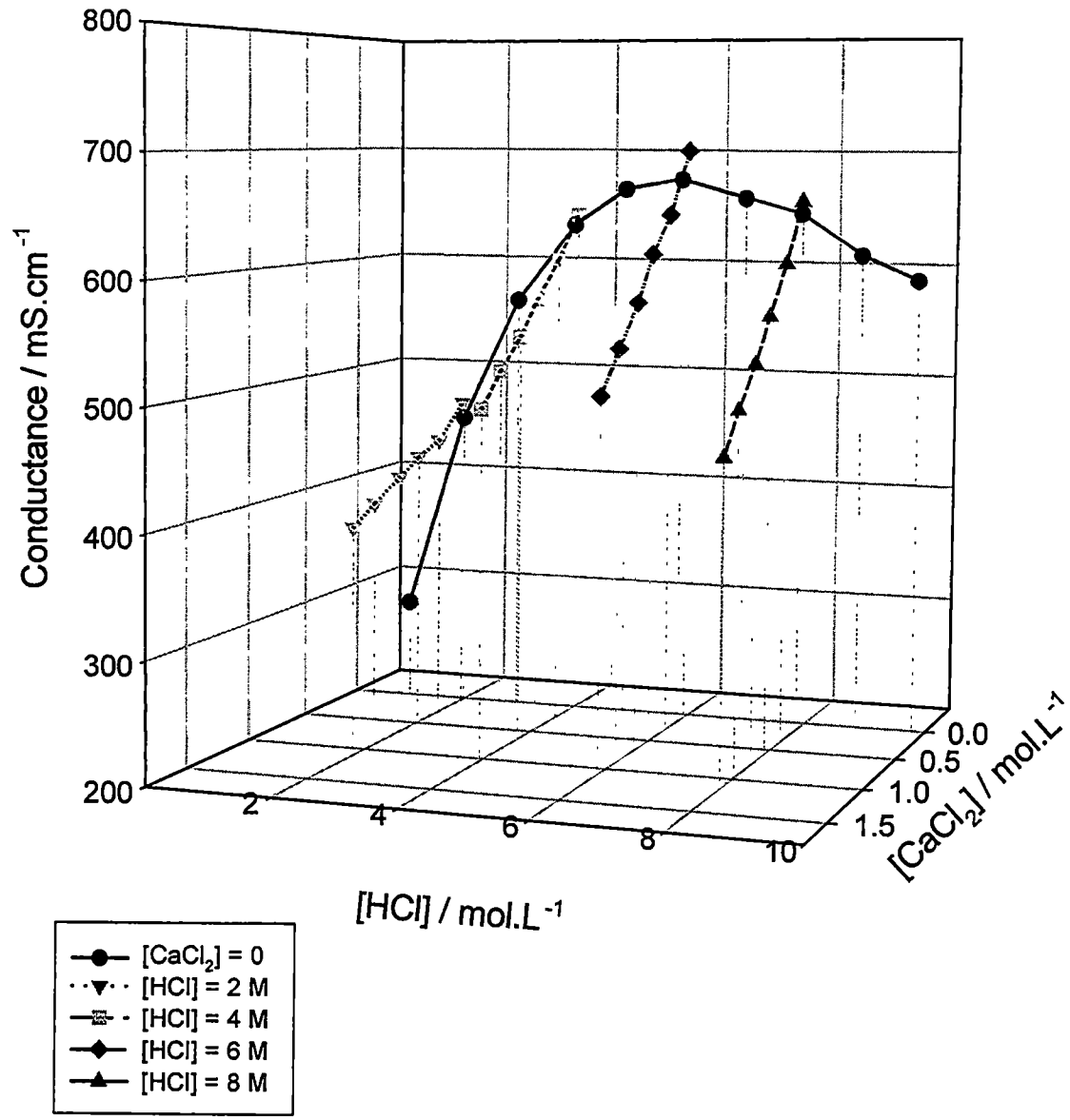

Figure 4.16. Conductance of $CaCl_2$/HCl solutions as a function of $CaCl_2$ and HCl concentrations.

words, different HCl concentrations can give an identical conductance reading. This limited the application of conductance measurements to a restricted analytical range.

Furthermore, the contribution of [$CaCl_2$] to the total conductance of the sample was large, and in the same order of magnitude as [HCl] itself. We concluded that conductivity was not an adequate secondary transducer to estimate [HCl] and C_{salt} in highly concentrated acids. However, for lower concentrations it may still be a feasible secondary transducer.

The dual-transducer approach reported here provides easy measurements of acid and salt concentrations in salt-containing concentrated strong acids. The effect of ionic strength on the optical sensor response can be a significant source of error if not corrected in the acidity measurement. The approach developed here is based on a novel linear relationship between $\left(\partial A/\partial C_{salt}\right)_{Cacid}$ and $\left(dA/dC_{acid}\right)_{C_{salt}=0}$. In essence, the approach reported here converts $\left(\partial A/\partial C_{salt}\right)_{Cacid}$, an unknown function of C_{acid}, into $\beta\left(dA/dC_{acid}\right)_{C_{salt}=0}$. Both β, a function free of C_{salt}, and $\left(dA/dC_{acid}\right)_{C_{salt}=0}$ could be determined experimentally, and thus lead to the computed solutions for C_{acid} and C_{salt}. If similar relationships exist between other analytes, the approach could be potentially applicable in their analysis.

The approach used here can be used to the development of sensors coupled to a single multiplex CCD (charged coupled device) spectrometer to coordinate and analyze multiple measurements automatically.

CHAPTER 5

Hysteresis in Optical Sensing and Its Impact on Analytical Error

5.1 Introduction

As optical sensors are increasingly used as measuring devices, a closer scrutiny of their properties is needed in order to better understand their operational principles and improve their efficiencies. One such property is reversibility of the sensor response. In general, sensors should operate in a reversible fashion. This would obviously not be the case if the sensor transducing mechanism is not reversible. However, even when the sensor transducing mechanism is reversible, the analyte diffusion process still has a profound effect on the reversibility of the sensing scheme. This is the subject of study in the current chapter.

Many sensing schemes in optical sensors are based on the transport of an analyte through a porous support where the transducing chemistry occurs. The transducing chemistry ranges from simple molecular interactions with specific dyes to minute changes in the swelling of a cross-linked polymer. A large number of optical sensors are based on the immobilization of a sensitive dye into a solid support, and mass transport of the analyte across the solid support is necessary to produce the analytical signal. If mass transport is not truly reversible, hysteresis of the sensor response is observed. Alabbas and coworkers[69] studied various aspects of sensor design (film thickness, porosity, and probe geometry) that were correlated with diffusion time, and their experimental data agreed with one-dimensional mass-transport diffusion models. Bousse

and coworkers[70] have investigated the time-dependence of the potentiometric response of silicon nitride-based sensors and the hysteresis profile of such sensors. The hysteresis profile was found to be a function of the time constant in an exponentially time-dependent response, and the magnitude of hysteresis was observed to be a direct function of the response time. Another sensor for SO_2 was reported to have a long response time and pronounced hysteresis.[71]

In general, a concentration gradient develops when the sensor element is placed in a solution of the analyte, and diffusion of the analyte through the sensor element is controlled by this gradient. Most available sensing schemes record the analytical response as a function of the concentration of the diffused analyte. In this case, the analytical error is large if the diffusion is not at equilibrium. When the concentration of the analyte in the exterior solution is larger than that inside the sensor, a positive concentration gradient is established and the analyte diffuses into the sensor. Conversely, when the concentration in the exterior solution is smaller than that inside the sensor, a negative gradient develops, and the analyte diffuses out of the sensor. The analyte transport properties may be different under a positive or negative gradient regime, and this difference usually leads to hysteresis in the sensor response.

A few sensing schemes are based on the analyte diffusion process itself. In these cases, the sensors are equipped with a semi-permeable membrane that isolates an internal chamber from the external analyte solution. A titrant continuously flows through this internal chamber and reacts with the analyte that has diffused in. The semi-permeable membrane allows the analyte to reach a steady state diffusion, and therefore the rate of analyte diffusion can be correlated with the external analyte concentration.[23,40]

In their review of fundamental properties of sensors, Göpel and coworkers[72] defined hysteresis as "the difference in the output of the sensor for a given input value X when X is reached from two opposite directions, i.e., from X^- and X^+." In a mechanical sensor, hysteresis is usually produced by a delay in the action of the sensor element. In magnetic sensors it is usually caused by a delay in the alignment of magnetic moments, in response to an external magnetic field.

Hysteresis is ubiquitous in a plethora of phenomena involving absorption/desorption and membrane permeation of analytes. Sensors cannot be operationally reversible when hysteresis is large. Hysteresis was found to be the major component of the analytical error in our optical sensor systems. In addition, we have observed a correlation between sensor response time and hysteresis. Efforts have been made to minimize the hysteresis in our optical acid and base sensors, and these efforts have led to the improvement of the sensor reversibility.

5.2 Experimental Section

The acid (Sensor 2) and base sensors (Sensors 7 – 9) were prepared by the procedures reported in Chapters 2 and 3, respectively.

Visible spectra were recorded using a single array, dual beam spectrometer system described in Chapter 1. To minimize response drifts caused by fluctuations in the light output collection, the absorbance at the most sensitive wavelength of each sensor was divided by their corresponding isosbestic absorbance. Analysis of Variance (ANOVA) was executed in the Matlab environment with the use of PLS_Toolbox 2.0 (Eigenvector Research, Inc., 830 Wapato Lake Road, Manson, WA 98831).

Prior to spectral data collection, the sensors were washed with acid or base solutions until no further changes in their absorbance were observed. This step usually required 2 to 15 min to complete. Each spectrum acquired was the average of 15 measurements, collected at 1 s intervals and 300 ms integration time.

5.3 Results and Discussion

5.3.1 Hysteresis in the Acid Sensor

The Sensor 2 response when the HCl concentration was increased from 2 to 10 M gave a plot (of sensor absorbance vs. HCl concentration) in Figure 5.1 with a positive concentration gradient. Afterwards, the HCl concentration was gradually reduced, and the response of the acid sensor in this process with a negative concentration gradient was recorded (Figure 5.1). If the sensor response were hyteresis-free, the two curves in Figure 5.1 would overlap. The larger the difference between the two curves is, the larger the hysteresis of the sensor response is. In the case of Sensor 2, the two curves are similar but do not overlap. In other words, the response hysteresis of Sensor 2 is small but observable. When the external HCl concentration was decreased, and after a long washing period (2 – 15 min), the sensor absorbances (under a negative gradient) were larger than those at the same concentrations when HCl concentration was increased (under a positive gradient). These observations, typical of the acid and base sensors, indicate that when the external acid concentration is decreased, it takes longer for the H^+ ions to diffuse out of the sol-gel sensor film.

Such hysteresis was also observed during the nine-month durability and reproducibility test discussed in Chapter 2 (Figure 2.16). During the durability tests, the

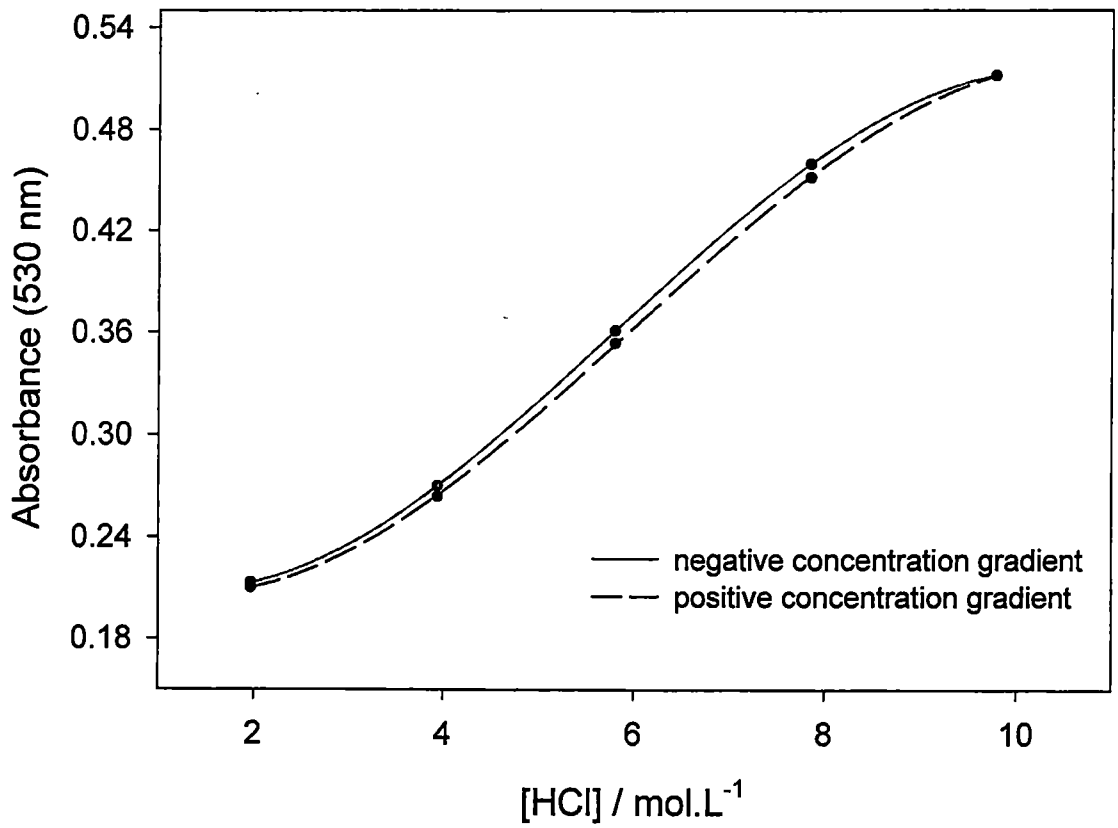

Figure 5.1. The hysteresis profile for Bromocresol Purple Sensor 2.

Sensor 2 film was kept in 6 M HCl for the entire nine-month period, except when measurements were collected. Periodically, the sensor film was transferred to the spectrometer cell and exposed to HCl solutions, with both incremental and decremental concentration cycles. Figure 5.2 shows the nine-month reproducibility data of Sensor 2 for 2 M HCl.

Analysis of variance (ANOVA) is a statistical tool that identifies sources of variation on samples. It compares the means and variances in different data sub-sets to confirm whether the subsets are statistically identical or not. In the current work, ANOVA was applied to the data set from the studies of Sensor 2 long-term reproducibility.

For 2 and 6 M HCl, a large data set was created for each concentration, and analysis of variance was performed on the collected data. The data set for each concentration was further divided into two sub-sets, corresponding to data collected when the sensor film was exposed to a positive acid concentration gradient, and a negative acid concentration gradient, respectively. Analysis of variance indicated that when the sensor was placed in solutions with the same HCl concentration (2 M), the two sub-sets of data are statistically different from each other at a 0.95 confidence level (Table 5.1).

Such analysis of variance (ANOVA) was also conducted for 6 M HCl as well. The results of this analysis are shown in Table 5.2. The data set for 6 M HCl was broken down into two different sub-sets (positive and negative gradient), which were confirmed to be statistically different from each other at a 0.95 confidence level.

In order to verify that the sensor response was not deteriorating over time, each data sub-set was divided further into another two groups, namely, measurements in the

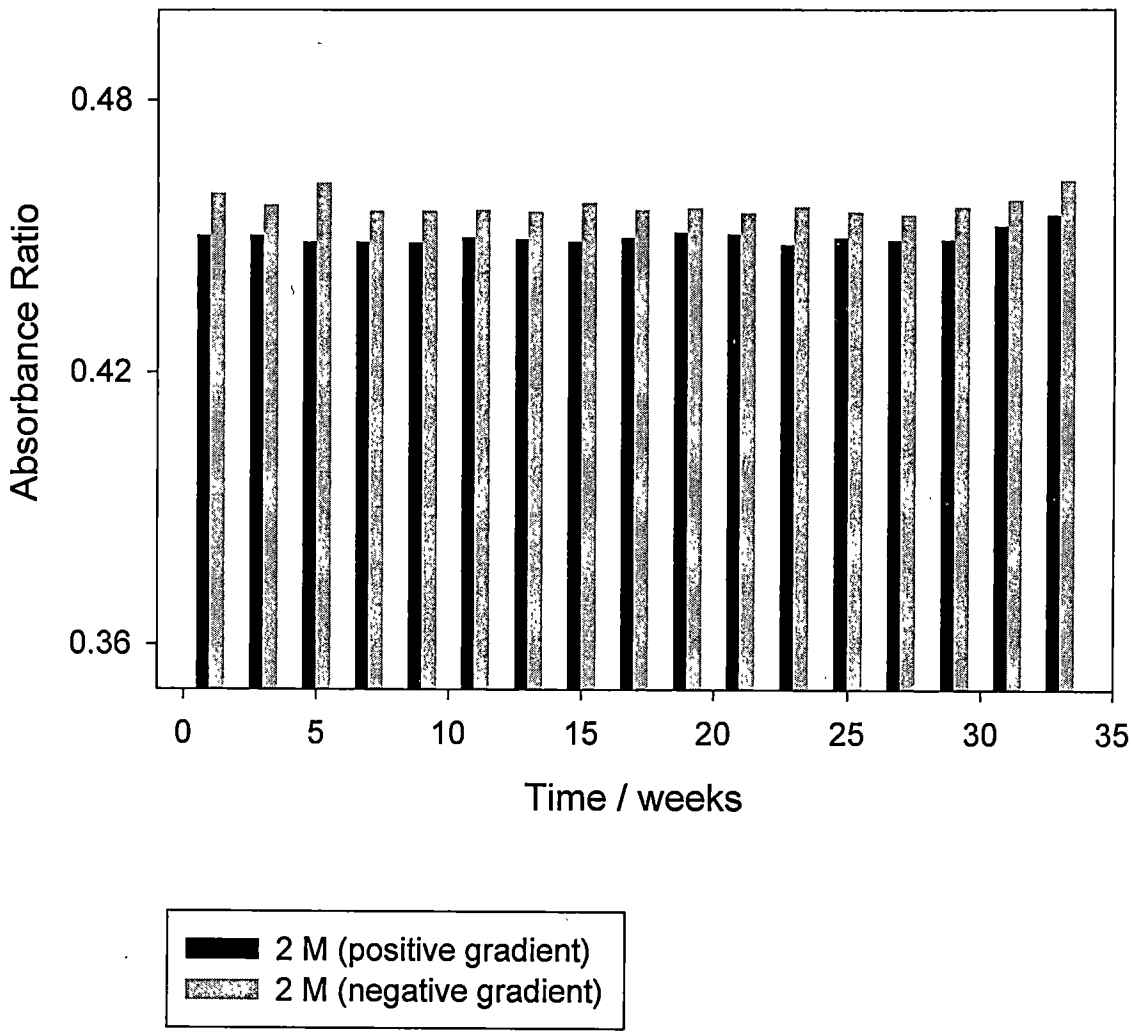

Figure 5.2. Nine-month reproducibility test of Sensor 2 in 2 M HCl. The sensor was exposed to positive and negative acid concentration gradients.

Table 5.1 Results from Analysis of Variance Applied to the Nine-Month Reproducibility Data (Sensor 2 Response in 2 M HCl under a Positive and a Negative Concentration Gradient)*

Source of Variation	Sum of Squares	Degrees of Freedom	Mean Square
Between factors	0.0004	1	0.0004
Residual	0.0001	32	0.0000
Total	0.0005	33	

Effect of factor = 0.000420/3.76e-006 = 112

F at 95 percent confidence = 4.148 ∴ Effect of factor is significant

* In this analysis the factor is the concentration gradient.

Table 5.2 Results from Analysis of Variance Applied to the Nine-Month Reproducibility Data (Sensor 2 Response in 6 M HCl under a Positive and a Negative Concentration Gradient)*

Source of Variation	Sum of Squares	Degrees of Freedom	Mean Square
Between factors	0.0004	1	0.0004
Residual	0.0001	30	0.0000
Total	0.0005	31	

Effect of factor = 0.000395/2.97e-006 = 133

F at 95 percent confidence = 4.171 ∴ Effect of factor is significant.

* In this analysis the factor is the concentration gradient.

first 4.5 months and measurements in the second 4.5 months. The difference in the means of both sub-groups was not statistically significant at 0.95 confidence (Table 5.3), confirming that the sensor response was steady over the nine-month period.

5.3.2 Quantifying the Hysteresis Error in Acid Sensor Response

The total variance of a sample, s^2, corresponds to the sum of variances from all independent sources of error. Assuming that hysteresis is independent of other sources of random error, the total variance of the sensor measurements, s^2_T, is the sum of the variances of two terms as shown in Eq. 5.1.

$$s^2_T = s^2_{hyst} + (s^2_{pos} + s^2_{neg}) \qquad (5.1)$$

s^2_{hyst} is the variance due to hysteresis; s^2_{pos} and s^2_{neg} are the variances due to experimental errors of the sensor under a positive and negative concentration gradient, respectively.

Using the standard deviation as an estimator for the variance, s^2_T, s^2_{pos}, and s^2_{neg} are directly calculated from the experimental data. Thus s^2_{hyst} can be calculated from Eq. 5.1. In the case of Sensor 6, the contribution of hysteresis to the total variance (s^2_{hyst}/s^2_T) is 54% and 62%, for 2 and 6 M HCl, respectively.

Hysteresis is thus the major component of the analytical error, and cannot be ignored when designing sensor systems.

Table 5.3 Results from Analysis of Variance Applied to the Nine-Month Reproducibility Data (Sensor 2 Response in 2 M HCl in the First 4.5 Months and in the Second 4.5 Months)*

Source of Variation	Sum of Squares	Degrees of Freedom	Mean Square
Between factors	0.0000	1	0.0000
Residual	0.0000	14	0.0000
Total	0.0000	15	

Effect of factor = 1.34e-006/1.01e-006 = 1.32

F at 95 percent confidence = 4.600 ∴ Effect of factor **is not** significant

* In this analysis the factor is time (blocks of 4.5 months).

5.3.3 Hysteresis in the Base Sensors

The hysteresis profile for three different hydroxide sensors (Sensors 7 - 9) are shown in Figures 5.3, 5.4, and 5.5, respectively. Each profile consists of two curves of the sensor response under a positive and a negative NaOH concentration gradient. If the sensor response were hysteresis-free, the two curves in each profile would overlap. The hysteresis of the sensor response is larger as the difference between the two curves becomes more pronounced. In the case of Sensors 7 – 9, the two curves do not overlap, and therefore, response hysteresis was observable. Sensor 8 had the smallest hysteresis, whereas Sensor 7 had the largest.

Under a positive gradient, when [NaOH] was increased from 0 to 5 M, Sensors 7 – 9 have a lower absorbance A than when the external NaOH concentration was decreased from 5 to 0 M (under a negative gradient). The absorbances were measured after a long washing period (2 – 15 min). This result indicated that when the external base concentration was decreased, the diffusion of OH^- from the sensor film to the solution occurred at a lower rate than that from a more concentrated solution into the sensor film.

5.3.4 Hysteresis and Response Time

It was observed that hysteresis in the sensors that have been discussed in previous chapters increased with their response time. In the case of the acid sensor discussed in this Chapter, the response time (to reach 90% of total response) varies in the range 1 – 5 s.

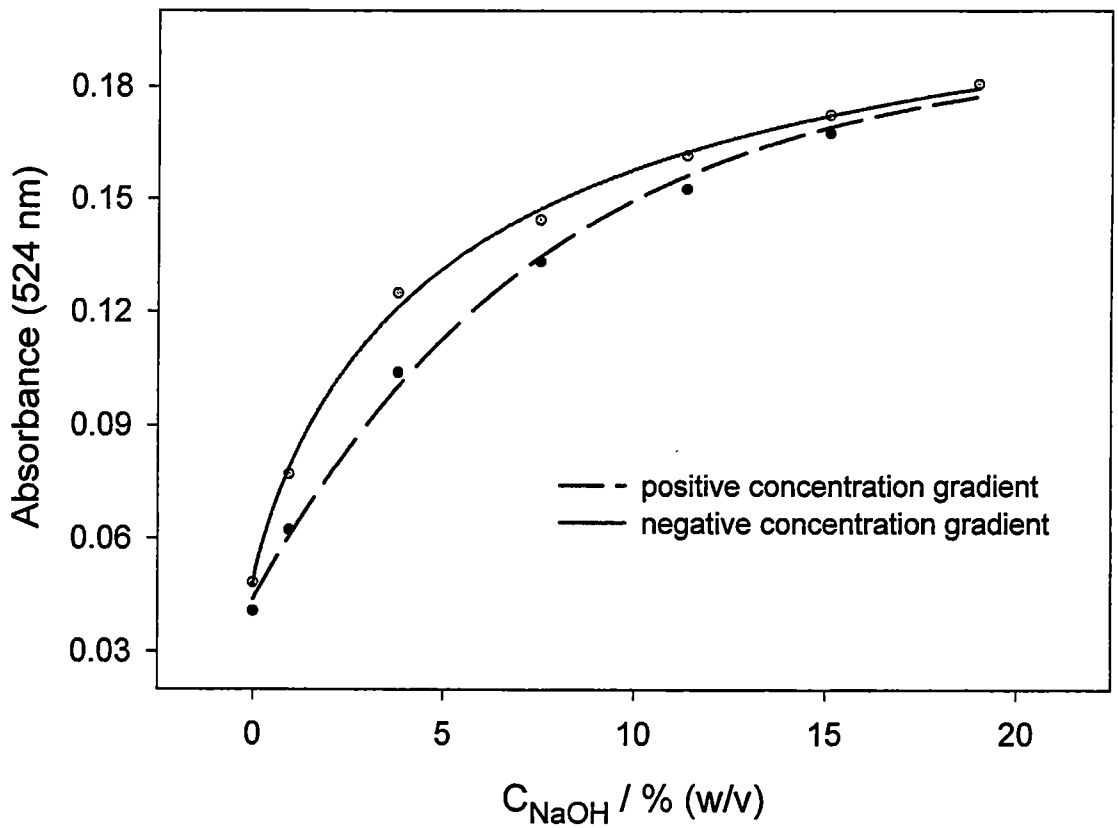

Figure 5.3. Hysteresis profile for Sensor 7.

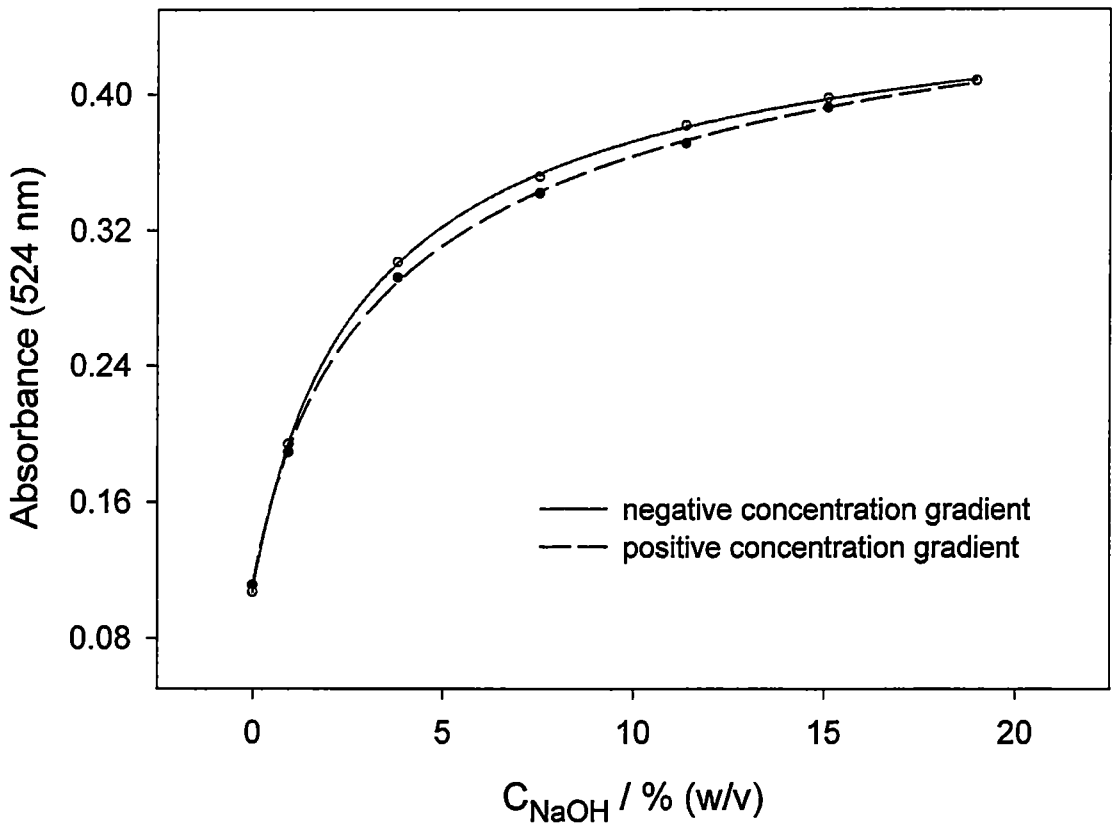

Figure 5.4. Hysteresis profile for Sensor 8.

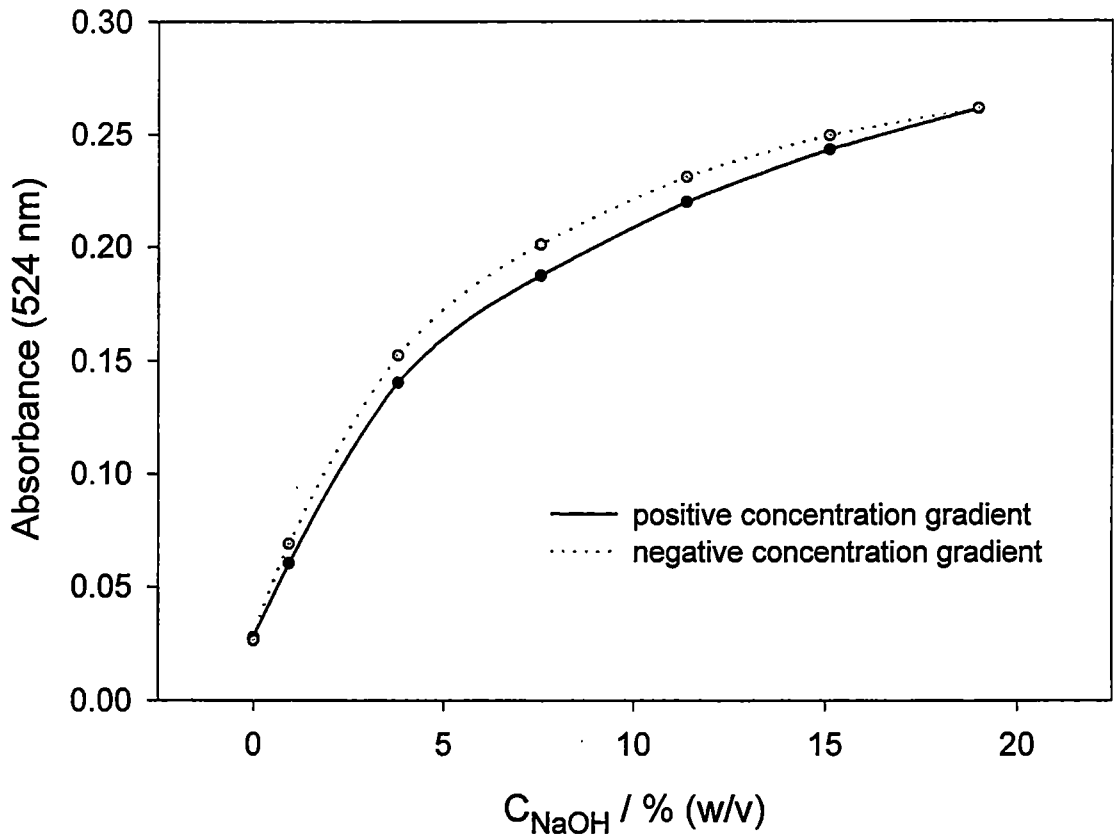

Figure 5.5. Hysteresis profile for Sensor 9.

The length of response time can be correlated with the magnitude of hysteresis. A linear correlation was found between the response time and the magnitude of hysteresis for the hydroxide sensors. The hysteresis profiles for Sensors 7 – 9 have been presented in the previous section (5.3.3). The response kinetics of these sensors has been discussed in Chapter 3 (Figure 3.11). The sensor with the slowest response time also showed the largest hysteresis, whereas the sensor with the fastest response time had the smallest hysteresis. A plot of the 90% of response time vs. hysteresis magnitude showed a clear linear correlation (Figure 5.6).

The different rates of inward/outward analyte diffusion across the sensor membrane seem to be the major source of hysteresis in our sensor systems. What is responsible for this variation in the diffusion rate?

We speculate that the diffusion rate difference reflects the ability of the solution to transfer H^+ (or OH^-) to/from the solid support containing the indicator. In other words, the buffer power of the solution in contact with the sensor film plays a major role in the analyte diffusion kinetics. The buffer power of acidic and basic solutions[59] as a function of pH is shown in Figures 5.7 and 5.8, respectively. The buffer power of these solutions increases with acid or base concentration, and is minimum at pH = 7.

In the case of the acid sensor, the driving force for the diffusion of H^+ across the sensor membrane is the acid concentration difference between a thin layer of solution closest to the sensor surface and that inside the sensor film. When the sensor film is under a positive concentration gradient, H^+ ions migrate from the thin layer into the sensor membrane, momentarily reducing the acid concentration of that thin solution layer. In a solution with large buffer power, the acidity decrease in the thin layer is

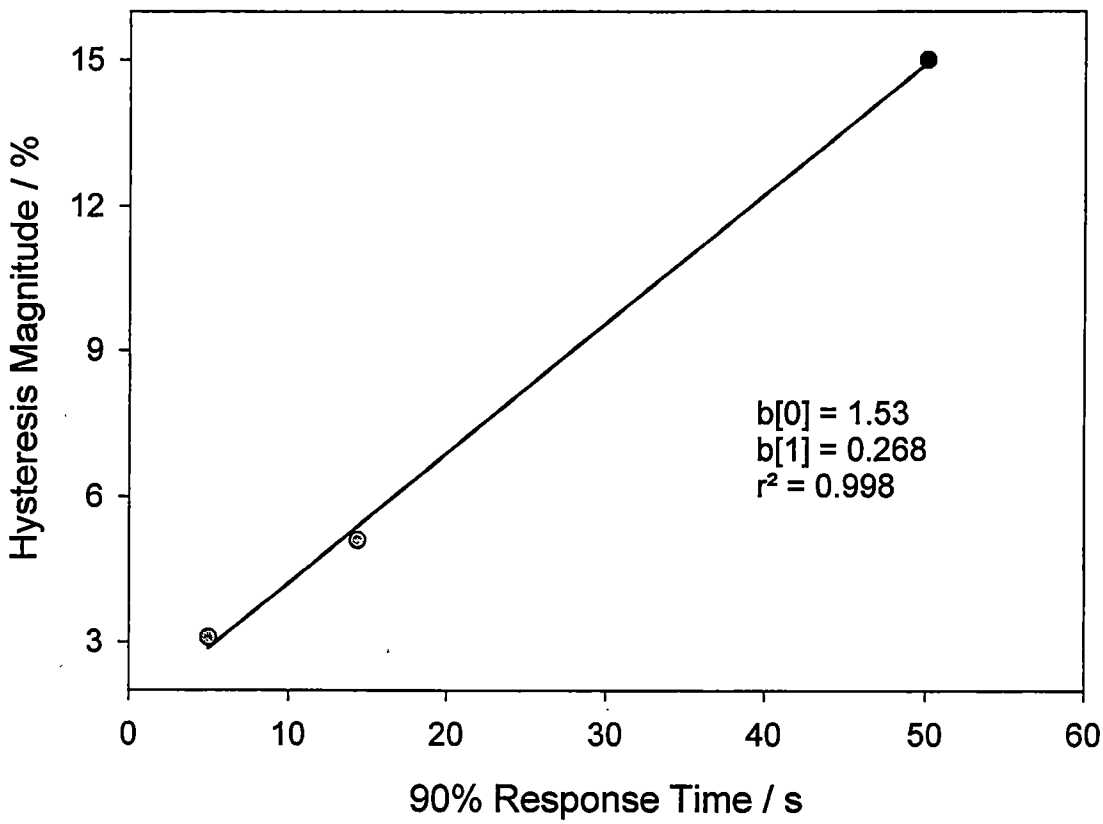

Figure 5.6. Plot of the response time vs. hysteresis magnitude for the hydroxide sensors (Sensors 7 – 9).

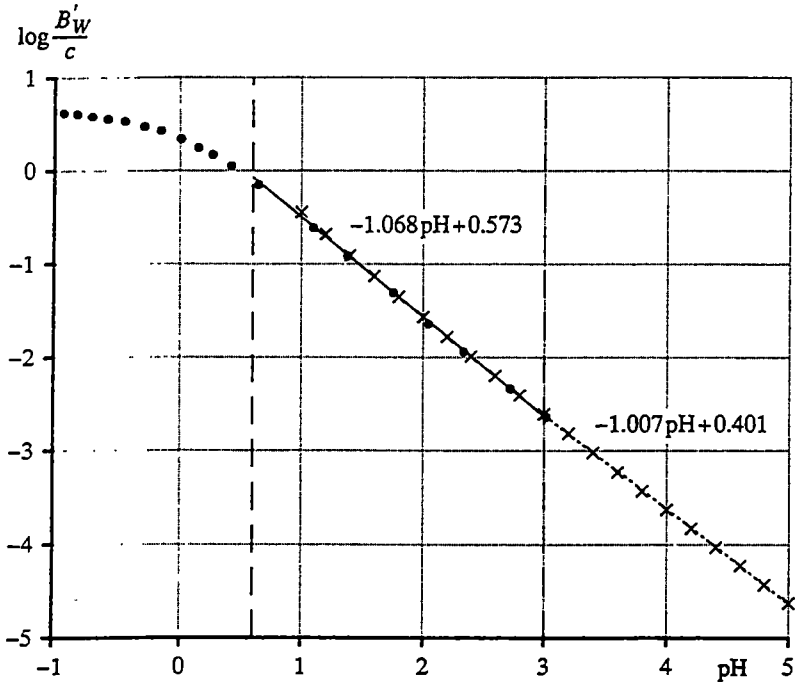

Figure 5.7. The logarithm of the buffer power per liter of water (B_w'/c) as a function of pH in the acidic region. Above pH = 3 and in the region between 0.6 and 3, the logarithm of buffer power is a linear function of pH with the equations given in the graph. Below pH = 0.6 there is a non-linear dependence, and, in extremely acidic solutions, the logarithm seems to approach a limiting value of 0.61. (Adapted from ref. 59).

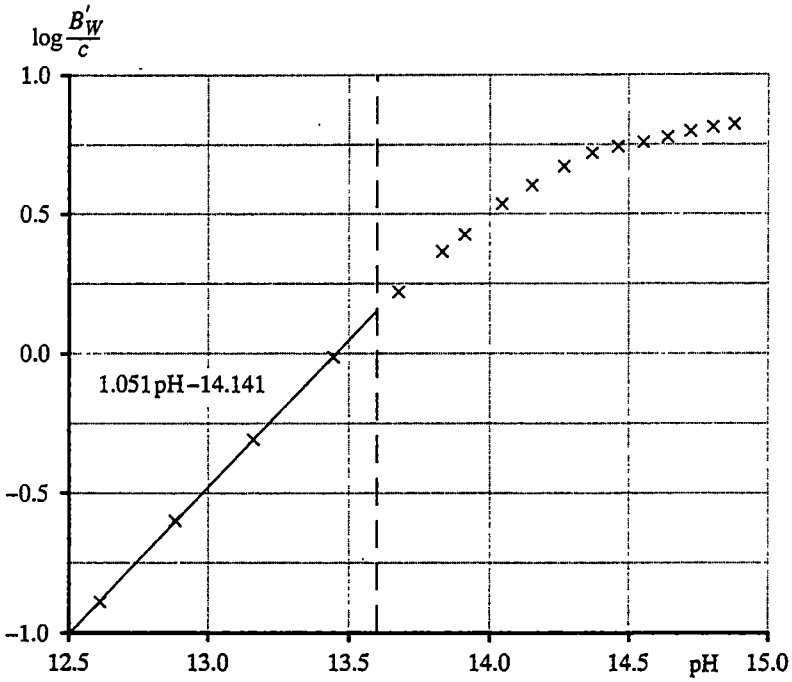

Figure 5.8. The logarithm of the buffer power per liter of water (B_w'/c) as a function of pH in the alkaline region. Below pH = 13.6 the logarithm is a linear function of pH with the equation given in the graph. Above this pH there is a non-linear dependence, and, in strongly alkaline solutions, the logarithm seems to approach a limiting value of 0.84. (Adapted from ref. 59).

quickly compensated to give fast H^+ diffusion into the film. A concentrated acid solution has larger buffer power. Thus when the sensor film is placed in such a solution, fast inward H^+ diffusion is often observed. However, the solution (often deionized water) used to wash an acid-containing sensor film often has small buffer power for H^+, limiting its ability to absorb H^+ ions from the film. The small buffer power of the wash solution thus gives slower H^+ outward diffusion from the sensor film and larger hysteresis of the sensor response.

In the current study, changing the film composition (Chapter 3) and increasing the film porosity (Chapter 2) were found to reduce the hysteresis of sensor response. However, the earlier approaches we took lead to severe leaching of doped indicators in the sensor films. In the current studies of acid and base sensors, we have developed approaches by balancing these two often competing requirements to give sensors with proper composition and pore sizes with minimal indicator leaching and hysteresis.

REFERENCES

1. *Terms and Definitions in Industrial Process Control*, IEC draft 65/84, International Electrotechnical Committee: Geneva, Switzerland, 1982.

2. (a) *CRC Fiber Optic Chemical Sensors and Biosensors*. Wolfbeis, O. S. Ed.; CRC Press: Boca Raton, 1991, Vol 1, p. 4. (b) *ibid* p. 246. (c) *ibid* p. 303. and Ch. 8. (d) *ibid* p. 303 and p. 359. (e) *ibid* p. 363.

3. Janata, J.; Josowicz, M. *Anal. Chem.* **1998**, *70*, 179R.

4. *Sensor Technology 2000*, Prognos AG: Basel, Switzerland, 1988.

5. *World Fiber-Optic Sensor Markets*, Frost & Sullivan: Mountain View, CA 1997.

6. Private communications with Technomic Publishing Co., Inc., Lancaster, PA.

7. Seitz, W. R. *CRC Crit. Rev. Anal. Chem.* **1988**, *19*, 135.

8. Rochester, C. H. *Acidity Functions*, Academic Press: London, 1970.

9. Wu, Y. C. *Standardization of pH Measurements*. U.S. Department of Commerce. National Bureau of Standards, 1988, Washington, C 13.10:260-53/988.

10. Hammett, L. P.; Deyrup, A. J. *J. Am. Chem. Soc.* **1932**, *54*, 2721.

11. Paul, M. A.; Long, F. A. *Chem. Rev.* **1957**, *57*, 1.

12. *Encyclopedia of Chemical Technology*, 4th ed.; Wiley: New York, 1991. (a) HCl, Vol. 13, p. 894; (b) HNO_3, Vol. 17, p. 80; (c) H_2SO_4 and SO_3, Vol. 23, p. 363; (d) NaOH, Vol. 1, p. 938.

13. Greenwood, N. N.; Earnshaw, A. *Chemistry of the Elements*, Pergamon Press: New York, 1997. (a) HCl, p. 811; (b) HNO_3, p. 466; (c) H_2SO_4, p. 708; (d) NaOH, p. 89.

14. Zaknoune, M.; Schuler, O.; Mollot, F.; Theron, D.; Crosnier, Y. *J. Vac. Sci. Technol.* **1998**, *16B*, 223.

15. Wolfbeis, O. S. *Fresenius J. Anal. Chem.* **1990**, *337*, 522.

16. *Chemical Sensors Special Issue. Acc. Chem. Res.*, **1998**, *31*, No. 5.

17. Atkins, P. W. *Physical Chemistry*, 4th ed. W. H. Freeman: New York, 1990, p. 249.

18. (a) *Technology Vision 2020: The U.S. Chemical Industry.* American Chemical Society, Washington, DC, 1996, p. 42. (b) *Expanding the Vision of Sensor Materials*, Committee on New Sensor Technologies: Materials and Applications, National Research Council, National Academy Press: Washington, DC, 1995, p. 73.

19. Bates, R. *Determination of pH*, Wiley: New York, 1973, p. 365.

20. McMillan, G. K. *Chem. Eng. Prog.* **1991**, *87*, 30.

21. Van Staden, J. F. *Fresenius Z. Anal. Chem.* **1987**, 328, 68.

22. (a) Carey, W. P.; Jorgensen, B. S. *Appl. Spectrosc.* **1991**, *45*, 834. (b) Carey, W. P.; DeGrandpre, M. D.; Jorgensen, B. S. *Anal. Chem.* **1989**, *61*, 1674. (c) Jorgensen, B. S.; Nekimken, H. L.; Carey, W. P.; O'Rourke, P. E. U.S. Patent 5650331, 1997. (d) Day, R. S. *J. Proc. Anal. Chem.* **1996**, *2*, 193.

23. Kuhn, K. J.; Dyke, J. T. *Anal. Chem.* **1996**, *68*, 2890.

24. Jensen, B.; Mickelson, J.; Jakhete, R.; Valentine, J. *Hydrocarbon Process., Int. Ed.* **1998**, *77*, 101.

25. (a) Rottman, C.; Ottolenghi, M.; Zusman, R.; Lev, O.; Smith, M.; Gong, G.; Kagan, M. I.; Avnir, D. *Mater. Lett.* **1992**, *13*, 293. (b) Ding, J. Y.; Shahriari, M. R.; Sigel, Jun. G. H. *Electron. Lett.* **1991**, *27*, 1560. (c) Lacan, P.; Gall, P. L.; Rigola, J.; Lurin, C.; Wettling, D.; Guizard, C.; Cot, L. *Sol-Gel Optics II, SPIE* **1992**, *1758*, 464. (d) Livingston, R. R.; Baylor, L.; Wicks, G. G. DOE Documents, Westinghouse Savannah River Company, 1992, WSRC-RP-92-1276.

26. (a) Lev, O. *Analusis* **1992**, *20*, 543. (b) Dunn, B.; Zink, J. I. *J. Mater. Chem.* **1991**, *1*, 903. (c) Klein, L. C. *Annu. Rev. Mater. Sci.* **1993**, *23*, 437. (d) Avnir, D. *Acc. Chem. Res.* **1995**, *28*, 328.

27. PC2000 or SD2000 by Ocean Optics, Dunedin, FL (http://www.oceanoptics.com).

28. (a) Brinker, C. J.; Scherer, G. W. *Sol-Gel Science*, Academic Press: San Diego, 1990. (b) *ibid* p. 103. (c) *ibid* p. 242.

29. (a) McDonagh, C.; McGraith, B. D.; McEvoy, A. K. *Anal. Chem.* **1998**, *70*, 45. (b) Cheetham, A. K.; Brinker, C. J.; Mecartney, M. L.; Sanchez, C., Eds.; *Mater. Res, Soc. Symp. Proc.* **1994**, Volume 346.

30. Klein, L. *Sol-Gel Optics: Processing and Applications*, Kluwer Academic Publishers: Lowell, MA, 1994.

31. *Chemistry, Spectroscopy, and Applications of Sol-Gel Glasses*, Reisfield, R.; Jorgenson, C. K. Eds.; Springer-Verlag: Berlin, 1992.

32. Grate, J. W.; Klusty, M.; McGill, R. A.; Abraham, M. H.; Whiting, G.; Andonian-Jaftvan, J. *Anal. Chem.* **1992**, *64*, 610.

33. Narang, U.; Dunbar, R. A.; Bright, F. V.; Prasad, P. N. *Appl. Spectr.* **1993**, *47*, 1700.

34. (a) Bishop, E. *Indicators*, Pergamon Press: Oxford, 1972. (b) *ibid* p. 347 and p. 672. (c) ibid p. 74.

35. (a) Kolthoff, I. M. *Indicators*, 1926, John Wiley & Sons: New York. (b) Matsuoka, M. *Infrared Absorbing Dyes*, 1990, Plenum Press: New York.

36. Gupta, V. D.; Reed, J. B. *J. Pharm. Sci.* **1970**, *59*, 1683.

37. Aragoni, M. C.; Arca, M.; Crisponi, G.; Nurchi, V. M.; Silvagni, R. *Talanta* **1995**, *42*, 1157.

38. Bell, R. P. *The Proton in Chemistry,* Cornell University Press: Ithaca, N.Y., 1973.

39. Gold, V.; Hawes, B. W. V. *J. Chem. Soc.* **1951**, 2102.

40. Berman, R.; Christian, G. D.; Burgess, L. W. *Anal. Chem.* **1990**, *62*, 2066.

41. Watson, E. Jr.; Baughman, E. H. *Spectroscopy* **1987**, *2*, 44.

42. (a) Price, J. M.; Xu, W.; Demas, J. N.; DeGraff, B. A. *Anal. Chem.* **1998**, *70*, 265. (b) Baldini, F.; Bracci, S.; Cosi, F. *Sens. Actuators A* **1993**, *37-38*, 180. (c) Zhang, L.; Langmuir. M. E.; Bai, M.; Seitz, R. W. *Talanta* **1997**, *44*, 1691.

43. (a) Jordan, D. M.; Walt, David R.; Milanovich, F. P. *Anal. Chem.* **1987**, *59*, 437. (b) Song, A.; Parus, S.; Kopelman, R. *Anal. Chem.* **1997**, *69*, 863. (c) Zhang, S.; Rolfe, P.; Wickramasinghe, Y. A. B. D. *Proc. SPIE-Int. Soc. Opt. Eng.* **1994**, *2085* (Biochemical and Medical Sensors), 22. (d) Bacci, M.; Baldini, F.; Scheggi, A. M. *Proc. SPIE-Int. Soc. Opt. Eng.* **1989**, *990* (Chem. Biochem. Environ. Appl. Fibers), 84.

44. Janata, J. *Anal. Chem.* **1987**, *59*, 1351.

45. Casay, G. A.; Meadows, F.; Daniels, N.; Roberson, A.; Patonay, G. *Spectrosc. Lett.* **1995**, *28*, 301.

46. Phelan, M. K.; Barlow, C. H.; Kelly, J. J.; Jinguji, T. M.; Callis, J. B. *Anal. Chem.* **1989**, *61*, 1419.

47. Werner, T.; Wolfbeis, O. S. *Fresenius J. Anal. Chem.* **1993**, *346*, 564.

48. Safavi, A.; Abdollahi, H. *Anal. Chim. Acta* **1998**, *367*, 167.

49. Safavi, A.; Pakniat, M. *Anal. Lett.* **1998**, *31*, 1297.

50. Courchene, C. E.; Suh, S.; McDonough, T. J. *Tappi J.* **1994**, *77(7)*, 101.

51. Parker, D.; Senanayake, P. K.; Gareth, J. A. W. *J. Chem. Soc., Perkin Trans. 2* **1998**, *10*, 2129.

52. Parker, D.; Senanayake, K.; Gareth, J. A. W. *J. Chem. Soc., Chem. Commun.* **1997**, 1777.

53. Perrin, D. D.; Armarego, W. L. F. *Purification of Laboratory Chemicals*, 3rd ed.; Pergamon Press: Oxford, 1988.

54. Paul, A. *J. Mater. Sci.* **1977**, *12*, 2246.

55. (a) Stone, V. F.; Davis, R. J. *Chem. Mater.* **1998**, *10*, 1468. (b) Toba, M.; Mizukami, F.; Niwa, S.; Sano, T.; Maeda, K.; Annila, A.; Komppa, V. *J. Mol. Catal.* **1994**, *94*, 85.

56. (a) Carpenter, J. P.; Lukehart, C. M.; Price, B. T.; Wittig, J. E. *Inorg. Chim. Acta* **1995**, *229*, 121. (b) Raman, N. K.; Anderson, M. T.; Brinker, C. J. *Chem. Mater.* **1996**, *8*, 1682. (c) Imhof, A.; Pine, D. J. *Nature*, **1997**, *389*, 948.

57. (a) Serjeant, E. P.; Dempsey, D. *Ionization Constants of Organic Acids in Aqueous Solutions*, IUPAC series; Pergamon Press: Oxford, 1979. (b) Perrin, D. D. *Dissociation Constants of Organic Bases in Aqueous Solutions*; Butterworths: London, 1965. (c) Vogel, W.; Andrusiow, K. *Dissociation Constants of Organic Acids in Aqueous Solution*; Butterworths: London, 1961. (d) Kolthoff, I.; Rosenblum, C. *Acid-Base Indicators*; MacMillan: New York, 1937. (e) Perrin, D. D. *Dissociation Constants of Organic Bases in Aqueous Solution*: supplement 1972; Butterworths: London, 1972.

58. (a) Bowden, K. *Chem. Rev.* **1966**, *66*, 119. (b) Edward, J. T.; Wang, I. C. *Can. J. Chem.* **1962**, *40*, 399.

59. Rilbe, H. *pH and Buffer Theory - a New Approach*, Wiley Series in Solution Chemistry, John Wiley & Sons: Chichester, England, Vol. 1, 1996.

60. Wolfbeis, O. S.; Offenbacher, H. *Sens. Actuators*, **1986**, *9*, 85.

61. Edmonds, T. E.; Flatters, N. J.; Jones, C. F.; Miller, N. A. *Talanta* **1988**, *35*, 103.

62. Optiz, N.; Lubbers, D. W. *Sens. Actuators* **1983**, *4*, 473.

63. Wolfbeis, O. S.; Offenbacher, H. *Sens. Actuators*, **1986**, *9*, 85.

64. Lavigne, J. J.; Savoy, S.; Clevenger, M. B.; Ritchie, J. E.; McDoniel, B.; Yoo, S. J.; Anslyn, E. V.; McDevitt, J. T.; Shear, J. B.; Neikirk, D. *J. Am. Chem. Soc.* **1998**, *120*, 6429.

65. Aussenegg, F. R.; Brunner, H.; Leitner, A.; Lobmaier, C.; Schalkhammer, T.; Pittner, F. *Sens. Actuators, B* **1995**, *B29*, 204.

66. (a) Cox, R. A.; Yates, K. *Can. J. Chem.* **1981**, *59*, 2116. (b) Vicente, M. E. S. *Curr. Top. Sol. Chem.* **1997**, *2*, 157.

67. Paul, M. A. *J. Am. Chem. Soc.* **1954**, *76*, 3236.

68. (a) Högfeldt, E.; Staples, P. J. *J. Chem. Soc.* A **1971**, 2074. (b) Perrin, C. *J. Am. Chem. Soc.* **1964**, *86*, 256.

69. Alabbas, S. H.; Ashworth, D. C.; Bezzaa, B., Momin, S. A.; Narayanaswamy, R. *Sens. Actuators A* **1996**, *51*, 129.

70. Bousse, L.; Hafeman, D.; Tran, N. *Sens Actuators* **1990**, *81*, 361.

71. Pichlmaier, J. *Sens. Actuators B* **1995**, *26-27*, 286.

72. Göpel, W.; Hesse, J.; Zemel, J. N. in *Sensors, a Comprehensive Survey*, VHC: Weiheim, 1989, Vol. 1, p. 21.

APPENDICES

Appendix A

The indicators that were tested and found to degrade in concentrated hydroxide are:

1-(2-pyridylazo)-2-naphthol, 1,1'-diethyl-2,2'-cyanine iodide, 1,2,3-indantrione (ninhydrin), 1-aminoantraquinone, 2,4-dinitroaniline, 2,4-dinitrodiphenylamine, 2,6,7-trihydroxy-9-phenylisoxanthene-3-one, 2,6-dichloro-4-nitroaniline, 2,6-dichlorophenol indophenol, 2',7'-dichlorofluorescein, 2-bromo-4,6-dinitroaniline, 2-naphthol benzein, 2-nitroaniline, 3-(4-dimethylamino-1-naphthylazo)-4-methoxibenzene sulfonate, 3-nitroaniline, 4,2-pyridylazo resorcinol, 4-amino-3-nitrophenol, 4-chloronitroaniline , 4-dinitrodiphenylamine, 4-methyl esculetin, 4-nitroaniline, acid alizarin violet N, acid blue 147, acid blue 29, acid fuchsin, acridine, alizarin, alizarin sodium monosulfonate, azocarmine, barbituric acid, barium diphenylamine sulphonate, bathocuproine disulfonate, brilliant black BN, brilliant cresol blue, brilliant green, brilliant yellow, bromo pyrogallol red, bromocresol green, bromocresol purple, bromophenol blue, bromothymol blue, calcium chrome, carbazole, celestine blue, chlorophenol red, chlorophenol red, chromoazurol S, chromoxane cyanine R, chrysoidin, congo red, copper phthalocyanine tetrasulfonic, cresol red, cryptocyanine, crystal violet, curcumin, cyclohexanone, 2,4-dinitrophenylhydrazone, diphenyltiocarbazone, disperse orange, dithizone, eosin Y, eriochrome blue blacl B, ethylviolet, Evan's blue, ferrozine, fluorescein mercuric acetate, gallein, Gurr James black, hydroxyhydroquinol sulfonephthalein, hydroxynaphthol blue, indigo blue, indigo carmine, indoine blue, indophenol, malachite green oxalate, meta-cresol purple, methyl green hue, methyl

orange, methylene blue, methylene violet, methylthymol blue, morin, murexide, naphthol blue, naphthol green, neutral red, night blue, Nile blue A, nitroresorcinol, oil red 0, orange G, palatine chrome black (eriochrome black R), phenol red, phenyl fluorone, pinacyanol, ponta chrome violet SW, pyrocathechol violet, pyrocathecol violet, pyrogallol red, rhodamine B, rhodamine GG, Sudan II, sulfonazo III, sulfur-containing dye, tetrabromo m-cresol sulfonephthalein (bromocresol green), tetrabromohydroxyhydroquinol sulfonephthalein, tetrabromophenol blue, thymol blue, tin(IV) phthalocyanine dichloride, toluidine blue, tropeolin G, variamine blue, victoria blue B, xylene cyanol FF, xylenol blue, xylenol orange.

Appendix B

Matlab m files used in the deconvolution of acid and salt concentration in the multi-transducer approach described in Chapter 4.

<bcptest.m>

```
%this m file defines both the absorbance vs. [acid] calibration curve
%and the effect of salt concentration on absorbance for a typical
%sensor,in this example, BCP.


function con = test1(x)

%parameters for the calibration curve

a=0.44220;
b=1.66700;
x0=6.03500;
y0=0.26660;

%expression for [H+] vs Abs

y=y0 + a./(1 + exp((x0 - x)./b));

%calculates the first derivative of calibration curve, if [HCl] is
%known returns predicted slope for ionic strength dependence

dy = (a./b)*(1./(1 + exp(-(x - x0)./b))^2)*exp(-(x - x0)./b);

%estimated slope (indicator)

b0= -6.8933e-3;
b1=1.5356;

slope = b0 + b1*dy;

%adding the absorbance reading

Abs =0.51909;

load xestim.txt;

Asalt = Abs + slope*(x - xestim);


%expression for the interception of y and Asalt

con= y - Asalt;
```

Matlab m file

<iteration.m>

```
%enter initial guess for HCl concentration
iniHCl= 6.511;

for i=1:90;

   n=300;  %for the step size

   temp =(iniHCl -i/n);
   estHCl(i) =(iniHCl -i/n);

   save c:\leonardo\matlab\xestim.txt temp -ascii

   %enter m.file for calculation of interception point
   fzero('bcptest', 5);

   x=ans;
   HCl(i)=ans;

   %enter m.file that estimates [CaCl2]
  bcpsalt;

   Csalt1(i)=Csalt;
end

% save estimated data points ([HCl], Csalt) calculated from
% from the differential equations into file "answer.txt"

save c:\leonardo\matlab\answer.txt estHCl HCl Csalt1 -ascii -tabs
load answer.txt;
temp1=answer'
save c:\leonardo\matlab\answer.txt temp1 -ascii -tabs
```

Matlab m file

<findvalue.m>

```
%this m file calculates the interception point for the two
%estimated [HCl] vs. Csalt curves using two different sensors

j=input('Which set of equations will be used?    ');
i=(j-1)*4;
clear p1 p2 n;
n=input('How many degrees used in the interpolation? [1 to 7]:   ');

p1=polyfit(a(:,i+1),a(:,i+2),n);
p2=polyfit(a(:,i+3),a(:,i+4),n);

   Csalt=roots(p1 - p2)
   m=input('Which concentration will be used? [1 2 3 4 5]:');
   HCl=polyval(p1,Csalt(m))
   Csalt1(j)=Csalt(m);
   HCl1(j)=HCl;


save c:\leonardo\matlab\evalconc.txt  Csalt1 HCl1 -ascii -tabs
```

VITAE

Leonardo Resende Allain was born in 1972 in São Paulo, Brazil. He graduated from the Colégio Santo Antônio in December 1990. In February 1991, he enrolled at Universidade Federal de Minas Gerais, Belo Horizonte, Brazil, where he studied chemistry. During the four years of undergraduate studies, Leonardo was awarded a research fellowship by the Brazilian government. Under the direction of Professor Carlos Alberto Filgueiras, he conducted research with the funds from this fellowship on synthesis and characterization of coordination and organometallic tin compounds, as well as on the mechanism of reactions involving nucleophilic organotin species. He graduated with a B.S. degree in Chemistry in January 1995, and was offered a teaching position at the high school he graduated from. After teaching for six months, Leonardo came to the University of Tennessee to start his graduate studies under the direction of Professor Ziling (Ben) Xue. He developed optical sensors for the on-line monitoring of concentrated strong acids and bases for process control in industrial streams. In addition, he investigated the origins of hysteresis in sensor response, and developed a dual-sensor approach to correct sensor response in salt-containing acid with high ionic strength.